AD-A124 863 BASIC EMC TECHNOLOGY ADVANCEMENT FOR C(3) SYSTEMS 1/2
VOLUME IV C CROSSTALK I.. (U) SOUTHEASTERN CENTER FOR
ELECTRICAL ENGINEERING EDUCATION INC S..
UNCLASSIFIED M B JOLLY ET AL. NOV 82 F/G 9/3 NL

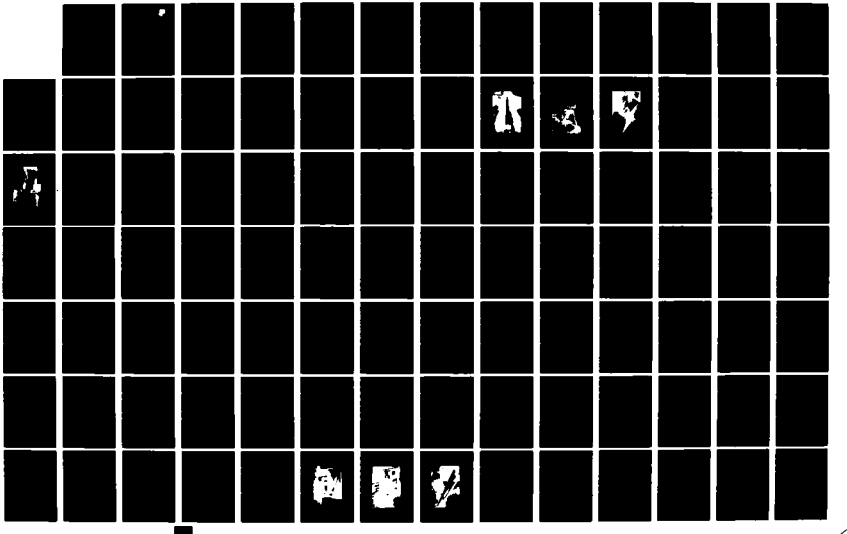

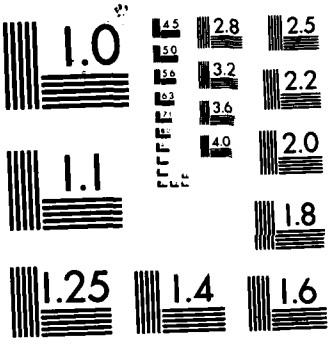

MICROCOPY RESOLUTION TEST CHART
NATIONAL BUREAU OF STANDARDS-1963-A

(12)

RADC-TR-82-286, Vol IV C (of six)
Phase Report
November 1982

BASIC EMC TECHNOLOGY ADVANCEMENT FOR C^3 SYSTEMS - Crosstalk in Twisted-Wire Circuits

Southeastern Center for Electrical Engineering Education

Marty B. Jolly
Clayton R. Paul

ROME AIR DEVELOPMENT CENTER
Air Force Systems Command
Griffiss Air Force Base, NY 13441

This report has been reviewed by the RADC Public Affairs Office (PA) and is releasable to the National Technical Information Service (NTIS). At NTIS it will be releasable to the general public, including foreign nations.

RADC-TR-82-286, Volume IV C (of six) has been reviewed and is approved for publication.

APPROVED Gerard T. Capraro

GERARD T. CAPRARO
Project Engineer

APPROVED: Edmund J. Westcott

EDMUND J. WESTCOTT
Technical Director
Reliability & Compatibility Division

FOR THE COMMANDER: John P. Huss

JOHN P. HUSS
Acting Chief, Plans Office

If your address has changed or if you wish to be removed from the RADC mailing list, or if the addressee is no longer employed by your organization, please notify RADC (RBCT) Griffiss AFB NY 13441. This will assist us in maintaining a current mailing list.

Do not return copies of this report unless contractual obligations or notices on a specific document requires that it be returned.

UNCLASSIFIED

SECURITY CLASSIFICATION OF THIS PAGE (When Data Entered)

REPORT DOCUMENTATION PAGE		READ INSTRUCTIONS BEFORE COMPLETING FORM
1. REPORT NUMBER RADC-TR-82-286, Vol IV C (of six)	2. GOVT ACCESSION NO. AD-A124	3. RECIPIENT'S CATALOG NUMBER 863
4. TITLE (and Subtitle) BASIC EMC TECHNOLOGY ADVANCEMENT FOR C^3 SYSTEMS - Crosstalk in Twisted-Wire Circuits		5. TYPE OF REPORT & PERIOD COVERED Phase Report Jun 81 - Dec 81 6. PERFORMING ORG. REPORT NUMBER N/A
7. AUTHOR(s) Marty B. Jolly Clayton R. Paul		8. CONTRACT OR GRANT NUMBER(s) F30602-81-C-0062
9. PERFORMING ORGANIZATION NAME AND ADDRESS Southeastern Center for Electrical Engineering Education 1101 Massachusetts Avenue, St Cloud FL 32796		10. PROGRAM ELEMENT, PROJECT, TASK AREA & WORK UNIT NUMBERS 62702F 23380335
11. CONTROLLING OFFICE NAME AND ADDRESS Rome Air Development Center (RBCT) Griffiss AFB NY 13441		12. REPORT DATE November 1982 13. NUMBER OF PAGES 122
14. MONITORING AGENCY NAME & ADDRESS(if different from Controlling Office) Same		15. SECURITY CLASS. (of this report) UNCLASSIFIED 15a. DECLASSIFICATION/DOWNGRADING SCHEDULE N/A

16. DISTRIBUTION STATEMENT (of this Report)

Approved for public release; distribution unlimited.

17. DISTRIBUTION STATEMENT (of the abstract entered in Block 20, if different from Report)

Same

18. SUPPLEMENTARY NOTES

RADC Project Engineers: Roy F. Stratton (RBCT)
Gerard T. Capraro (RBCT)

Work was performed at the University of Kentucky, Dept of Electrical Engineering, Lexington KY 40506 (See reverse)

19. KEY WORDS (Continue on reverse side if necessary and identify by block number)

Electromagnetic Compatibility	Twisted Wires
Cabe Coupling	Digital Transmission
Transmission Lines	Line Drivers
Multiconductor Transmission Lines	Line Receivers
Wire-to-Wire Coupling	

20. ABSTRACT (Continue on reverse side if necessary and identify by block number)

An investigation of wire-to-wire crosstalk is presented in an attempt to accurately predict the magnitude of the voltage coupled to a twisted wire pair. A sensitivity analysis of the twisted wire pair is conducted to determine the effect that line twist has on the coupled differential mode voltage when the twisted pair is connected in an unbalanced configuration. An improved computer model is developed to aid in the prediction of the voltage coupled to the twisted wire pair when it is terminated in low

DD FORM 1 JAN 73 1473 EDITION OF 1 NOV 65 IS OBSOLETE

UNCLASSIFIED

SECURITY CLASSIFICATION OF THIS PAGE When Data Entered)

impedance loads. Another circuit configuration which is investigated consists of a differential line driver connected to a differential line receiver by a twisted wire pair. Predictions of the common mode voltage coupled to the twisted pair are computed with a single wire model and a comparison is made with experimental results.

Block 18 (Cont'd)

Volumes I - III, V and VI will be published at a later date.

TABLE OF CONTENTS

I. Introduction

Most sophisticated electronic equipment consists of fairly complex subsystems. In order for these subsystems to communicate, they are interconnected with a network of wires. These wires in turn carry the modulated signal, usually digital data, necessary for communication. Most system networks require many such wires which are grouped into cable bundles. Since the wires in these bundles are closely packed, wire to wire interaction (crosstalk) is inevitable. Some of this crosstalk may be detrimental to the overall system performance because false data could be coupled into other subsystems.

Many techniques of reducing this interference have been proposed and used. Placing filters on the lines where the crosstalk level is 'high' is effective but costly, and the additional weight due to the filters may exceed limitations for certain systems. Shielding these lines is also an apparent method for crosstalk reduction but in some instances the additional weight factor of the shielding cannot be tolerated. The twisted wire pair (TWP) is used extensively in connecting electronic equipment to effectively reduce electromagnetic coupling to transmission lines due to crosstalk.

The TWP consists of two wires wound in the form of a bifilar helix. Although extensive analytical analysis has

been done for this special wire configuration an exact solution (or model) has not been obtained. Since the TWP is a bifilar helix, a translation along the x axis (the line axis) produces an apparent continuous rotation of any cross-section taken in the y-z plane; the rate of rotation is proportional to the pitch of the twist (see Fig. 1-1).

Although the wires in Fig. 1-1 represent a 'true' TWP, they cannot remain physically separated without some type of support. Circular-cylindrical dielectic insulation provides this support and insures that the wire separation remains constant (Fig. 1-2). However, the presence of this dielectic introduces inhomogeneity into the cross-section of the TWP. For simplicity in modeling it is assumed that the TWP consists of bare wires (Fig. 1-1).

The TWP is also inherently nonuniform. A transmission line is uniform if cross-sectional views of the line are identical for any point along the line. Clearly different cross-sectional views of the TWP can be obtained at different points along the line. Note, however, that the structure replicates with each full twist. Each twist of the TWP is identical to any other twist in the line except for its position along the line. This is further discussed in Chapter III where it is shown that this property greatly simplifies the process of modeling the coupling to the TWP.

Electromagnetic coupling to transmission lines is induced through the effects of both capacitive and inductive phenomena. The twisting of the lines is thought to reduce

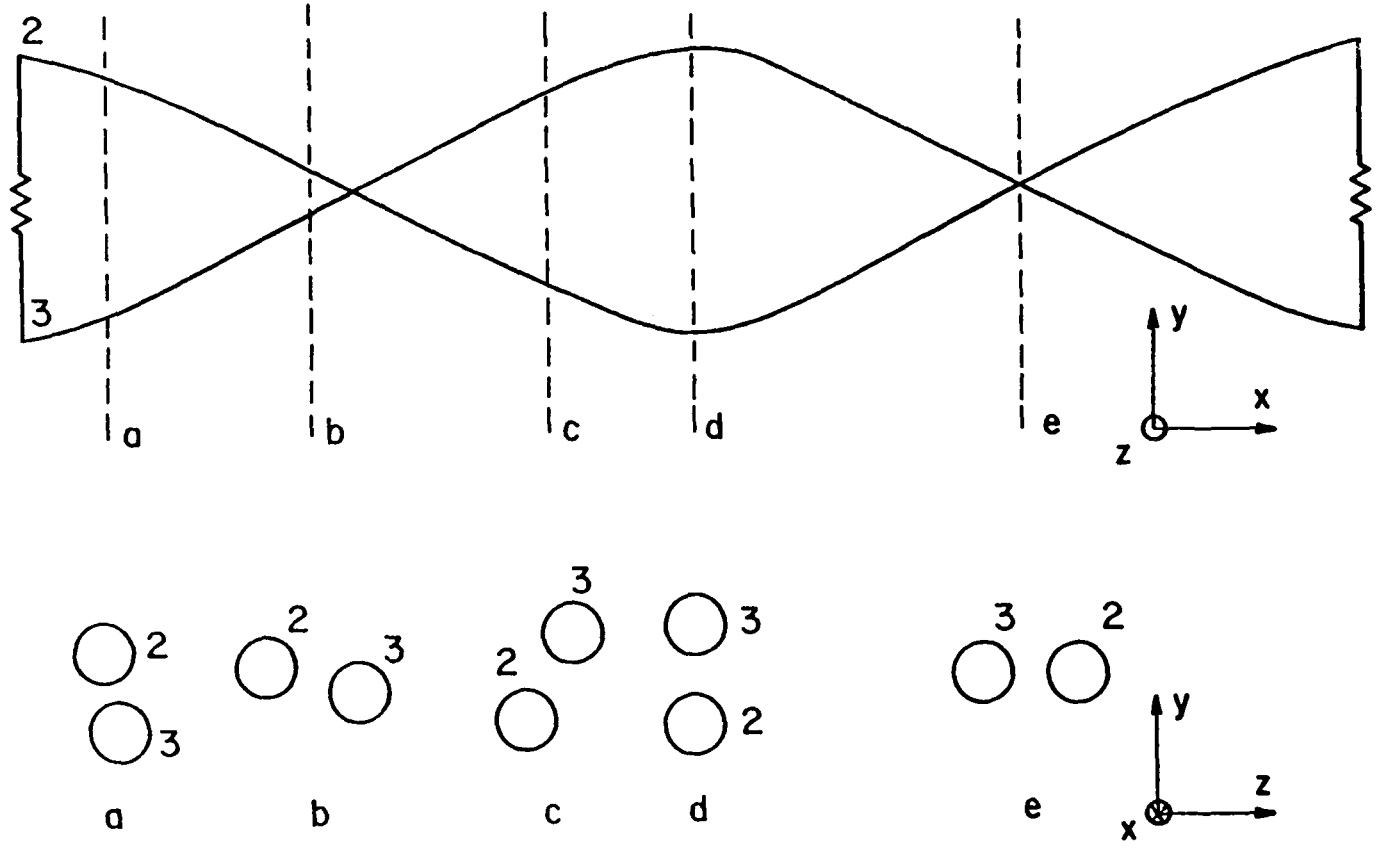

Fig. 1-1

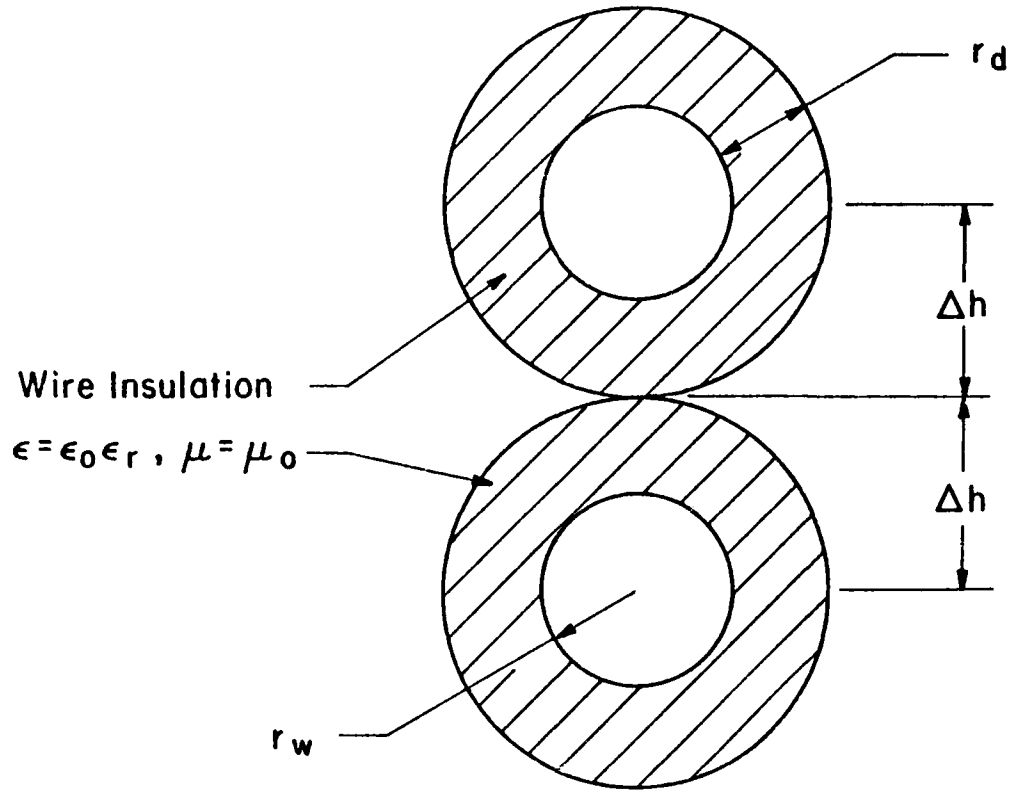
r_d
Δh
Wire Insulation
$\epsilon = \epsilon_0 \epsilon_r$, $\mu = \mu_0$
Δh
r_w

Fig. 1-2

crosstalk through the reduction of inductive coupling. This is precisely the case when the values of the end terminations of the TWP are sufficiently small and inductive coupling is dominant. To illustrate the concept of this reduction, consider the current induced in the straight wire pair (SWP) (Fig. 1-3). This induced current is directly proportional to the flux of the generating line penetrating the area enclosed by the two wires [1]. If the wires are twisted (as in Fig. 1-4) the flux penetrating the enclosed area is significantly reduced, therefore reducing the induced current. If the flux is idealized as being perpendicular to the TWP and if the twists are perceived as small circular loops then the induced currents would be excited as in Fig. 1-4. The currents induced in either wire appear to cancel, resulting in a very low level of inductive coupling.

The cancellation of the induced current would be greater when an even number of half-twists is present in the TWP than when an odd number of half-twists is present. This can be deduced from the illustration given above. For an even number of half-twists the induced currents cancel entirely, but for an odd number of half-twists there remains one half-twist where the current is not cancelled.

After obtaining experimental data for the differential mode voltage, an extreme sensitivity of the voltage transfer

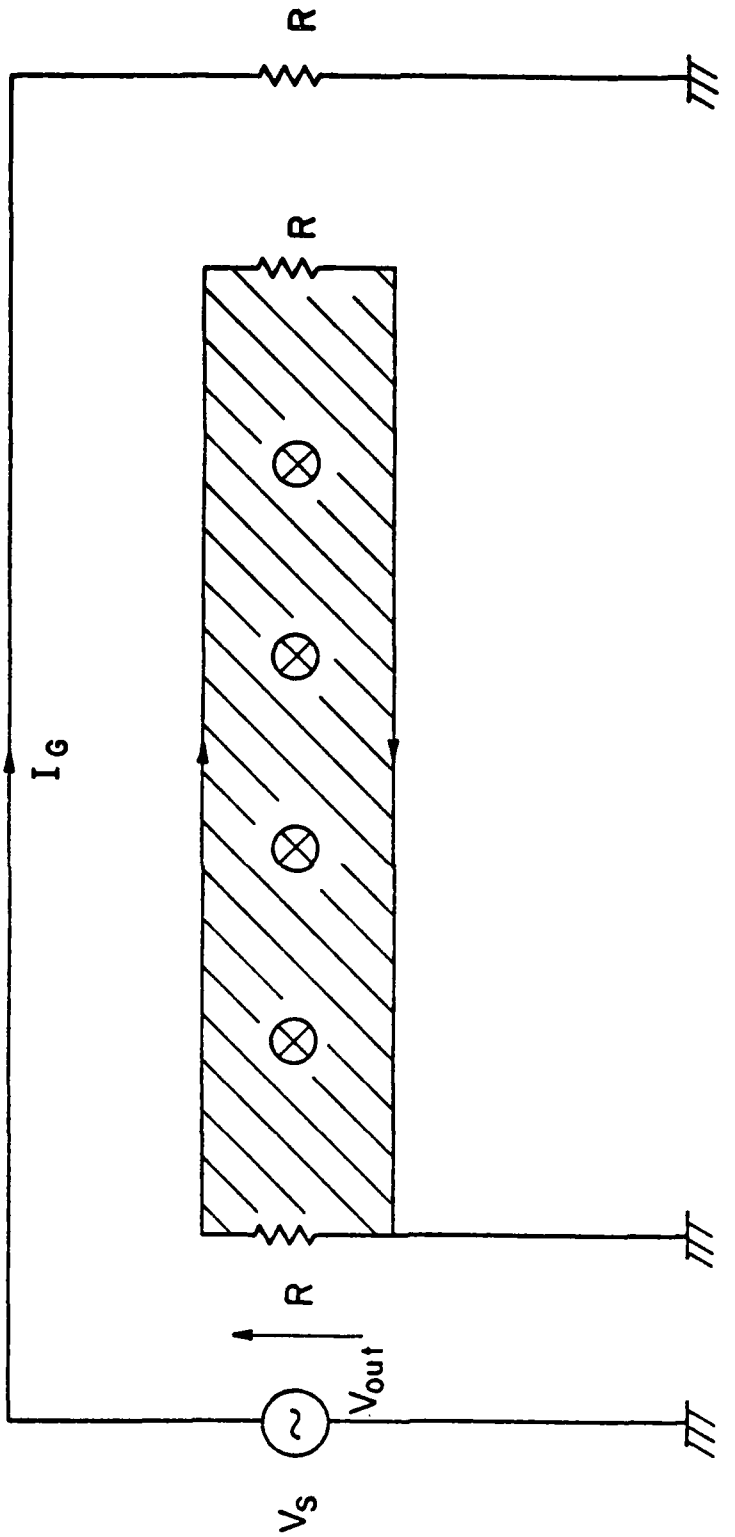

Fig. 1-3

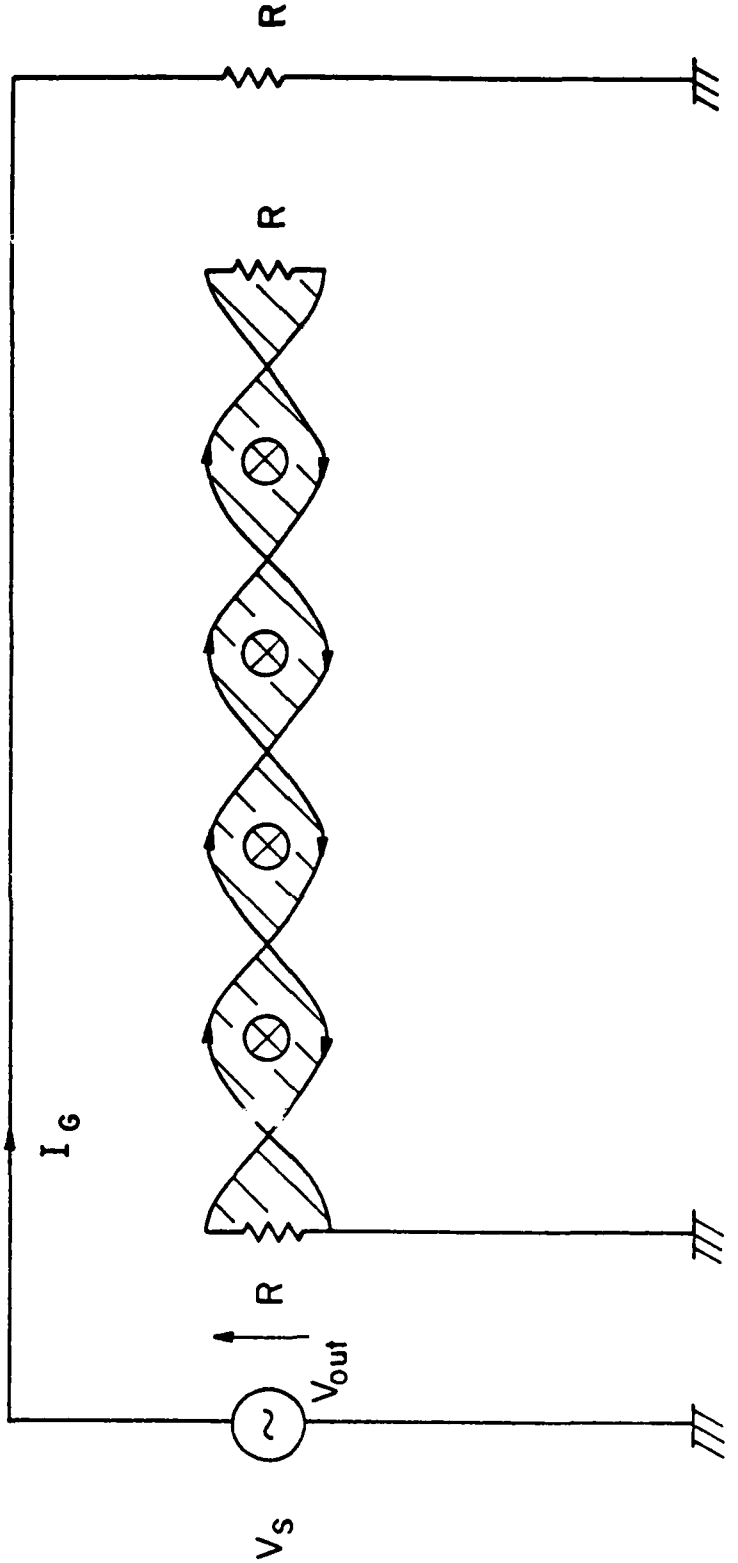

Fig. 1-4

ratio is noticed for 'low' terminal impedances. The voltage transfer ratio is defined as

$$VTR = \frac{|V_{OUT}|}{|V_s|}$$

The wires are arranged so one end of the TWP can be rotated and hence, change the number of twists in the line without altering the physical configuration. For these 'low' termination impedances a difference of 35 dB in the coupled differential voltage can be obtained by merely rotating one end of the TWP 180 degrees. This has the effect of changing the number of twists in the line by only one half-twist! The first objective of this work is to examine this sensitivity of the TWP.

A previous work [1] which examines the prediction of crosstalk either to or from TWP's uses the concept described above. In this model each 'loop' is considered as a separate transmission line pair excited by a corresponding adjacent section of generator line [1]. An illustration is given in Fig. 1-5. This loop model, although a seemingly crude approximation, provides accurate prediction of the voltage transfer ratio against experimental results for 'high' impedance loads, i.e., where capacitive coupling is dominant. For low impedance loads experimental results were not obtained in [1] so a comparison with the 'loop' model predictions could not be made.

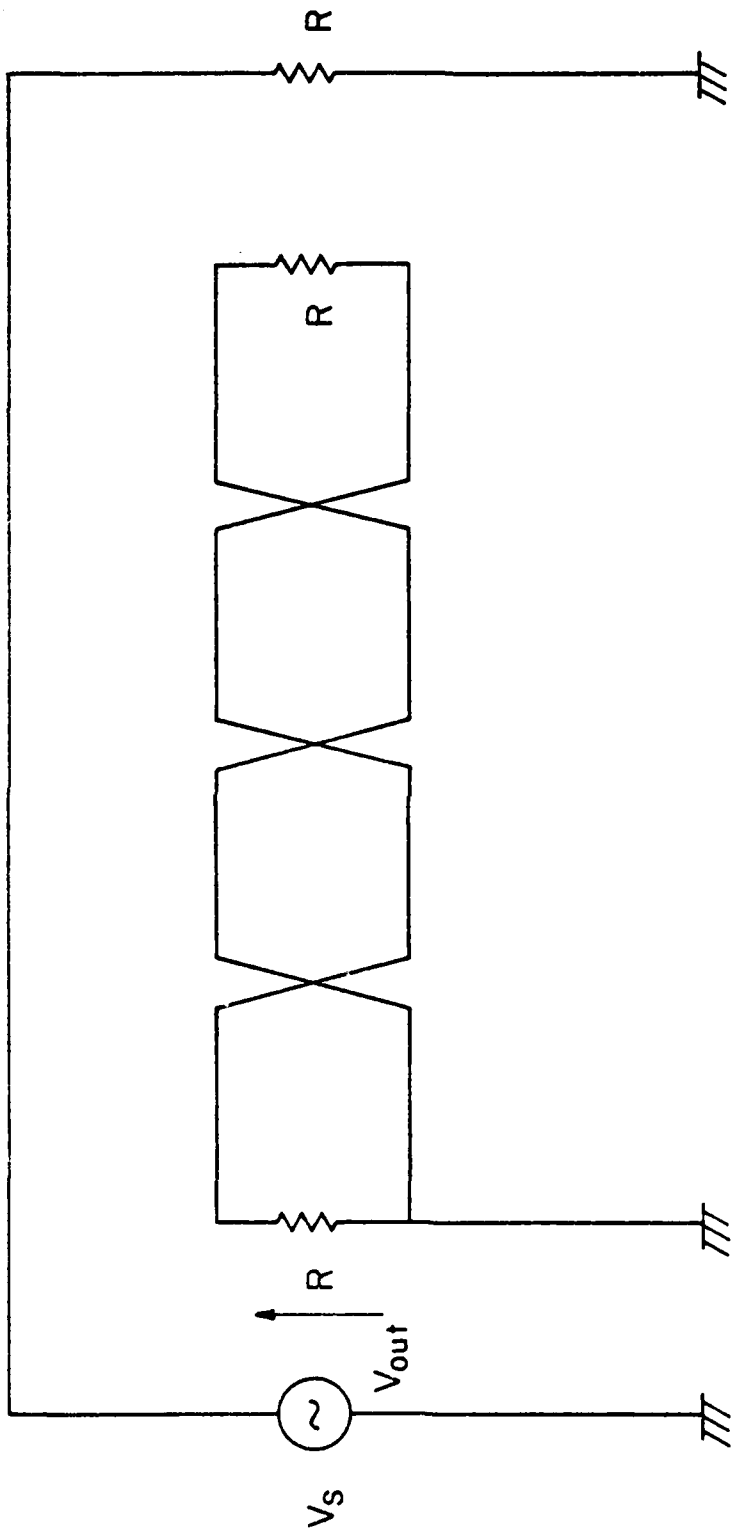

Fig. 1-5

Since the loop model does not predict the drastic 35 dB change in the VTR for an even or odd number of loops, which was observed experimentally in this effort, an improved model is considered, which is the second objective of this work.

In this model, parallel wire lines are used to approximate the TWP. Small incremental parallel segments, when rotated in space appear as a TWP (Fig. 1-6). The model illustrated in Fig. 1-6 incorporates rotation of the line whereas the loop model does not. Although this model provides a more realistic representation of the TWP than the loop model, the actual skewness of the wires of the TWP (which the current traverses) is not incorporated. The 'click model' (so named because of the abrupt incremental rotation of the segments) provides a moderate improvement in the prediction of the VTR over the loop model when the TWP has very low values of impedance terminations. It does not, however, predict the 35 dB change in the VTR when the number of twists in the line are changed by one half-twist.

The third and final phase of this work concerns the prediction of electromagnetic coupling to the TWP when it is terminated in the differential line driver and line receiver (Shown in Fig. 1-7). The majority of digital data is transmitted on modern electronic systems via this configuration. The diffferential line driver is readily used to transmit digital data because it provides both AND and NAND output. Whatever change in voltage might occur at one output results in an equal and opposite change at the

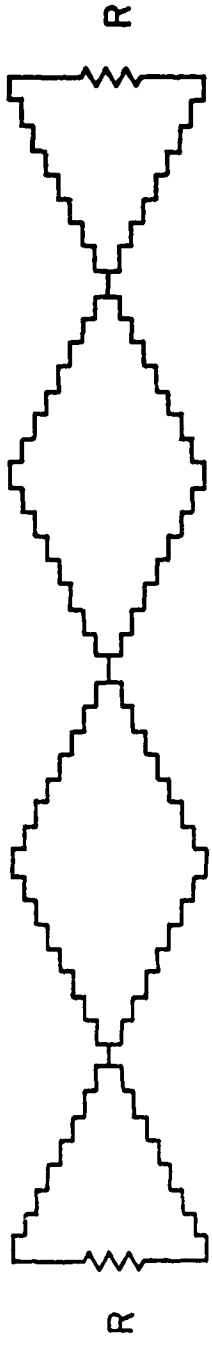

Fig. 1-6

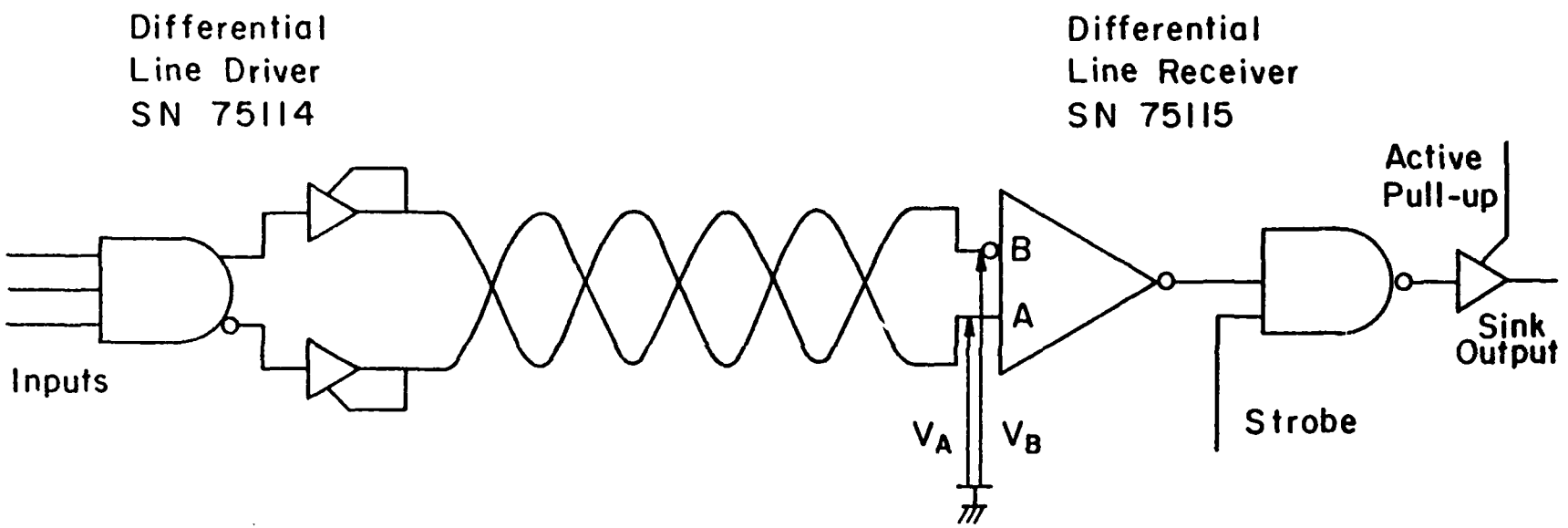
Differential
Line Driver
SN 75114
Differential
Line Receiver
SN 75115
Active
Pull-up
B
A
Inputs
Sink
Output
V_A
V_B
Strobe

Fig. 1-7

other output. The difference in the AND and NAND outputs provides a differential mode voltage which is transmitted via the TWP to the differential line receiver. The differential line receiver is designed to sense small differential signals in the presence of large common mode noise. This electrical noise is usually present due to crosstalk from another signal path. The differential mode noise is very small and sensitive to measurement since a signal induced in one wire of the TWP is normally induced in the other wire because of their close proximity. Hence, the common mode signal is measured. Predictions of crosstalk for the common mode voltage are computed for the TWP configured in this manner (Fig. 1-7) and a comparison is made with experimental results.

II. SENSITIVITY ANALYSIS

The lines were arranged as shown in Fig. 2-1 to demonstrate the sensitivity of the VTR. This configuration of the wires has been sometimes referred to as unbalanced, since one end of the TWP is not connected to the ground plane. Stranded 22 gauge wires (with polyvinyl chloride insulation) were used because stranded wire bends more easily than solid wire and should provide a uniform length of the twists in the TWP. Although care was taken when twisting the wires, this uniform length of the twists was probably not achieved. The line length was 4.705 meters (15' 5 1/4") and the wires were supported above a 1/8" aluminum ground plane by 4"x3"x3' styrofoam blocks (Fig. 2-2). Slots were cut in these blocks to provide a 2 cm height of the wires above the ground plane and to insure 2 cm separation between the generating line and the TWP. The generating line was the single wire with ground return, which is excited by a sinusoidal generator.

End terminations for the TWP and generating line were constructed of 1/8" aluminum so that BNC bulkhead connectors could be attached. At the generator end of the line the wires of the TWP were positioned horizontal with respect to the ground plane (Fig. 2-3). They were then twisted counter-clockwise as progression is made toward the load end. The load end termination consisted of an aluminum frame with an end plate made of plexiglass (Fig. 2-4).

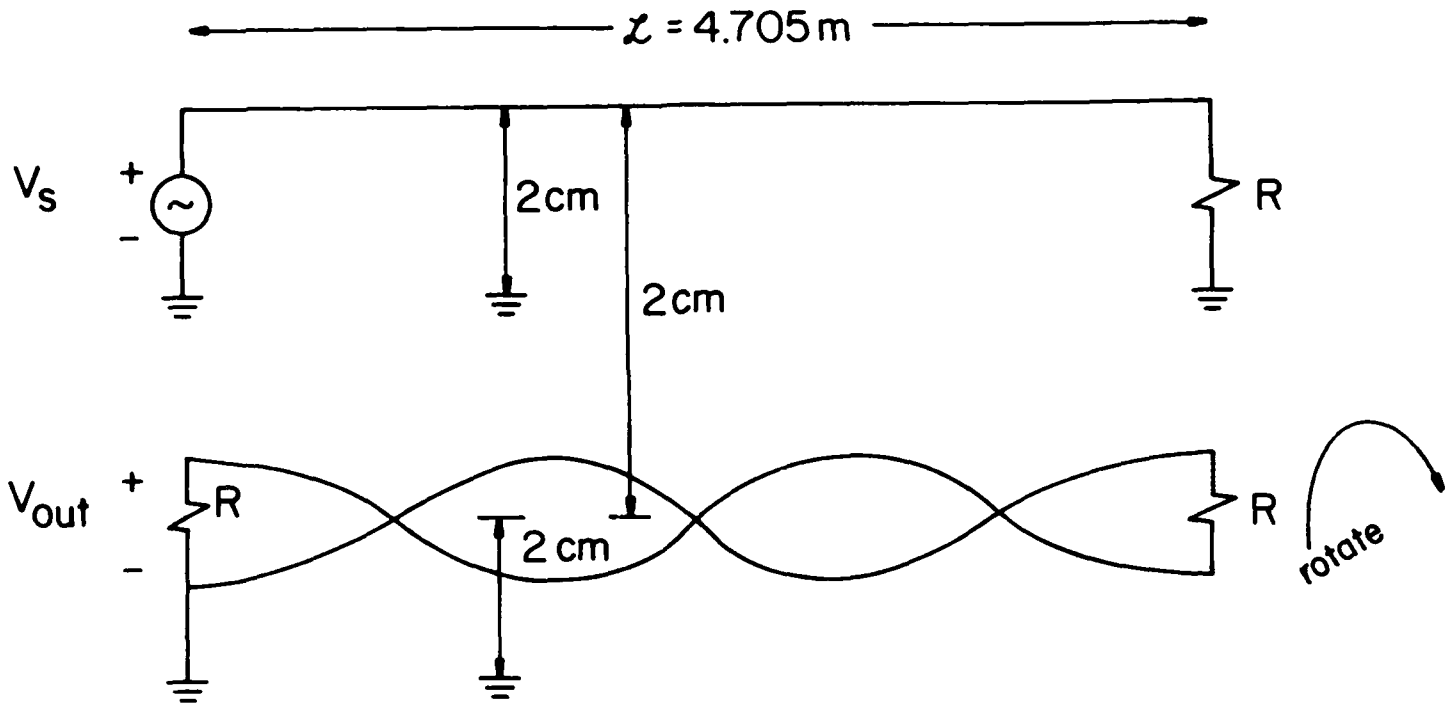

Fig. 2-1

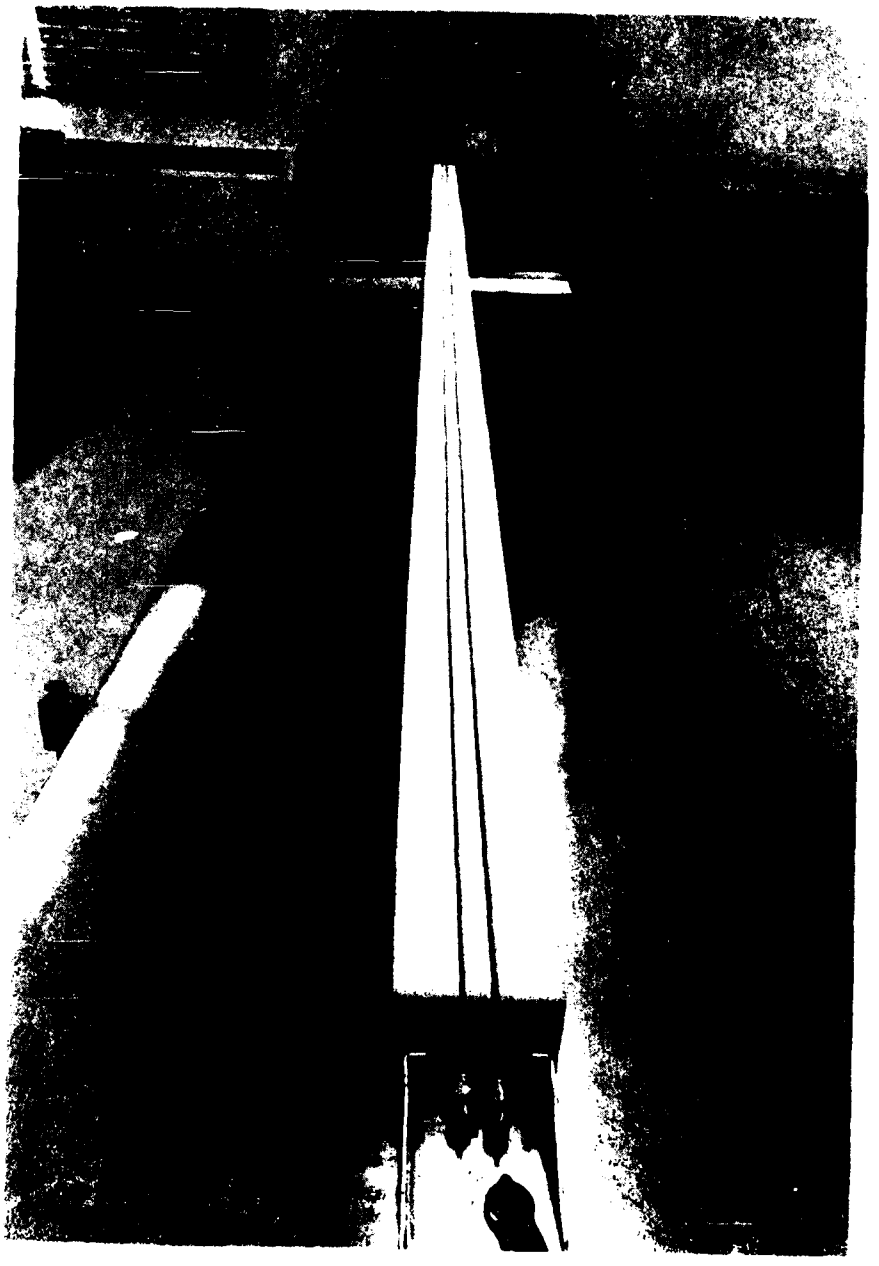

Fig. 2-2

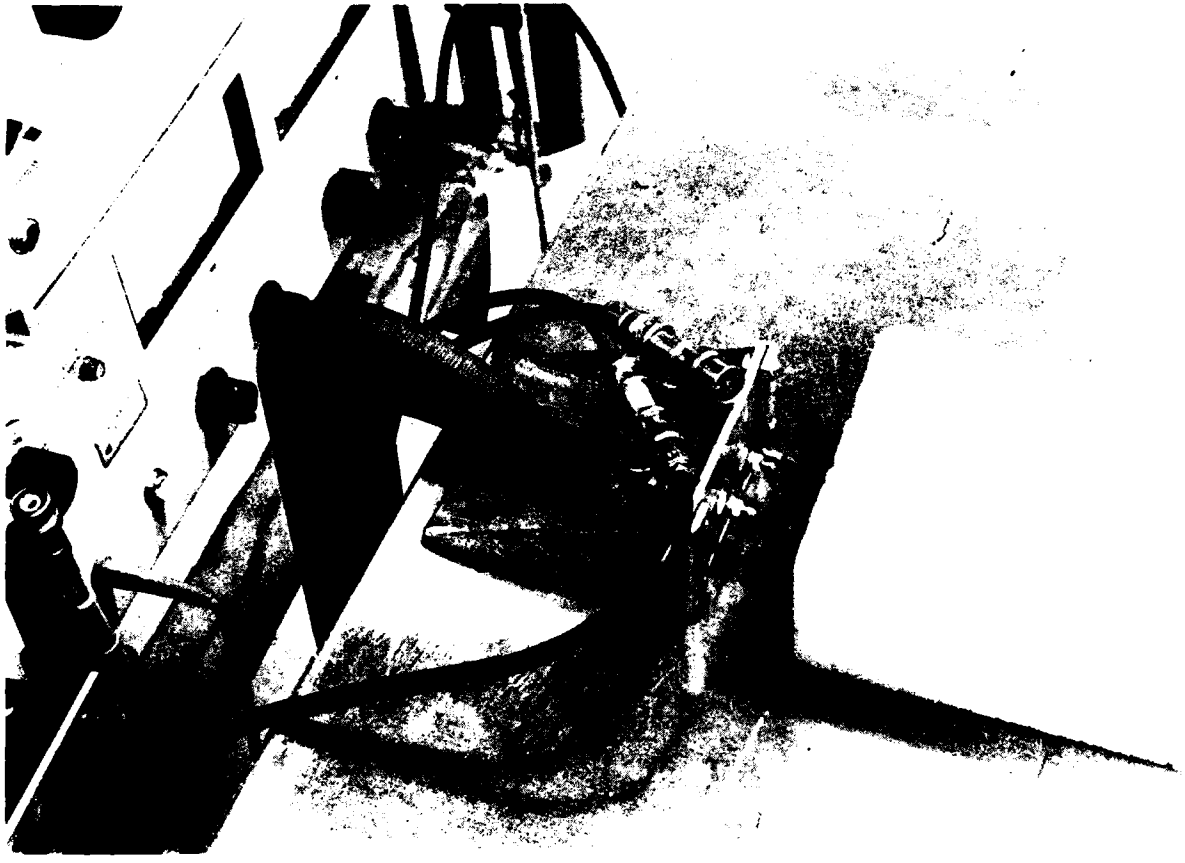

Fig. 2-3

Fig. 2-4

Plexiglass was used to keep the wires of the TWP from being grounded. An aluminum strip was used to ground the outer conductor of the BNC bulkhead connector which was connected to the generator line. This provided a return path through the 1/8" aluminum ground plane for the generator signal. Provision was made so the BNC bulkhead connector attached to the TWP at the load end could be rotated 360 degrees. Thus, the number of twists in the TWP could be changed without having to unsolder the wires. Loads were attached through BNC plugs (Fig. 2-5). The outer conductor of these plugs provided shielding for the load resistors from stray electromagnetic fields. Resistive loads, R, of 1 ohm, 3 ohms, 50 ohms, and 1k ohms were used.

The VTR (i.e., V_{OUT}/V_s) for each load was measured over the frequency range of 100 Hz to 1 MHz in steps of 1, 1.5, 2, 2.5, 3, 4, 5, 6, 7, 8, 9 in each decade. An HP RMS 3400A voltmeter was used to continuously moniter the input voltage to the generator line. A Tektronix 501 frequency meter was connected in parallel with this voltmeter to assure the accurate frequency. The output signal V_{OUT} was a very low voltage and very sensitive to electrical noise at low frequencies. The HP 3580A Spectrum Analyzer (SA) was used to measure V_{OUT} for frequencies below 50 kHz. The narrow bandwidth (3 Hz) of the SA provided essential noise rejection so that the low voltage levels of V_{OUT} could be measured. Above 50 kHz an Electrometrics EMC-25 Interference Analyzer was used to measure V_{OUT}. The narrow

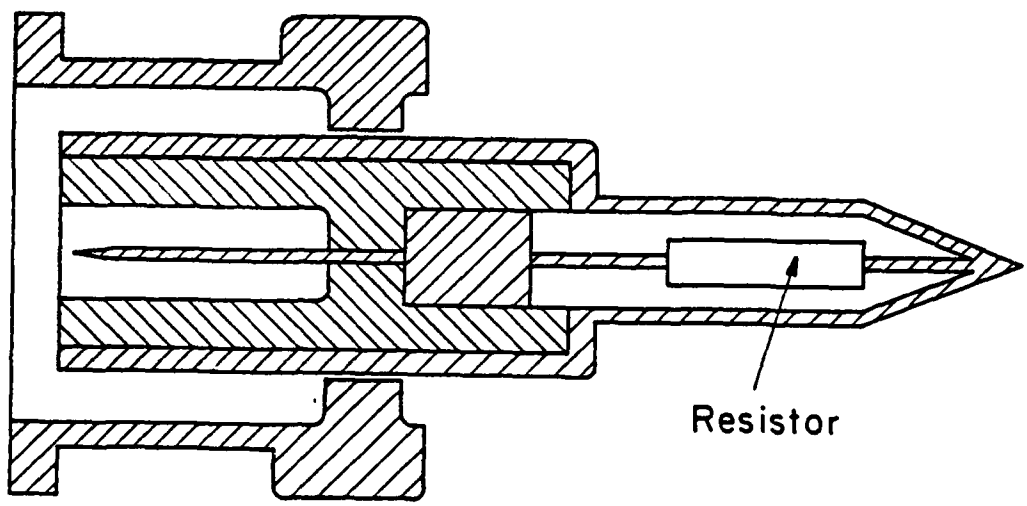

BNC Plug

Fig. 2-5

bandwidth setting of the EMC-25 was 500 Hz. This bandwidth was sufficient for signal detection since the electrical noise level was much lower than the output signal at these frequencies. Both the HP 3580A and the EMC-25 were battery powered to reduce incoming noise from the power bus. Electrical noise from the power bus still entered the system through the connections of the generator and the RMS voltmeter.

Once the lines were properly arranged, the 1 ohm loads were attached to the end terminations. The frequency was set to 15 kHz and the EMC-25 was attached to monitor the output voltage V_{OUT}. The EMC-25 has needle deflection with a dynamic range of 60 dB. As the BNC bulkhead connector of the TWP was rotated, a significant change in the needle reading was observed. The needle deflection was proportional to the angle of rotation of the BNC connector. The minimum reading occured when the position of the two wires attached to the BNC connector was approximately 65 degrees from horizontal (Fig. 2-6). The maximum deflection occured when the BNC connector was further rotated approximately 180 degrees. The difference in these two readings was around 35 dB.

With the frequency still set at 15 kHz the BNC connector was rotated until a low voltage reading was obtained on the EMC-25. The twists were counted and there appeared to be 94 1/5 twists in the TWP. The twists were, however, of slightly nonuniform length. Measurement of the

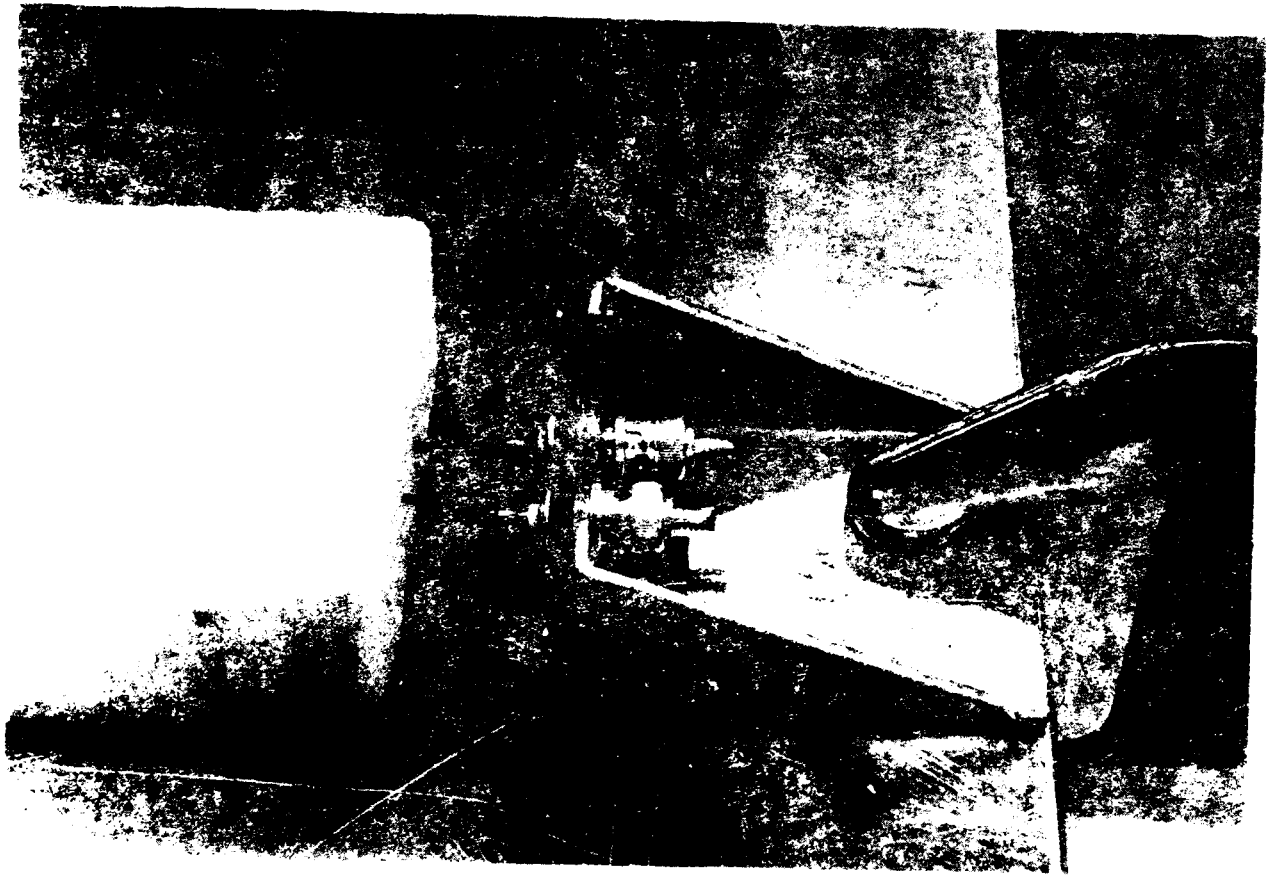

Fig. 2-6

frequency response was then made for 1 ohm loads as well as for 3 ohm, 50 ohm, and 1k ohm loads without disturbing the line configuration. Extreme care was taken, while changing load resistors, not to move the TWP.

After these measurements were taken, the frequency was once again returned to 15 kHz and the 1 ohm load terminations reattached. The BNC connector was then rotated approximately 180 degrees until a high voltage reading was obtained on the EMC-25. The 'high' measurements of the frequency response were then made for the different values of load terminations. The results of this experiment are shown in Figs. 2-7 through 2-10.

For the 1 ohm resistive loads a drastic sensitivity was observed for the VTR. Around 10 kHz a 35 dB change in the VTR was noticed between the high and low voltage levels. When changing the voltage levels, a slight rotation of the BNC connector produced a substantial difference in the VTR. The maximum change occured when the receptor was rotated about 180 degrees from the original position. For the 3 ohm loads a change of approximately 23 dB in the VTR was observed between the high and low voltage levels. The VTR for the 50 ohm and 1k ohm loads was relatively insensitive to the rotation of the BNC connector, and therefore, insensitive to the number of twists in the TWP.

The sensitivity of the VTR (to the number of twists in the line) for low impedance loads and the insensitivity of the VTR for high impedance loads can be explained using the

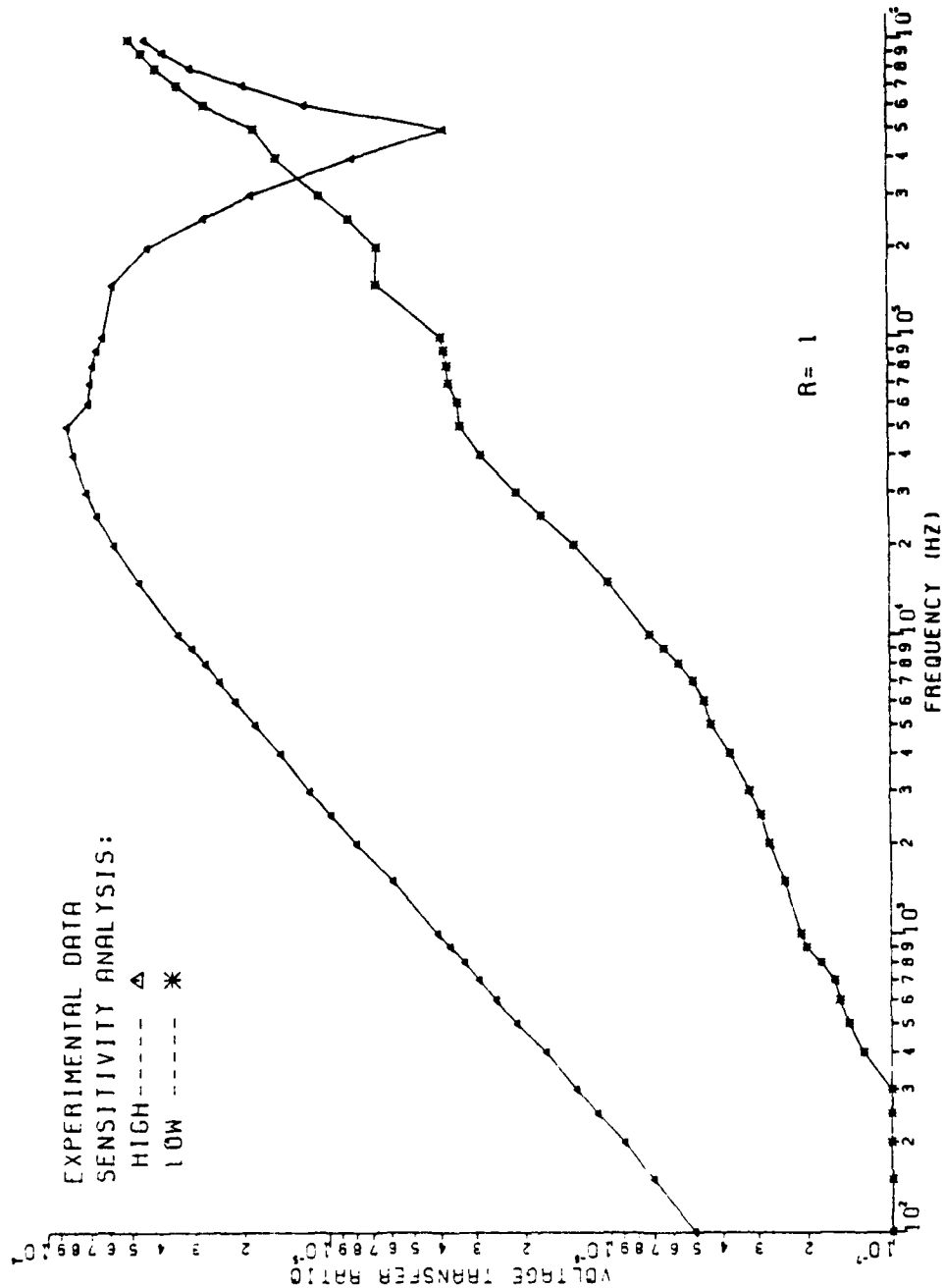
EXPERIMENTAL DATA
SENSITIVITY ANALYSIS:
HIGH----- Δ
LOW ----- *
R= 1
VOLTAGE TRANSFER RATIO
FREQUENCY (HZ)

Fig. 2-7

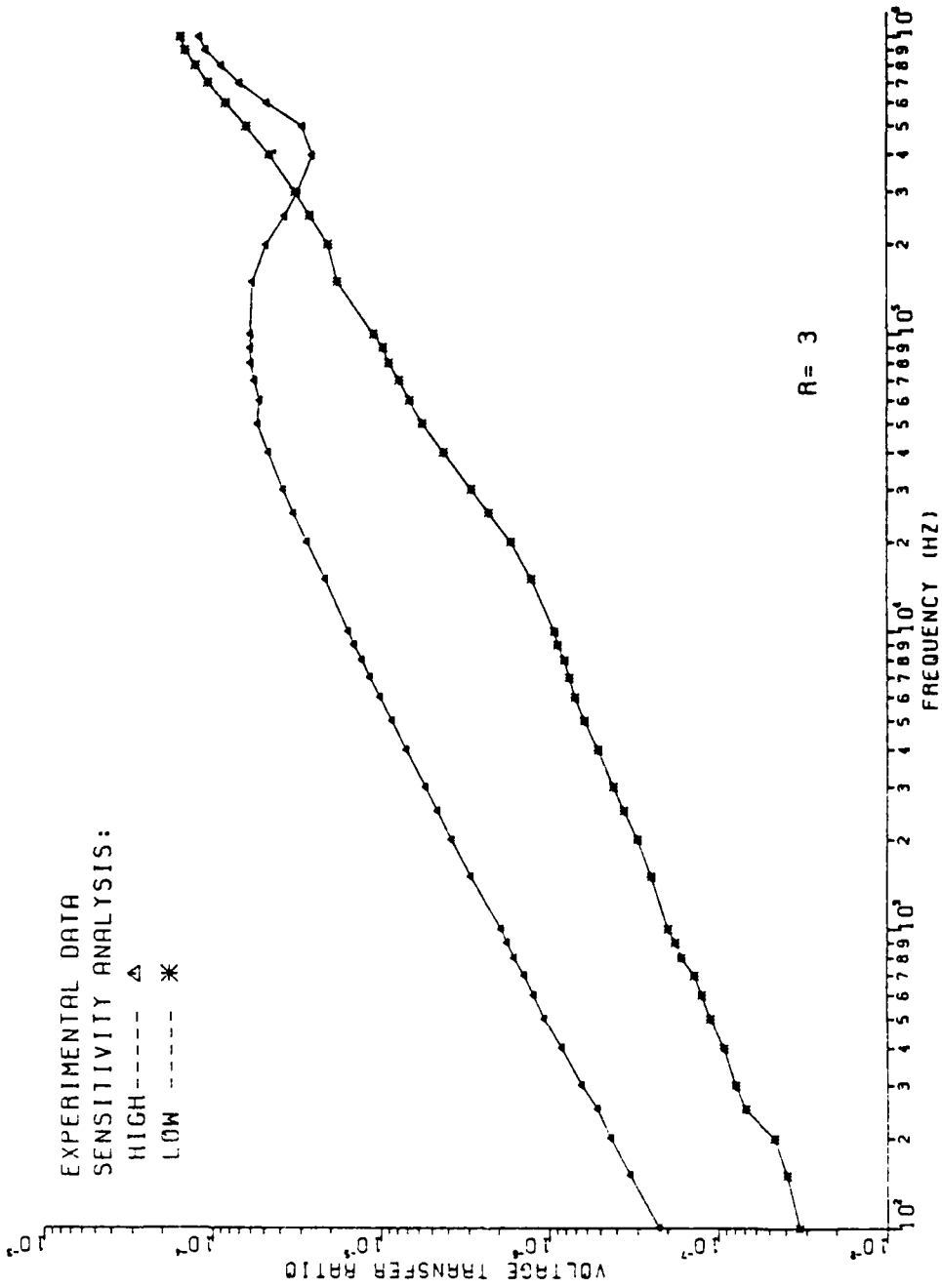
EXPERIMENTAL DATA
SENSITIVITY ANALYSIS:
HIGH----- Δ
LOW ----- ✳
R= 3
VOLTAGE TRANSFER RATIO
FREQUENCY (HZ)

Fig. 2-8

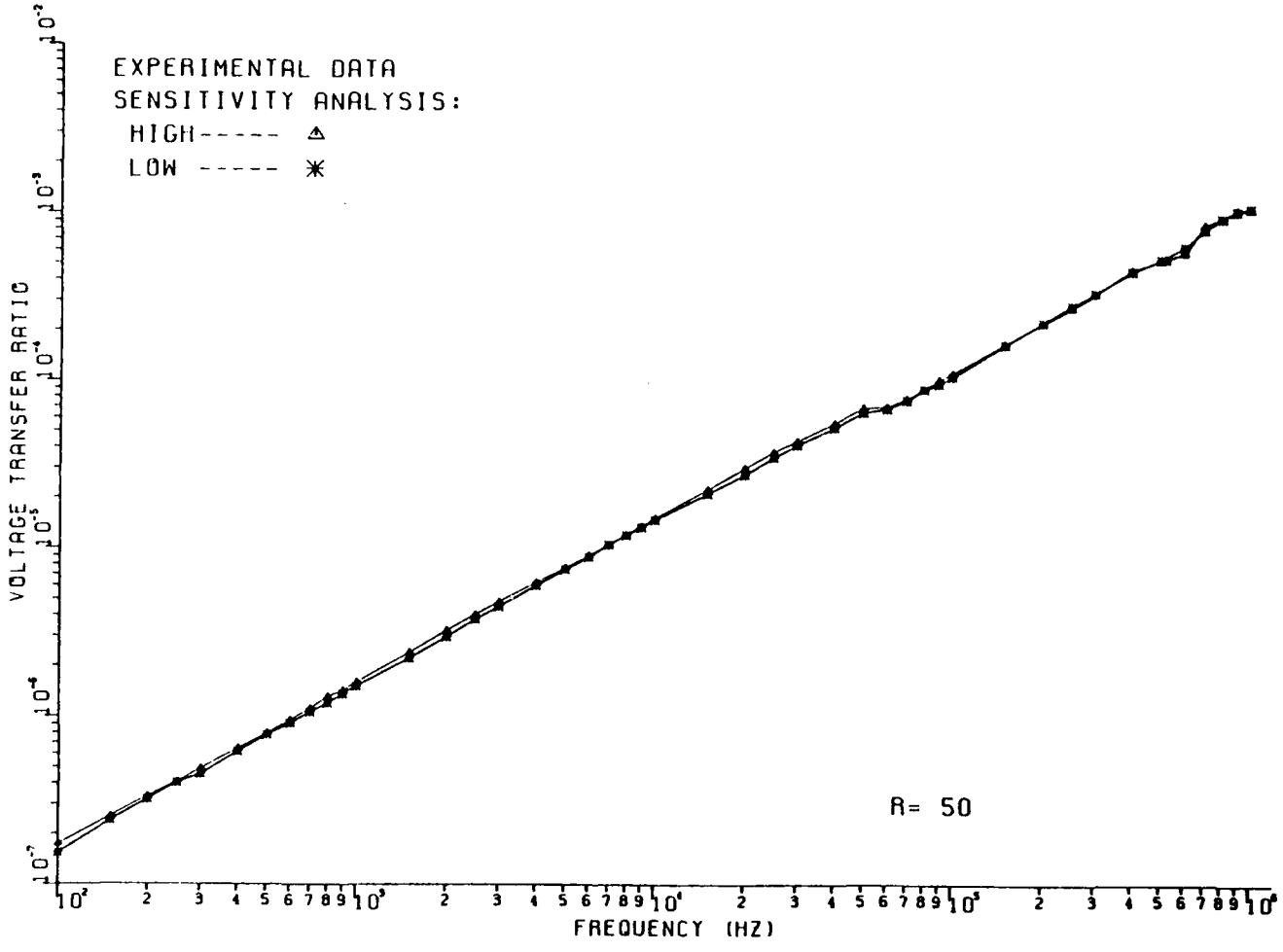
EXPERIMENTAL DATA
SENSITIVITY ANALYSIS:
HIGH----- Δ
LOW ----- ✳
VOLTAGE TRANSFER RATIO
FREQUENCY (HZ)
R= 50

Fig. 2-9

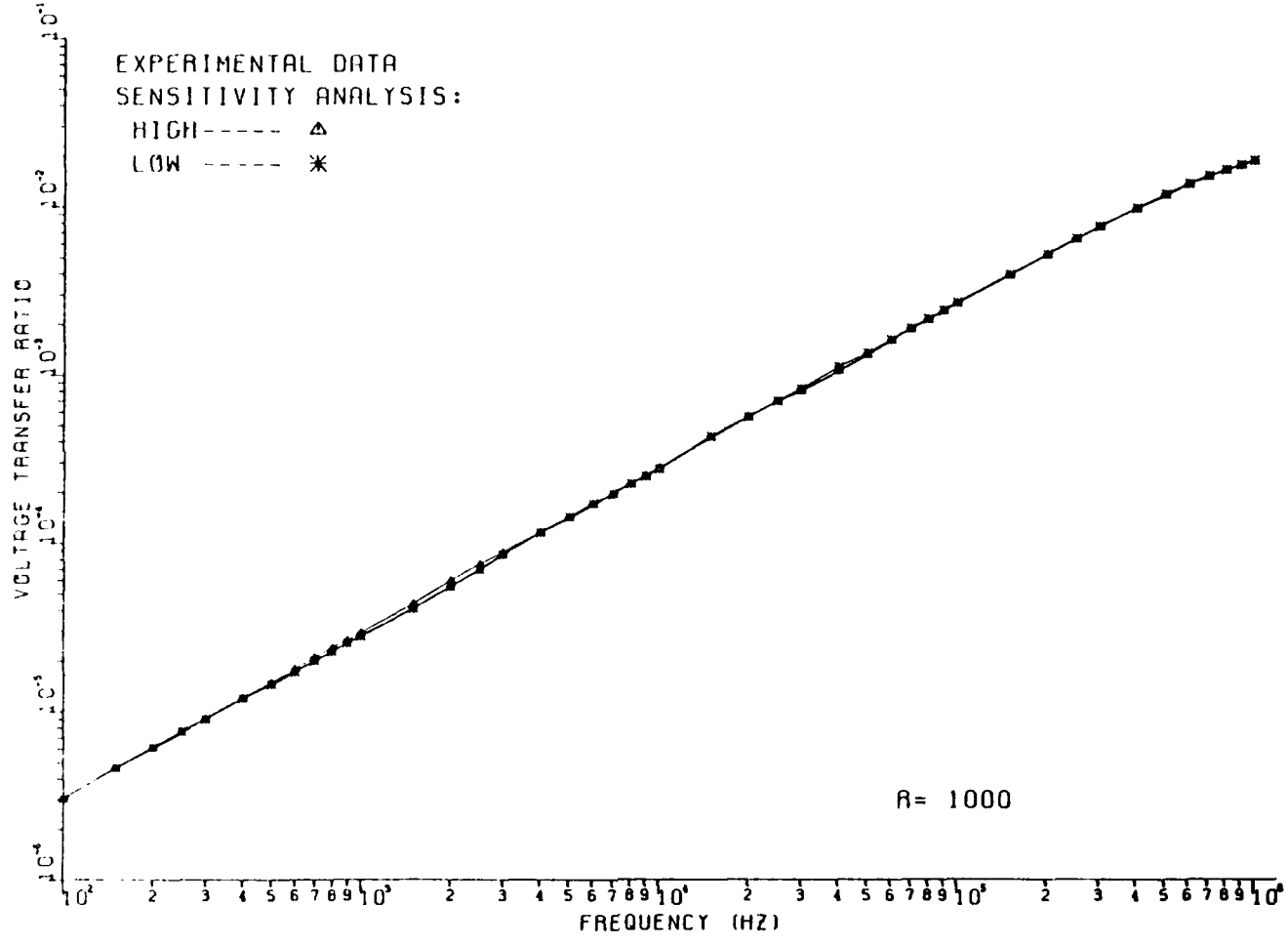
EXPERIMENTAL DATA
SENSITIVITY ANALYSIS:
HIGH----- Δ
LOW ----- ✳
VOLTAGE TRANSFER RATIO
FREQUENCY (HZ)
R= 1000

Fig. 2-10

concepts of inductive and capacitive coupling. It has been shown that the overall coupling to the SWP and the TWP was the sum on the inductive and capacitive coupling [2].

$$V_{OUT} = V_{OUT}^{CAP} + V_{OUT}^{IND}$$

The coupling due to the mutual capacitance of the lines is proportional to the position of the lines. Since the lines in the TWP are in close proximity with each other they experience approximately the same level of capacitive coupling. Thus, twisting the wires does not greatly effect the level of coupling due to mutual capacitance. However, twisting the lines does reduce inductive coupling to the wire pair because the current induced in either line of the TWP appears to cancel. If one type of coupling dominates, then the other has little effect in the overall coupling.

For the SWP with low impedance terminations (i.e., 1 ohm, 3 ohms) inductive coupling dominates capacitive coupling (Fig. 2-11a). As the SWP is twisted and as the number of twists in this TWP is increased, inductive coupling is reduced, thereby reducing the overall coupling to the TWP (Fig. 2-11a). With high impedance terminations of 50 ohms, capacitive coupling is of the same order of magnitude as inductive coupling for the SWP. With 1k ohm loads, capacitive coupling dominates inductive coupling whether the line is twisted or not (Fig. 2-11b). If the SWP is now twisted, inductive coupling is reduced, but this has no substantial effect in reducing the overall coupling to the TWP (Fig.

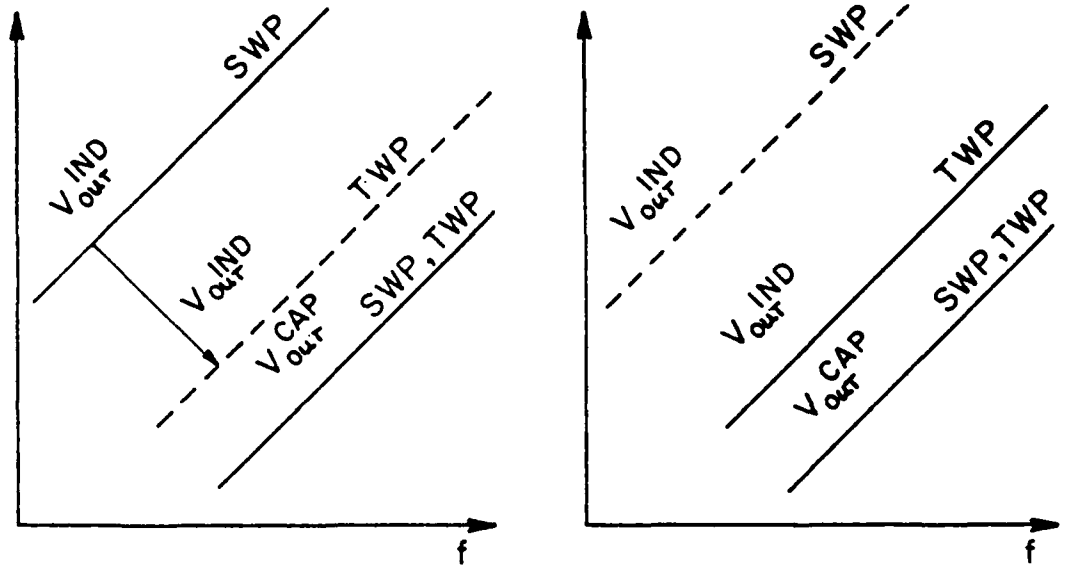

(a)

Low Impedance

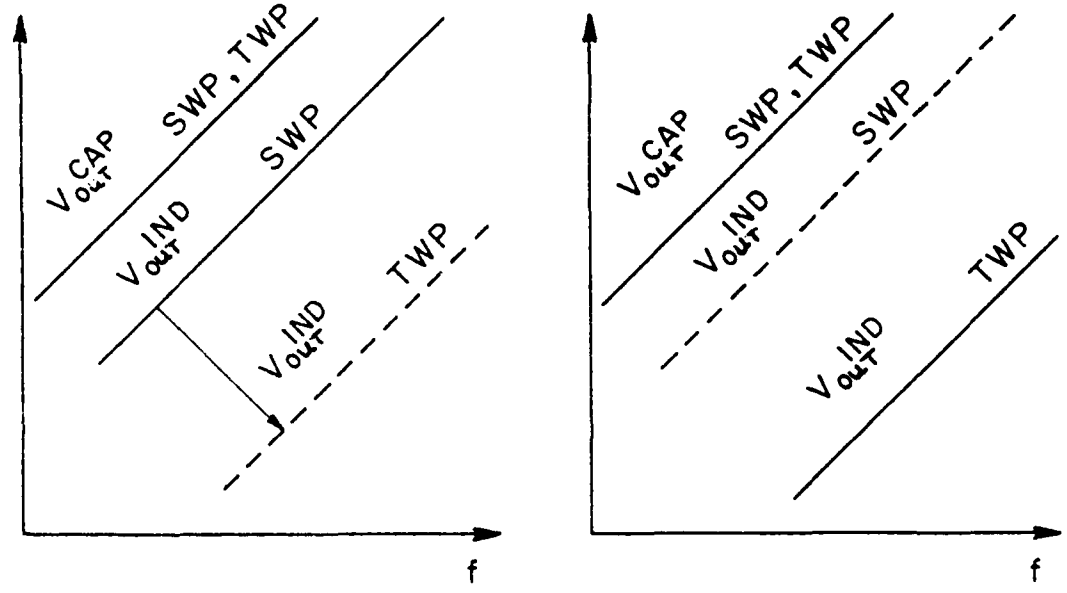

(b)

High Impedance

Fig. 2-11

2-11b). A further reduction of inductive coupling (due to increasing the number of twists in the TWP) would not effect the overall coupling because capacitive coupling is dominant. The TWP, therefore, seems insensitive to the number of twists when the load terminations are 'high' impedance.

This analysis has shown that the VTR is very sensitive to the number of twists in the TWP for small impedance loads but quite insensitive for high impedance loads. Prediction of the VTR for small impedance loads of the TWP would not be practical (from an application point of view) since a slight rotation of the wires as they are being installed could drastically effect the overall coupling.

III. AN IMPROVED PREDICTION MODEL FOR THE TWP

In previous papers [1], [2], [3], an attempt is made to predict the electromagnetic coupling from adjacent wires to the TWP. However, since the TWP is a bifilar helix, the skewness of the helix complicates an exact solution or model. In this chapter a model (the 'click' model) is presented which uses short wire segments, which are parallel to each other and the ground plane, to approximate the TWP (Fig. 3-1). As can be seen from Fig. 3-1 the skewness of the wires of the TWP is never achieved with the short parallel wire segments. However, the rotation of the wires is incorporated. The abrupt loop model did not incorporate this smooth rotation of the wires. Although the skewness of the helix is not precisely modeled, the model should give a more accurate prediction than the abrupt loop model, if these wire segments are taken short enough. The abrupt loop model, presented in [1], gave accurate predictions (against experimental results) for 'high' impedance loads. The model to be presented should improve the accuracy in the prediction of coupling to the TWP when it is terminated in 'low' impedance loads. For 'high impedance loads', both models should be adequate.

The 'click' model uses abruptly rotating parallel wire segments to approximate the TWP (Fig. 3-1). Each parallel segment used in modeling the twist has a different orientation above the ground plane, but it is a short

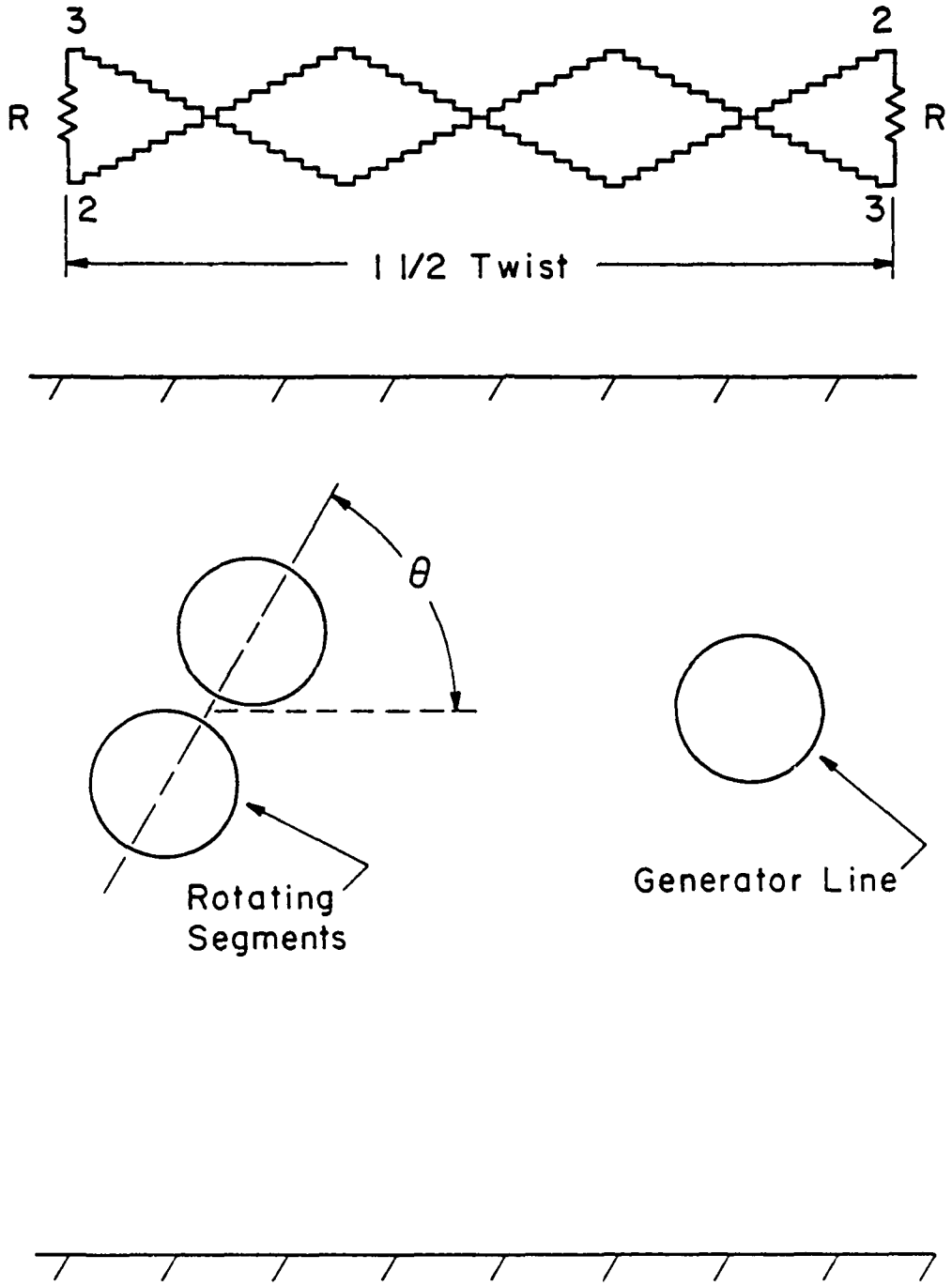

Fig. 3-1

section of a parallel wire pair. The TEM mode approximation is therefore a valid representation for the waves on each segment used in modeling the TWP. If we view the 'click' model as a cascade of parallel wire lines, then it is sufficient to cascade the chain parameter matrices for each parallel wire pair segment. Thus, we need only investigate the characterization of a set of parallel wires above ground. Two of the wires constitute the wires of a segment of the TWP and the third wire constitutes the adjacent generator wire segment.

The transmission line equations for such a segment S_i (Fig. 3-2) are given in [1]:

$$\frac{dV_1(x)}{dx} = -j\omega l_{11}I_1(x)-j\omega l_{12}I_2(x)-j\omega l_{13}I_3(x)$$

$$\frac{dV_2(x)}{dx} = -j\omega l_{12}I_1(x)-j\omega l_{22}I_2(x)-j\omega l_{23}I_3(x)$$

$$\frac{dV_3(x)}{dx} = -j\omega l_{13}I_1(x)-j\omega l_{23}I_2(x)-j\omega l_{33}I_3(x)$$

$$\frac{dI_1(x)}{dx} = -j\omega(c_{11}+c_{12}+c_{13})V_1(x)+j\omega c_{12}V_2(x)+j\omega c_{13}V_3(x)$$

$$\frac{dI_2(x)}{dx} = j\omega c_{21}V_1(x)-j\omega(c_{22}+c_{12}+c_{23})V_2(x)+j\omega c_{23}V_3(x)$$

$$\frac{dI_3(x)}{dx} = j\omega c_{13}V_1(x)+j\omega c_{23}V_2(x)-j\omega(c_{33}+c_{13}+c_{23})V_3(x)$$

The electrically short section Δx of the line shown in

figure 3-2 is characterized by the lumped, per-unit-length line parameters of self inductance l_{11}, l_{22}, l_{33}, mutual inductance l_{12}, l_{13}, l_{23}, self capacitance c_{11}, c_{22}, c_{33}, and mutual capacitance, c_{12}, c_{13}, c_{23}. The voltages and current $V_1(x)$, $I_1(x)$, are those of the generator line segment. The voltages and currents of the TWP segment are represented by $V_2(x)$, $I_2(x)$, $V_3(x)$, $I_3(x)$.

By relating the voltages and currents at one end of the line segment $V_1(x_R)$, $V_2(x_R)$, $V_3(x_R)$, $I_1(x_R)$, $I_2(x_R)$, $I_3(x_R)$, to the voltages and currents at the other end of the line segment $V_1(x_L)$, $V_2(x_L)$, $V_3(x_L)$, $I_1(x_L)$, $I_2(x_L)$, $I_3(x_L)$, a solution to the transmission line (TL) equations is provided by the matrix chain parameters [5],

$$\begin{bmatrix} \underline{V}(x_R) \\ \underline{I}(x_R) \end{bmatrix} = \underbrace{\begin{bmatrix} \underline{\Phi}_{11} & \underline{\Phi}_{12} \\ \underline{\Phi}_{21} & \underline{\Phi}_{22} \end{bmatrix}}_{\underline{\Phi}_i} \begin{bmatrix} \underline{V}(x_R) \\ \underline{I}(x_L) \end{bmatrix}$$

where,

$$\underline{V}(x_R) = \begin{bmatrix} V_1(x_R) \\ V_2(x_R) \\ V_3(x_R) \end{bmatrix} \qquad \underline{I}(x_R) = \begin{bmatrix} I_1(x_R) \\ I_2(x_R) \\ I_3(x_R) \end{bmatrix}$$

$$\underline{V}(x_L) = \begin{bmatrix} V_1(x_L) \\ V_2(x_L) \\ V_3(x_L) \end{bmatrix} \qquad \underline{I}(x_L) = \begin{bmatrix} I_1(x_L) \\ I_2(x_L) \\ I_3(x_L) \end{bmatrix}$$

are 3x1 column matrices.

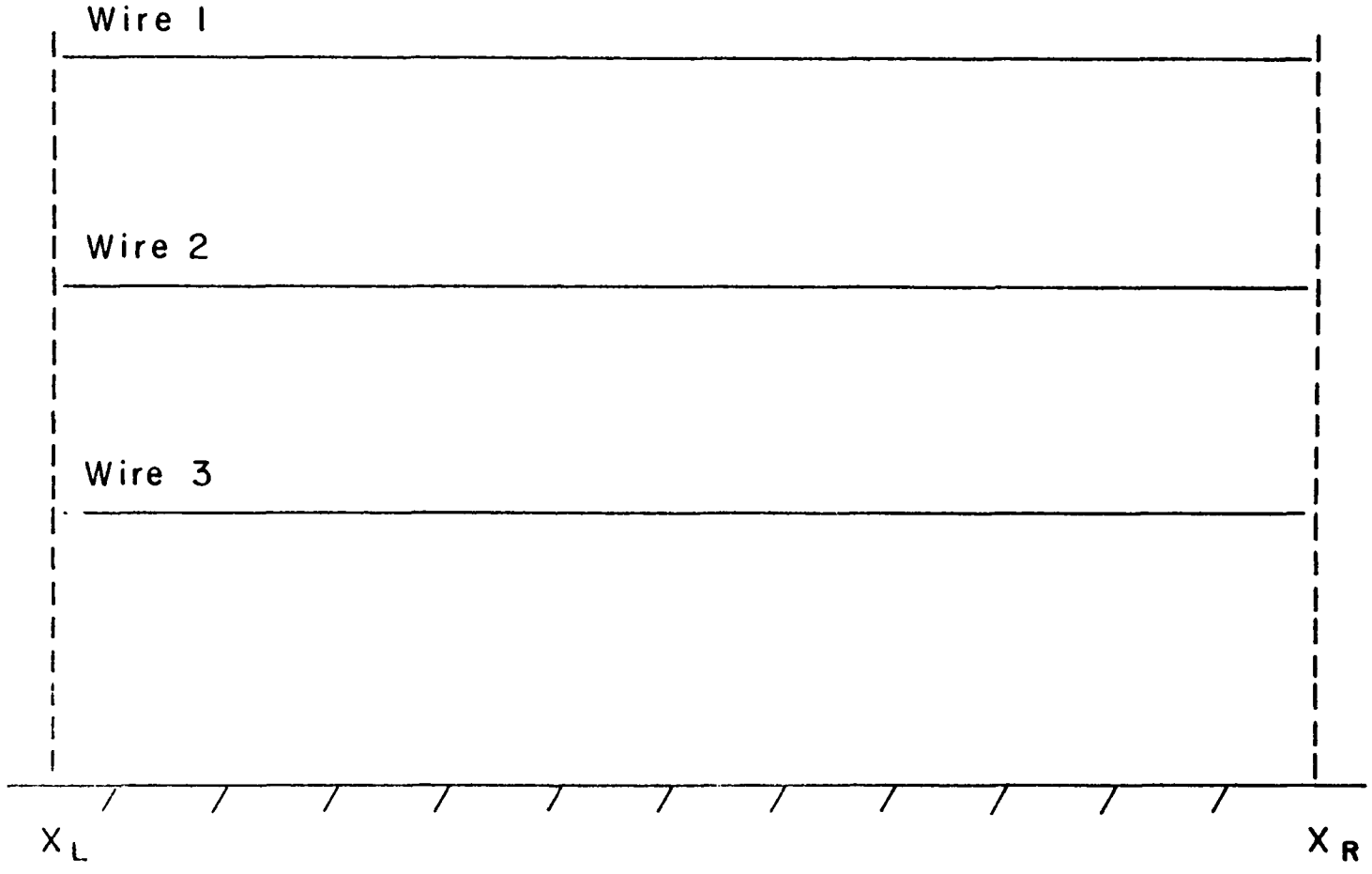

Fig. 3-2a

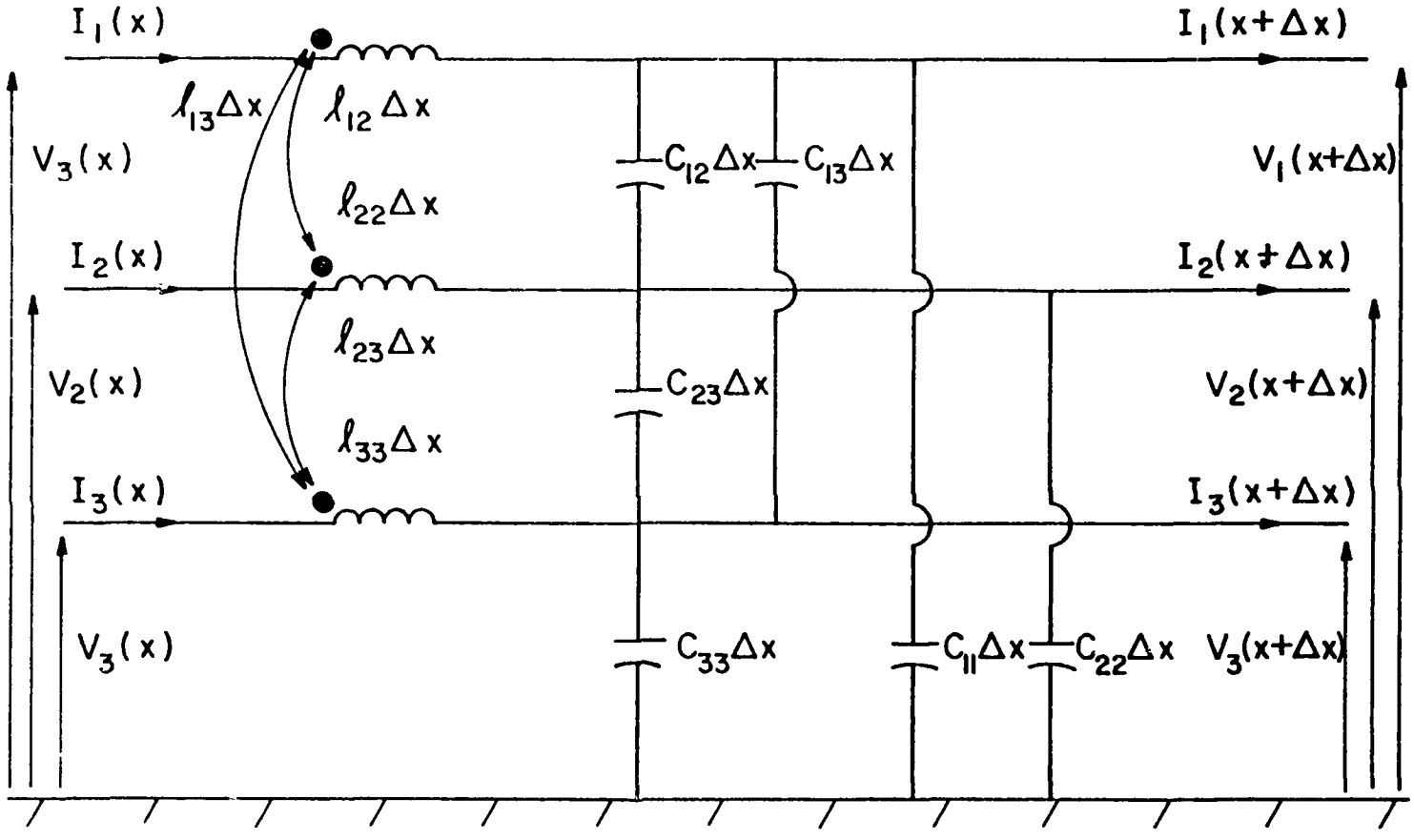
$I_1(x)$
$I_1(x+\Delta x)$
$\ell_{13}\Delta x$
$\ell_{12}\Delta x$
$V_3(x)$
$C_{12}\Delta x$
$C_{13}\Delta x$
$V_1(x+\Delta x)$
$\ell_{22}\Delta x$
$I_2(x)$
$I_2(x+\Delta x)$
$\ell_{23}\Delta x$
$V_2(x)$
$C_{23}\Delta x$
$V_2(x+\Delta x)$
$\ell_{33}\Delta x$
$I_3(x)$
$I_3(x+\Delta x)$
$V_3(x)$
$C_{33}\Delta x$
$C_{11}\Delta x$
$C_{22}\Delta x$
$V_3(x+\Delta x)$

Fig. 3-2b

The $\underline{\Phi}_{ij}$ elements of the $\underline{\Phi}_i$ matrix are 3x3 matrices given in [1].

$$\underline{\Phi}_{11}(\mathcal{L}) = \cos(\beta\mathcal{L})\underline{1}_3$$
$$\underline{\Phi}_{12}(\mathcal{L}) = -jv\sin(\beta\mathcal{L})\underline{L}_i$$
$$\underline{\Phi}_{21}(\mathcal{L}) = -jv\sin(\beta\mathcal{L})\underline{C}_i$$
$$\underline{\Phi}_{22}(\mathcal{L}) = \cos(\beta\mathcal{L})\underline{1}_3$$

The phase constant, β, is given by $\beta=\omega/v$, v is the velocity of propagation in the surrounding medium, $v=1/\sqrt{\mu\varepsilon}$, and ω is the radian frequency of excitation. The nxn identity matrix, denoted by $\underline{1}_n$ has ones on the main diagonal and zeros elsewhere, i.e., $[1_n]_{ii}= 1$ and $[1_n]_{ij}= 0$; $i,j=1,\cdots,n$ and $i\neq j$.

These equations are valid for each segment of line in the click model if the proper 3x3 per-unit-length inductance and capacitance matrices, $\underline{L}_i$ and $\underline{C}_i$, are used:

$$\underline{L}_i = \begin{bmatrix} l_{11} & l_{12} & l_{13} \\ l_{12} & l_{22} & l_{23} \\ l_{13} & l_{23} & l_{33} \end{bmatrix}$$

$$\underline{C}_i = \begin{bmatrix} (c_{11}+c_{12}+c_{13}) & -c_{12} & -c_{13} \\ -c_{12} & (c_{22}+c_{12}+c_{23}) & -c_{23} \\ -c_{13} & -c_{23} & (c_{33}+c_{13}+c_{23}) \end{bmatrix}$$

Since an abrupt rotation of the segments along the line is used, these per-unit-length parameters, l_{ij} and c_{ij}, are a

function of the angle of rotation, θ, for each segment.

Consider the three wires above a reference or ground plane shown in Fig. 3-3a. If the wire pair is rotated by θ degrees as in Fig. 3-3b, the per-unit-length parameters will obviously change. The per-unit-length inductance parameters of each parallel segment may be determined from transmission line theory using the geometry given in Fig. 3-3c. i.e.,

$$l_{11} = \frac{\mu}{2\pi} \ln \frac{h}{r_w}$$

$$l_{22} = \frac{\mu}{2\pi} \ln \frac{h + \Delta h \sin\theta}{r_w}$$

$$l_{33} = \frac{\mu}{2\pi} \ln \frac{h - \Delta h \sin\theta}{r_w}$$

$$l_{12} = \frac{\mu}{2\pi} \ln \frac{r_{12}}{r_{12}^*}$$

$$l_{13} = \frac{\mu}{2\pi} \ln \frac{r_{13}}{r_{13}^*}$$

$$l_{23} = \frac{\mu}{2\pi} \ln \frac{r_{12}^* r_{13}}{r_{13}^* r_{12}}$$

where,

$$r_{12} = \sqrt{(D - \Delta h\cos\theta)^2 + (\Delta h \sin\theta)^2}$$

$$r_{13} = \sqrt{(D + \Delta h\cos\theta)^2 + (\Delta h \sin\theta)^2}$$

$$r_{12}^* = \sqrt{(D - \Delta h\cos\theta)^2 + (2h + \Delta h \sin\theta)^2}$$

$$r_{13}^* = \sqrt{(D + \Delta h\cos\theta)^2 + (2h - \Delta h \sin\theta)^2}$$

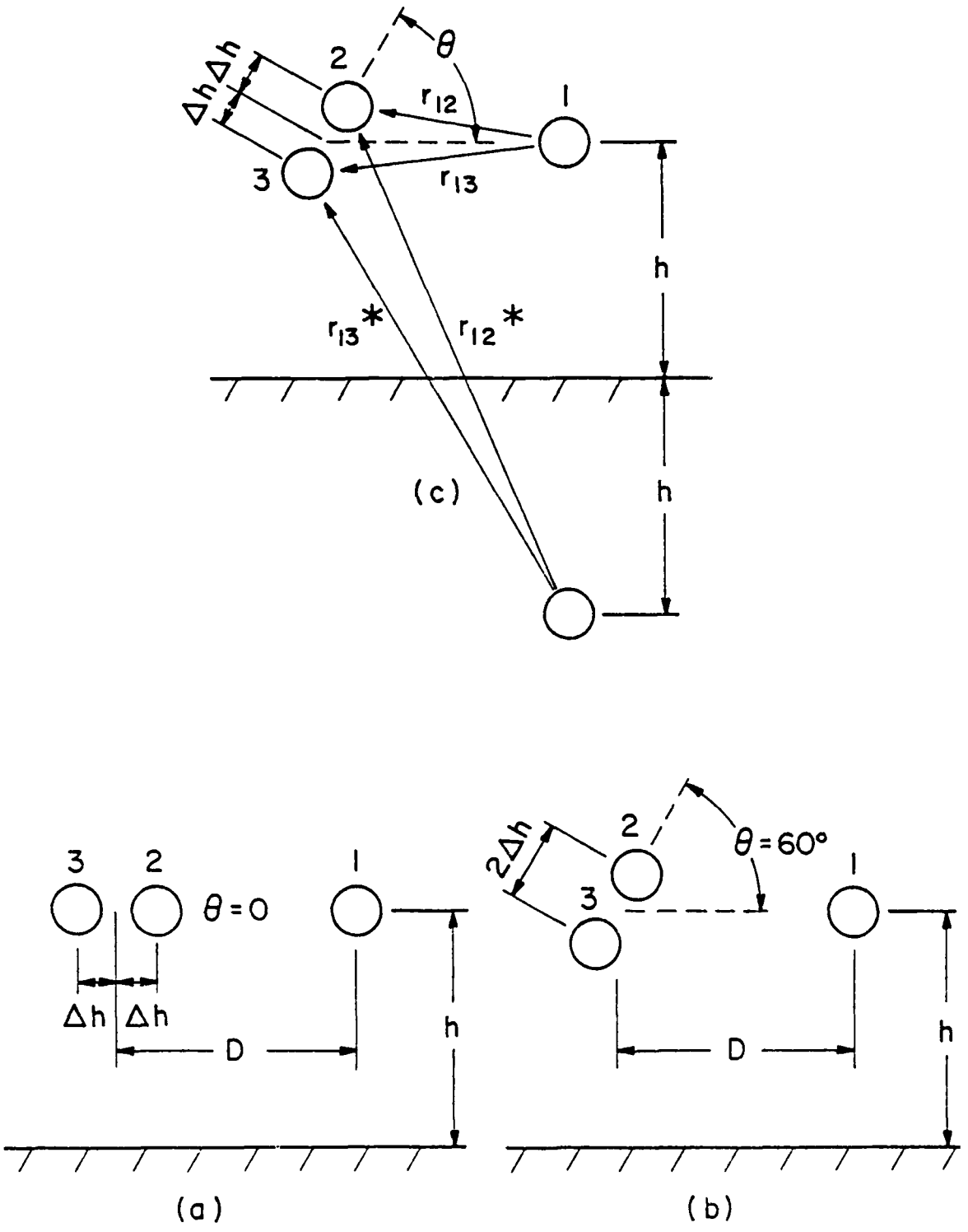

Fig. 3-3

h is the wire height above the ground plane, D is the separation between the generator wire and the TWP, r_w is the wire radius, Δh is the distance from the center of the TWP to the center of the wire in the wire pair, and θ is the angle of rotation of the wire segment with respect to the horizontal ground plane.

Since we assume a homogeneous surrounding medium, the permittivity and permeability are those of free space. Thus, the per-unit-length capacitance parameters can be derived from the per-unit-length inductance parameters [4].

$$\underline{C}_i = \mu\varepsilon \underline{L}_i^{-1} = 1/v^2 \underline{L}_i^{-1}$$

The click model of the TWP is constructed by connecting these abruptly rotating incremental segments. The only difference in any one section from another is in their per-unit-length parameters. This is a result of their different wire positions above the ground plane (Fig. 3-4). If the $\underline{\phi}_i$ matrix for each incremental segment is calculated, then expressions are obtained relating the voltage and current at one end of the segment to the voltage and current at the other end of the segment (Fig. 3-4).

$$\begin{bmatrix} \underline{V}(b) \\ \underline{I}(b) \end{bmatrix} = \underline{\phi}_i \begin{bmatrix} \underline{V}(a) \\ \underline{I}(a) \end{bmatrix} \qquad \begin{bmatrix} \underline{V}(d) \\ \underline{I}(d) \end{bmatrix} = \underline{\phi}_{i+1} \begin{bmatrix} \underline{V}(c) \\ \underline{I}(c) \end{bmatrix}$$

Since the line segments are connected over a zero interval of distance, $\Delta x \rightarrow 0$, the voltages and currents at

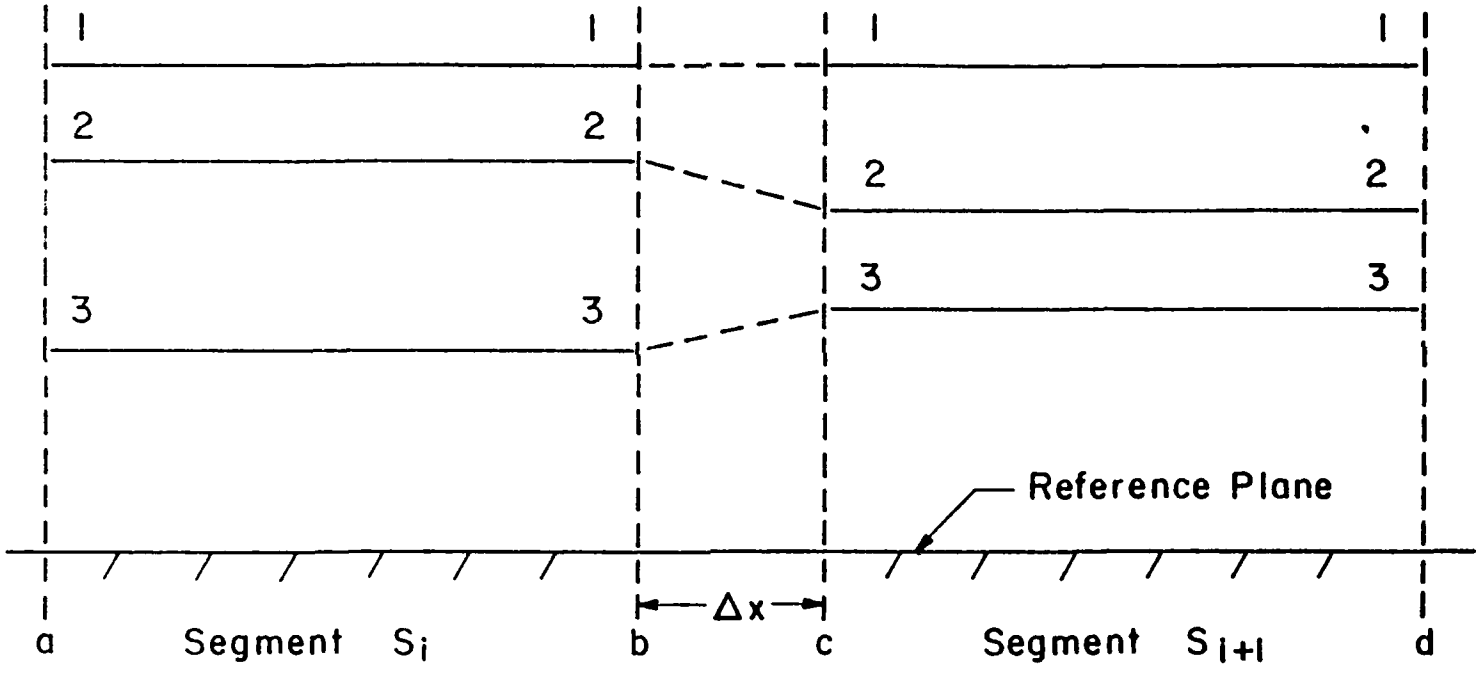
1
1
1
1
2
2
2
2
3
3
3
3
Reference Plane
Δx
a
Segment S_i
b
c
Segment S_{i+1}
d

Fig. 3-4a

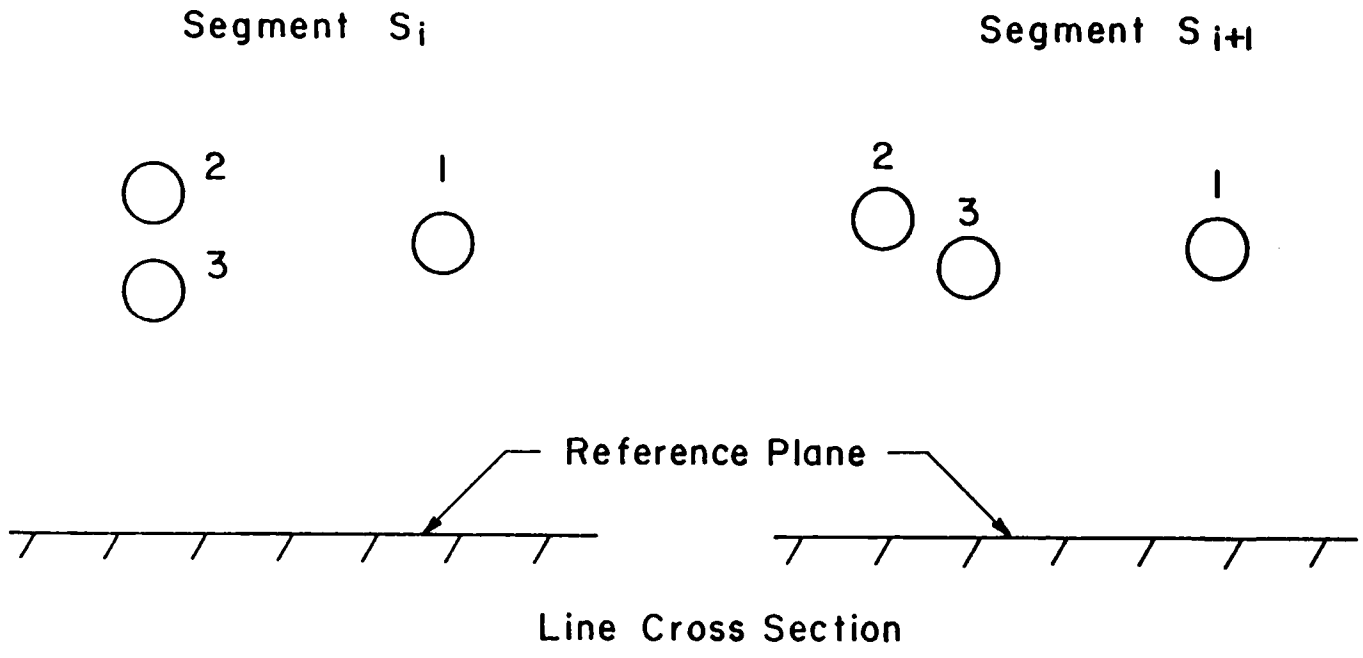
Segment S_i
Segment S_{i+1}
2
3
1
2
3
1
Reference Plane
Line Cross Section

Fig. 3-4b

position c are equal to the voltages and currents at position b.

$$\begin{bmatrix} \underline{V}(b) \\ \underline{I}(b) \end{bmatrix} = \begin{bmatrix} \underline{V}(c) \\ \underline{I}(c) \end{bmatrix}$$

Then,

$$\begin{bmatrix} \underline{V}(d) \\ \underline{I}(d) \end{bmatrix} = \underline{\phi}_{i+1} \begin{bmatrix} \underline{V}(b) \\ \underline{I}(b) \end{bmatrix}$$

$$\begin{bmatrix} \underline{V}(d) \\ \underline{I}(d) \end{bmatrix} = \underline{\phi}_{i+1}\, \underline{\phi}_i \begin{bmatrix} \underline{V}(a) \\ \underline{I}(a) \end{bmatrix}$$

If n segments are cascaded to represent the TWP, then the voltage and current at one end of the modeled TWP is related to the other end by the equation

$$\begin{bmatrix} \underline{V}(\ell) \\ \underline{I}(\ell) \end{bmatrix} = \underline{\Phi} \begin{bmatrix} \underline{V}(0) \\ \underline{I}(0) \end{bmatrix}$$

where,

$$\underline{\Phi} = \underline{\phi}_n\, \underline{\phi}_{n-1} \cdots \underline{\phi}_2\, \underline{\phi}_1 \quad .$$

To compute the $\underline{\Phi}$ matrix, which represents the transfer function of the voltages and currents from one end of the line to the other end, n-1 complex matrix multiplications would have to be performed. Since each of the $\underline{\phi}_i$ matrices are 6x6 complex matrices, this multiplication can become costly with a very few line segments per twist. To reduce

this cost, the transfer function matrix for each twist, $\underline{\Phi}_T$, could be found using the parallel $\underline{\phi}_i$ segments, and then the $\underline{\Phi}_T$ matrices cascaded to represent the TWP.

When viewing a TWP, each twist seems identical to any other twist except for its position along the line. If different twists in the TWP are modeled the same way, then the $\underline{\Phi}$ matrix transfer function can be computed with fewer multiplications. For example, if each twist consists of k segments, the chain parameter matrix of each twist, $\underline{\Phi}_T$, is

$$\underline{\Phi}_T = \underline{\phi}_k \, \underline{\phi}_{k-1} \cdots \underline{\phi}_2 \, \underline{\phi}_1$$

If the line has N twists then,

$$\underline{\Phi} = \underline{\Phi}_T^N$$

Figure 3-5 represents a view of one twist of the model as it would look from above if seen against the ground plane. This view shows nine segments used to represent one full twist. This model of one full twist also posesses symmetry. Since the wires of the TWP are considered to be identical, a twist can be modeled using two half-twists (Fig. 3-6). By making the length of the first and last segment of each half-twist half as long as the other segments, the TWP can be modeled by cascading the half-twist sections.

As a result of dividing the model of one full twist (FT) into two half-twist (HT) models, the voltages and currents at the center of the full twist are out of

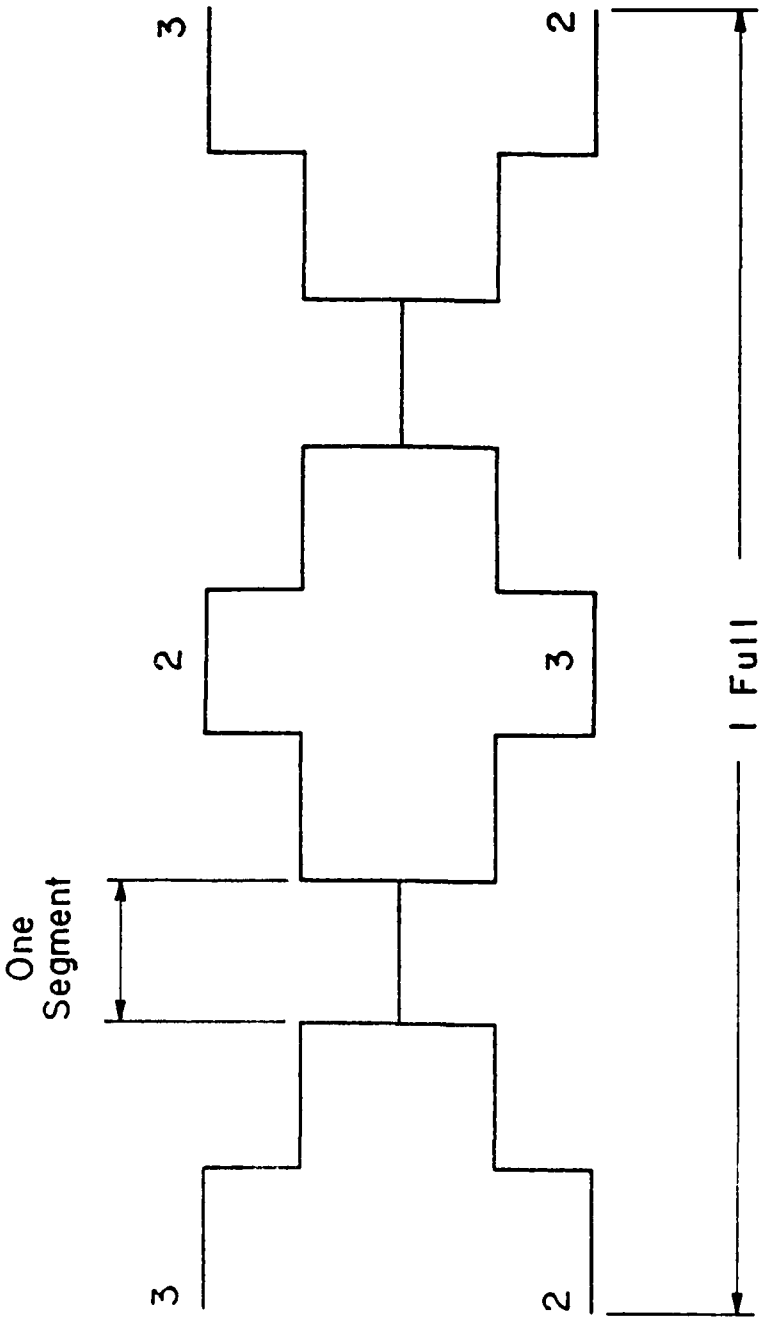

Fig. 3-5

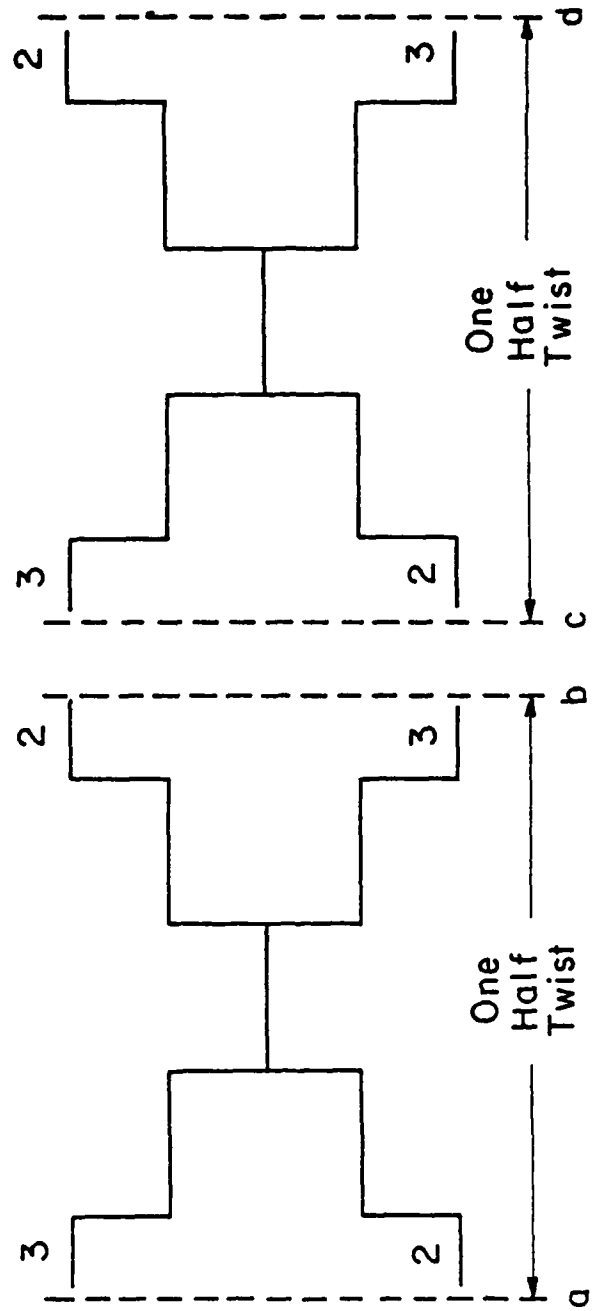

Fig. 3-6

sequence. To properly sequence the voltages and currents of wire #2 and wire #3 at this junction, the voltage and current relations of wire #2 and wire #3 must be interchanged. i.e.,

$$\begin{bmatrix} V_1(d) \\ V_2(d) \\ V_3(d) \\ I_1(d) \\ I_2(d) \\ I_3(d) \end{bmatrix} = \underline{\phi}_{HT2} \begin{bmatrix} V_1(c) \\ V_2(c) \\ V_3(c) \\ I_1(c) \\ I_2(c) \\ I_3(c) \end{bmatrix} ; \begin{bmatrix} V_1(b) \\ V_2(b) \\ V_3(b) \\ I_1(b) \\ I_2(b) \\ I_3(b) \end{bmatrix} = \underline{\phi}_{HT1} \begin{bmatrix} V_1(a) \\ V_2(a) \\ V_3(a) \\ I_1(a) \\ I_2(a) \\ I_3(a) \end{bmatrix}$$

$$\begin{bmatrix} V_1(c) \\ V_2(c) \\ V_3(c) \\ I_1(c) \\ I_2(c) \\ I_3(c) \end{bmatrix} = \begin{bmatrix} V_1(b) \\ V_3(b) \\ V_2(b) \\ I_1(b) \\ I_3(b) \\ I_2(b) \end{bmatrix} = \underline{P} \begin{bmatrix} V_1(b) \\ V_2(b) \\ V_3(b) \\ I_1(b) \\ I_2(b) \\ I_3(b) \end{bmatrix}$$

where $\underline{P}$ is the 6x6 permutation matrix given by

$$\underline{P} = \begin{bmatrix} \underline{p} & \underline{0}_3 \\ \underline{0}_3 & \underline{p} \end{bmatrix} \qquad \underline{p} = \begin{bmatrix} 1 & 0 & 0 \\ 0 & 0 & 1 \\ 0 & 1 & 0 \end{bmatrix}$$

Then,

$$\begin{bmatrix} V_1(d) \\ V_2(d) \\ V_3(d) \\ I_1(d) \\ I_2(d) \\ I_3(d) \end{bmatrix} = \underline{\phi}_{HT} \, \underline{P} \, \underline{\phi}_{HT} \begin{bmatrix} V_1(a) \\ V_2(a) \\ V_3(a) \\ I_1(a) \\ I_2(a) \\ I_3(a) \end{bmatrix}$$

Then the $\underline{\Phi}_T$ matrix for each full twist is given by

$$\underline{\Phi}_T = \underline{\phi}_{HT}\, P\, \underline{\phi}_{HT}$$

where,

$$\underline{\phi}_{HT} = \underline{\phi}_m\, \underline{\phi}_{m-1} \cdots \underline{\phi}_2\, \underline{\phi}_1$$

and each half twist consists of m segments.

The $\underline{\Phi}$ matrix for the entire TWP can then be computed by cascading the $\underline{\Phi}_T$ matrices for the number of twists present in the line. If an odd number of half twists is present, one additional matrix multiplication is necessary, i.e., $\underline{\phi}_{HT}$.

Even though the matrix multiplications for the transfer function of the TWP have been reduced by computing the transfer function of each twist $\underline{\Phi}_T$, another substantial reduction can be achieved by utilizing the fact that the transfer function of any twist, $\underline{\Phi}_{T_i}$, is identical to the transfer function of any other twist, $\underline{\Phi}_{T_j}$. Consider the cascade of matrices $\underline{\Phi}_T$ shown in Fig. 3-7. The overall transmission line matrix for the line consisting of N twists is given by

$$\begin{bmatrix} V_1(\ell) \\ V_2(\ell) \\ V_3(\ell) \\ I_1(\ell) \\ I_2(\ell) \\ I_3(\ell) \end{bmatrix} = \underbrace{\underline{\Phi}_T\, \underline{\Phi}_T\, \underline{\Phi}_T \cdots \underline{\Phi}_T\, \underline{\Phi}_T}_{\underline{\Phi}_T^N = \underline{\Phi}} \begin{bmatrix} V_1(0) \\ V_2(0) \\ V_3(0) \\ I_1(0) \\ I_2(0) \\ I_3(0) \end{bmatrix}$$

The computation of the $\underline{\Phi}$ matrix consists of N

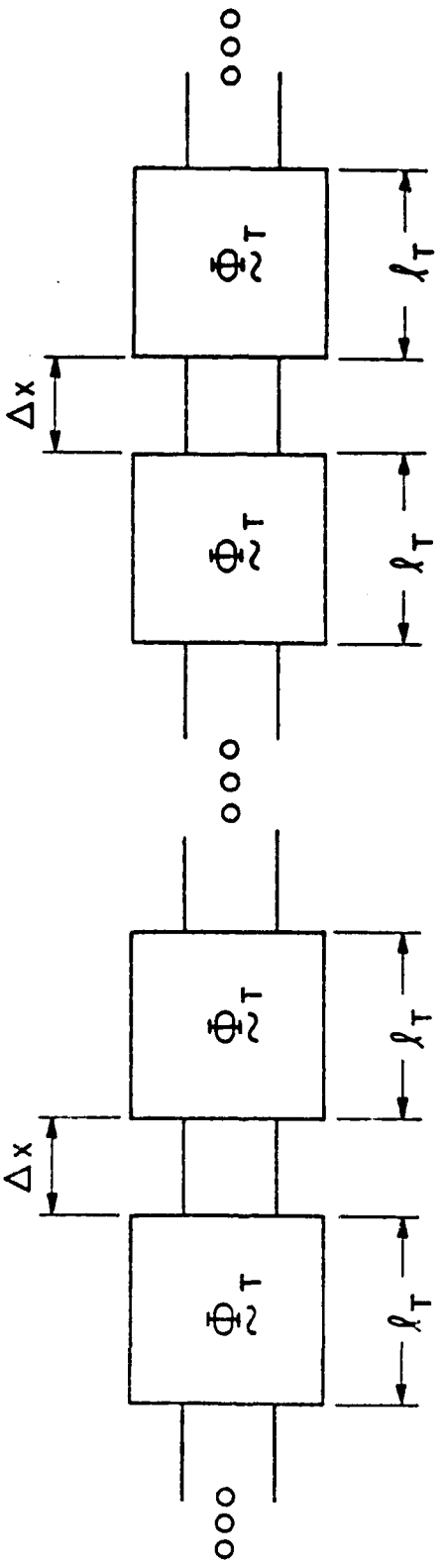

Fig. 3-7

multiplications of 6x6 complex matrices. However, if additional matrix storage is used, these multiplications can be drastically reduced.

The first multiplication of the $\underline{\Phi}_T$ matrices would yield a transfer function for a TL consisting of two twists.

$$\underline{\Phi}_T \, \underline{\Phi}_T = \underline{\Phi}_{2T}$$

The two twists represented by this $\underline{\Phi}_{2T}$ matrix are identical to any other two twists along the line.

If we now multiply the $\underline{\Phi}_{2T}$ matrix with itself a matrix representing any four twists of the line is obtained.

$$\underline{\Phi}_{4T} = \underline{\Phi}_{2T} \, \underline{\Phi}_{2T}$$

This process can be repeated until the $\underline{\Phi}$ matrix is obtained that represents the desired number of twists in the line.

If the number of twists in the line is not a power of two, i.e., 2^N, an additional number of matrices must be stored in the computer so that the proper $\underline{\Phi}$ matrix can be obtained. As an example, say we choose a TL which consists of 20 twists. The desired matrix multiplication for $\underline{\Phi}$ becomes

$$\underline{\Phi} = \underline{\Phi}_{20T} = \underline{\Phi}_{16T} \, \underline{\Phi}_{4T}$$

The matrix multiplications of the 6x6 complex matrices are reduced from 19 to 5. For a TL consisting of 226 twists the complex 6x6 matrix multiplications necessary to compute the $\underline{\Phi}$ matrix are reduced from 225 to 10. This constitutes a substantial saving in computer time. Solving the TL

equations once the $\underline{\ell}$ transfer function matrix is computed takes a small amount of computer time.

The equations for the end conditions of the line can be determined from Fig. 3-8 .

$$V_1(0) = V_s - Z_{0G} I_1(0)$$

$$V_2(0) = -Z_{0R} I_2(0)$$

$$V_3(0) = 0$$

$$I_1(\ell) = \frac{1}{Z_{\ell G}} V_1(\ell)$$

$$I_2(\ell) = \frac{1}{Z_{\ell R}} (V_2(\ell) - V_3(\ell))$$

$$I_3(\ell) = \frac{1}{Z_{\ell R}} (V_3(\ell) - V_2(\ell))$$

In matrix form these equations become:

$$\underline{V}(0) = \underline{V} - \underline{Z}_0 \underline{I}(0)$$

$$\underline{I}(\ell) = \underline{Y}_\ell \, \underline{V}(\ell)$$

where,

$$\underline{I}(0) = \begin{bmatrix} I_1(0) \\ I_2(0) \\ I_3(0) \end{bmatrix} \qquad \underline{I}(\ell) = \begin{bmatrix} I_1(\ell) \\ I_2(\ell) \\ I_3(\ell) \end{bmatrix}$$

$$\underline{V}(0) = \begin{bmatrix} V_1(0) \\ V_2(0) \\ V_3(0) \end{bmatrix} \qquad \underline{V}(\ell) = \begin{bmatrix} V_1(\ell) \\ V_2(\ell) \\ V_3(\ell) \end{bmatrix} \qquad \underline{V} = \begin{bmatrix} V_s \\ 0 \\ 0 \end{bmatrix}$$

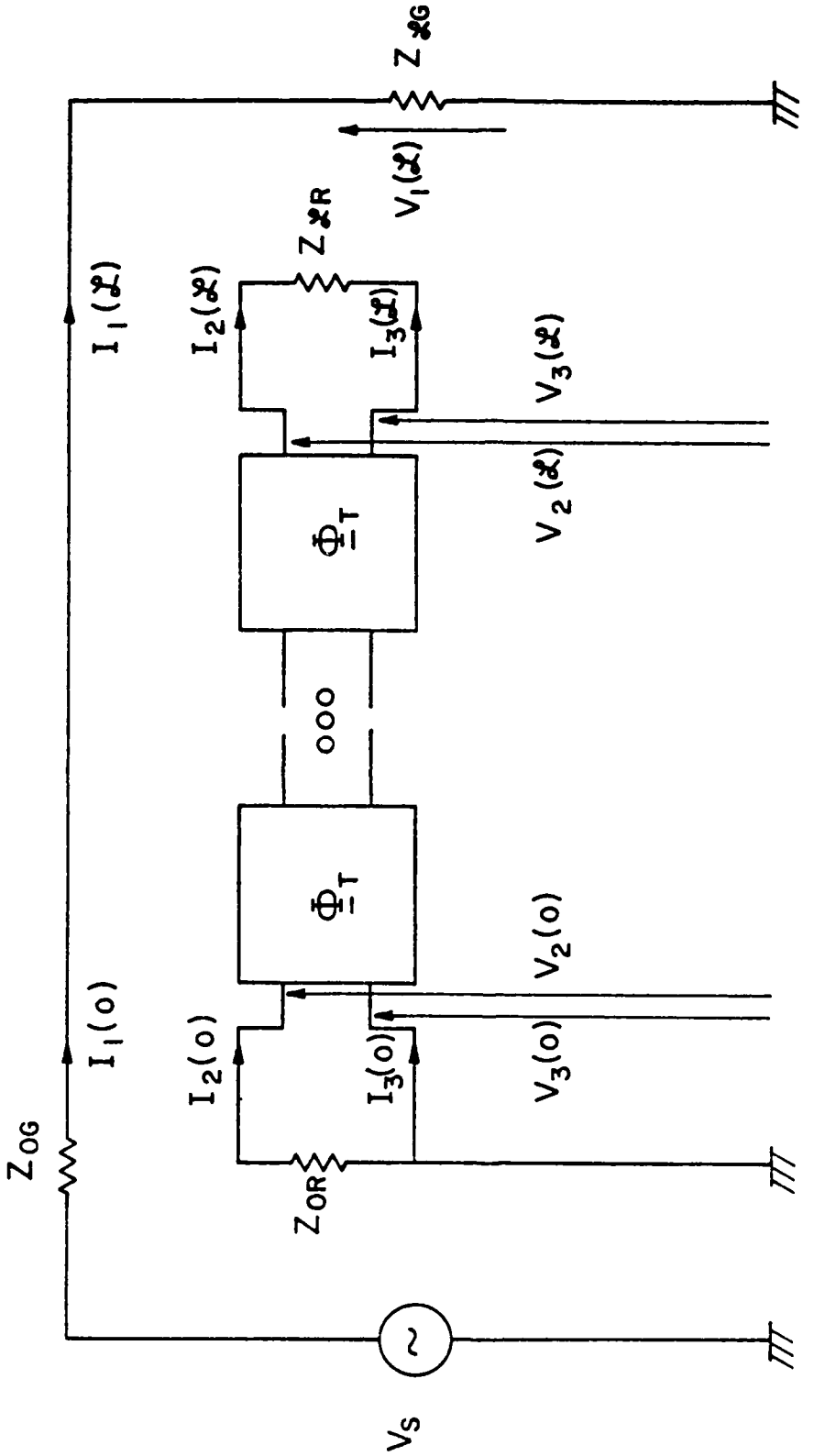
$Z_{\ell G}$
$V_1(\ell)$
$Z_{\ell R}$
$I_1(\ell)$
$I_2(\ell)$
$I_3(\ell)$
$V_3(\ell)$
$V_2(\ell)$
Φ_T
ooo
Φ_T
$V_2(0)$
$I_1(0)$
$I_2(0)$
$I_3(0)$
$V_3(0)$
Z_{OG}
Z_{OR}
V_S

Fig. 3-8

$$\underline{Z}_0 = \begin{bmatrix} Z_{0G} & 0 & 0 \\ 0 & Z_{0R} & 0 \\ 0 & 0 & 0 \end{bmatrix} \qquad \underline{Y} = \begin{bmatrix} \frac{1}{Z_{\chi G}} & 0 & 0 \\ 0 & \frac{1}{Z_{\chi R}} & -\frac{1}{Z_{\chi R}} \\ 0 & -\frac{1}{Z_{\chi R}} & \frac{1}{Z_{\chi R}} \end{bmatrix}$$

Substituting into the overall chain parameter matrix [1] gives

$$[\underline{Y}_{\chi}\underline{\Phi}_{11}(\chi)\underline{Z}_0 - \underline{Y}_{\chi}\underline{\Phi}_{12}(\chi) - \underline{\Phi}_{21}(\chi)Z_0 + \underline{\Phi}_{22}(\chi)]\underline{I}(0) = [\underline{Y}_{\chi}\underline{\Phi}_{11}(\chi) - \underline{\Phi}_{21}(\chi)]\underline{V}$$

$$\underline{I}(\chi) = \underline{\Phi}_{21}(\chi)\underline{V} + [\underline{\Phi}_{22}(\chi) - \underline{\Phi}_{21}(\chi)\underline{Z}_0]\underline{I}(0)$$

These simultaneous equations are solved for terminal currents at x=0.

Since the click model incorporated the rotation of parallel segments as a function of θ, the initial condition of the angular position of the TWP could be chosen. The direction of rotation of the TWP could also be changed, simply by taking the incremental rotation, $\Delta\theta$, to be negative.

The results of the click model are shown in figures 3-9 through 3-16 where the initial position of the wire pair is chosen to be horizontal with respect to the ground plane. These figures show the predicted VTR where a comparison of the loop model prediction is made with the click model prediction as the number of incremental segments per half-twist is changed from 3, 5, 10, to 25 for 225 and 226 half-twists in the TWP. The maximum deviation between the loop

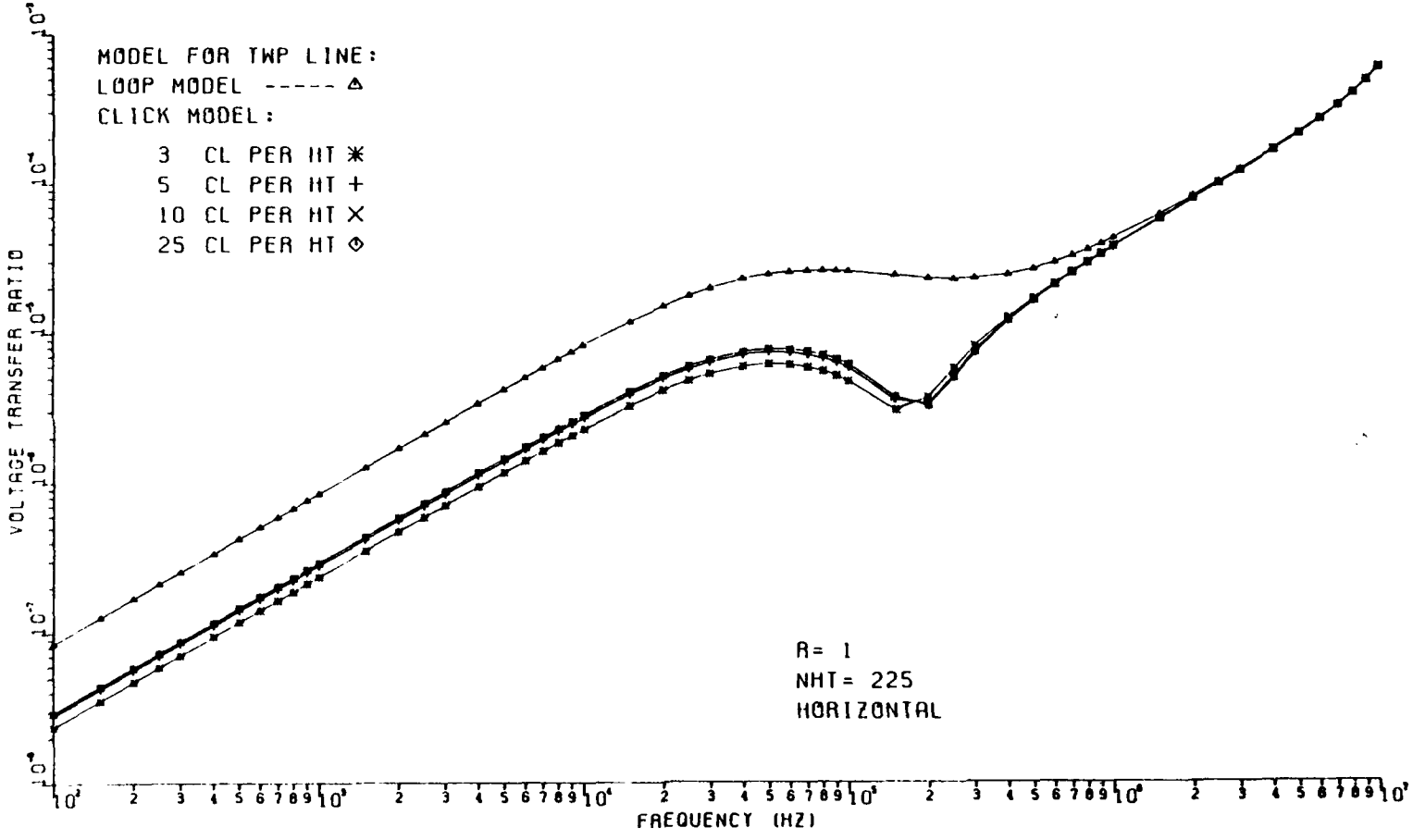
MODEL FOR TWP LINE:
LOOP MODEL ----- Δ
CLICK MODEL:
3 CL PER HT ✳
5 CL PER HT +
10 CL PER HT X
25 CL PER HT ◇
VOLTAGE TRANSFER RATIO
FREQUENCY (HZ)
R= 1
NHT= 225
HORIZONTAL

Fig. 3-9

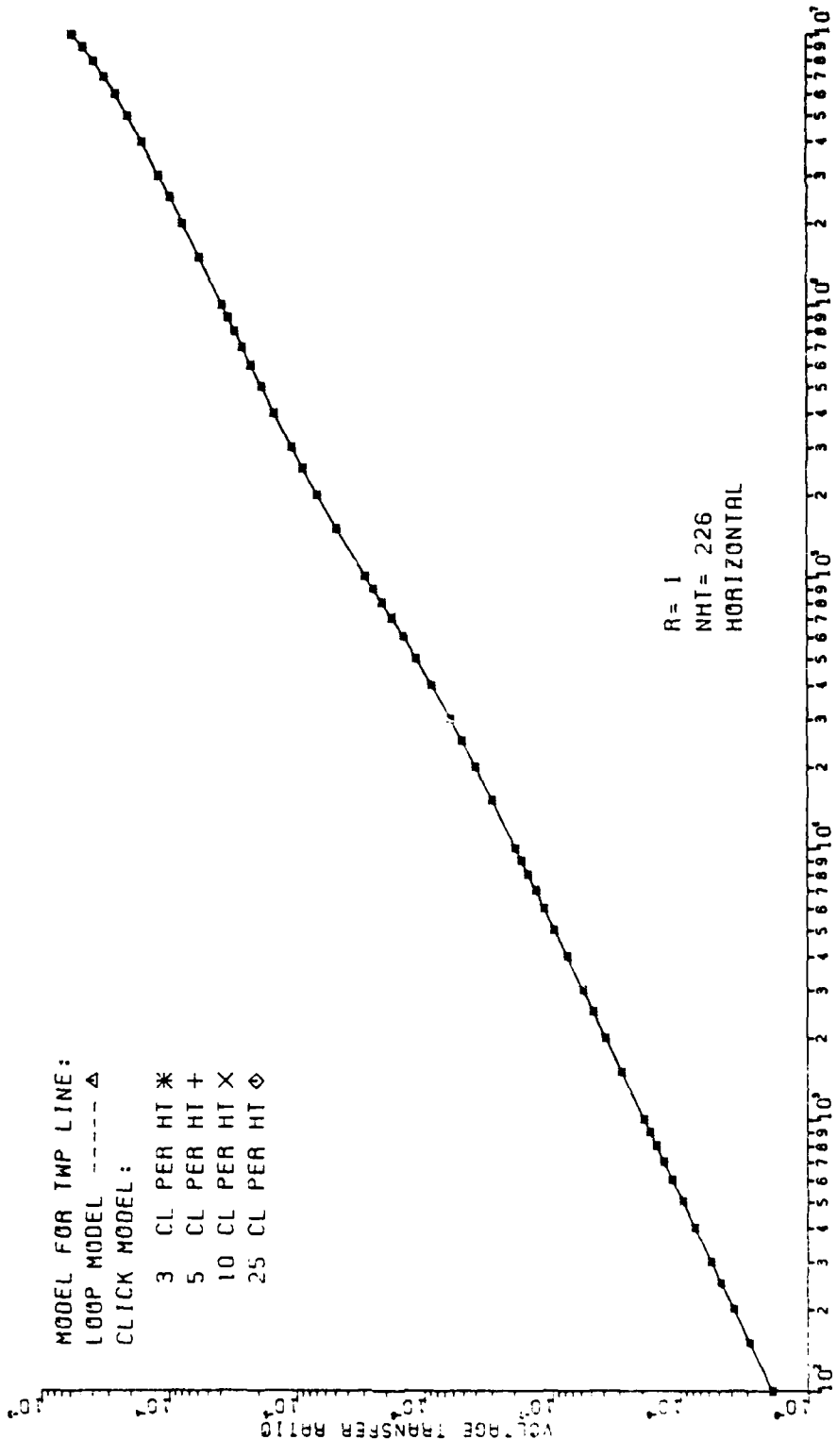
MODEL FOR TWP LINE:
LOOP MODEL ----- Δ
CLICK MODEL:
3 CL PER HT ✳
5 CL PER HT +
10 CL PER HT X
25 CL PER HT ◇
R= 1
NHT= 226
HORIZONTAL
FREQUENCY (HZ)

Fig. 3-10

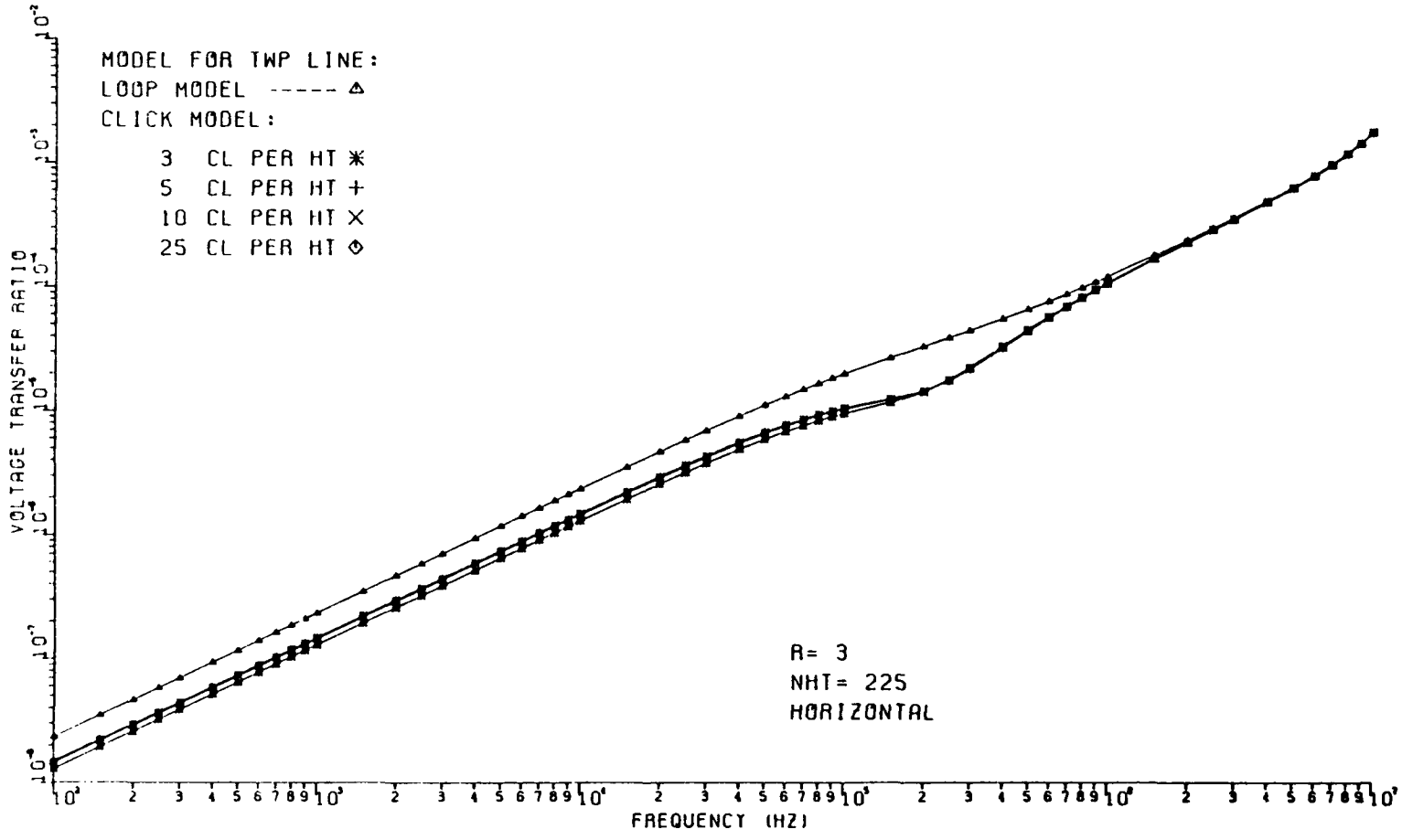
MODEL FOR TWP LINE:
LOOP MODEL ----- △
CLICK MODEL:
3 CL PER HT ✳
5 CL PER HT +
10 CL PER HT ×
25 CL PER HT ◇
VOLTAGE TRANSFER RATIO
FREQUENCY (HZ)
R= 3
NHT= 225
HORIZONTAL

Fig. 3-11

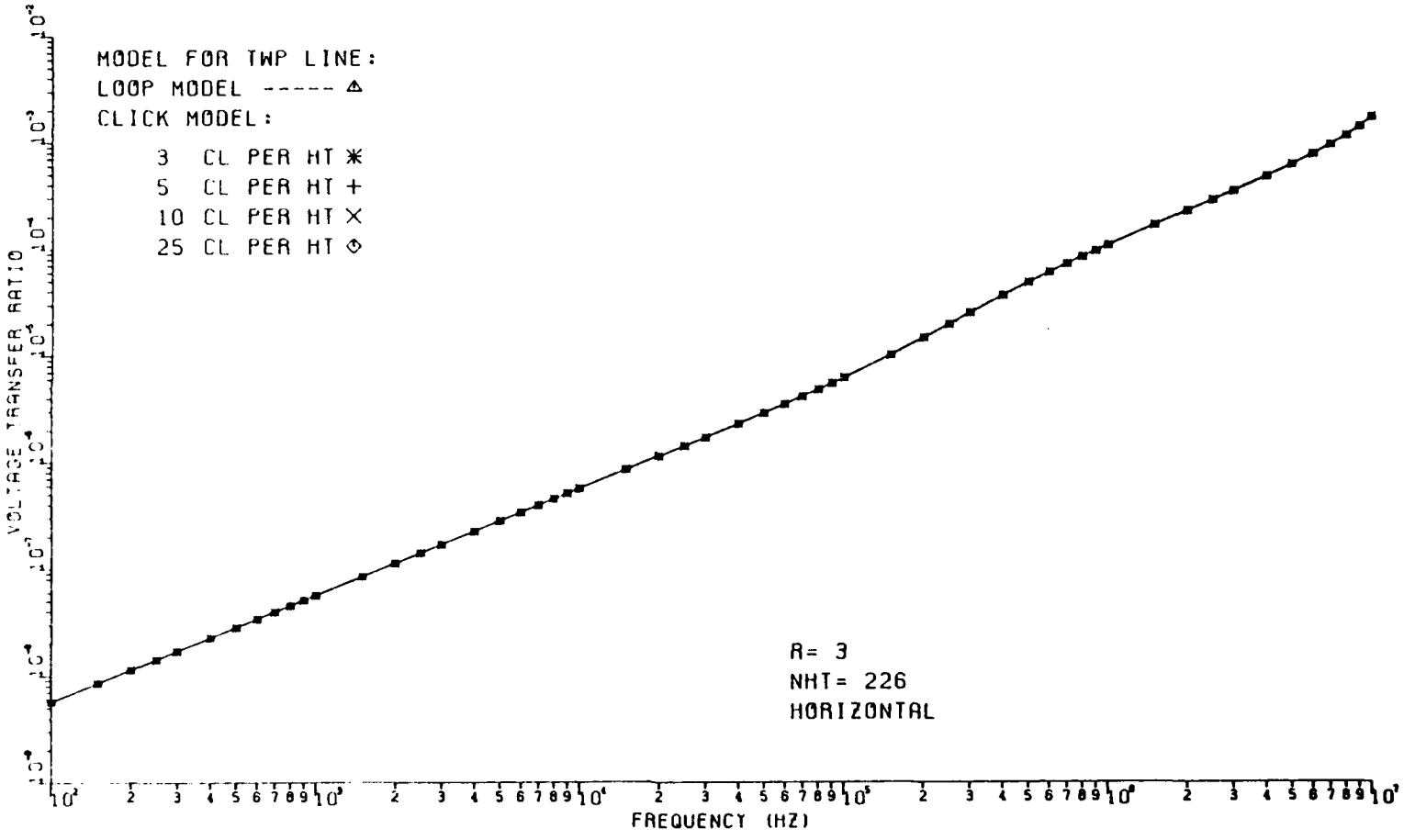
MODEL FOR TWP LINE:
LOOP MODEL ----- △
CLICK MODEL:
3 CL PER HT ✳
5 CL PER HT +
10 CL PER HT ×
25 CL PER HT ◇
VOLTAGE TRANSFER RATIO
FREQUENCY (HZ)
R= 3
NHT= 226
HORIZONTAL

Fig. 3-12

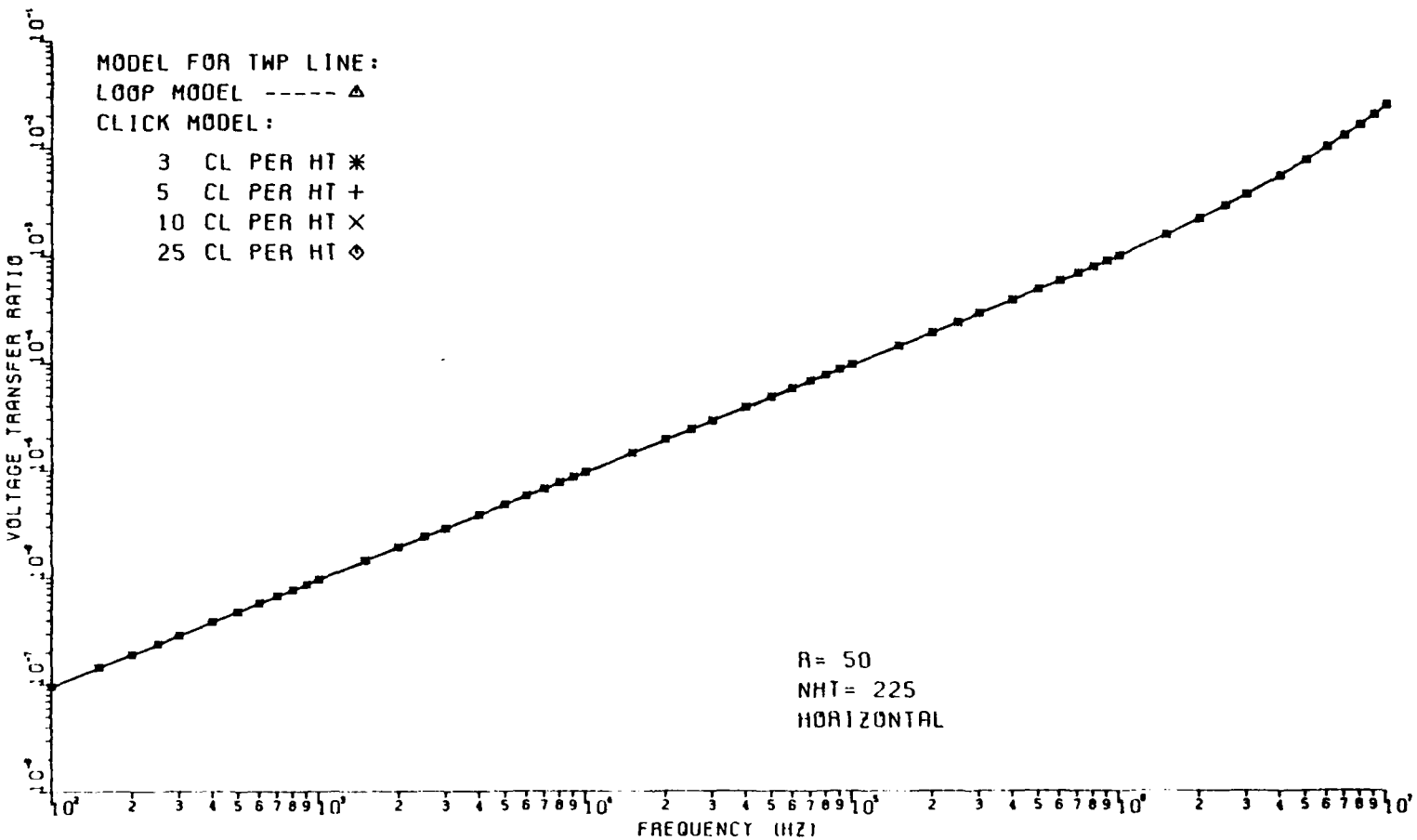
MODEL FOR TWP LINE:
LOOP MODEL ----- Δ
CLICK MODEL:
3 CL PER HT ✳
5 CL PER HT +
10 CL PER HT ×
25 CL PER HT ◇
VOLTAGE TRANSFER RATIO
FREQUENCY (HZ)
R= 50
NHT= 225
HORIZONTAL

Fig. 3-13

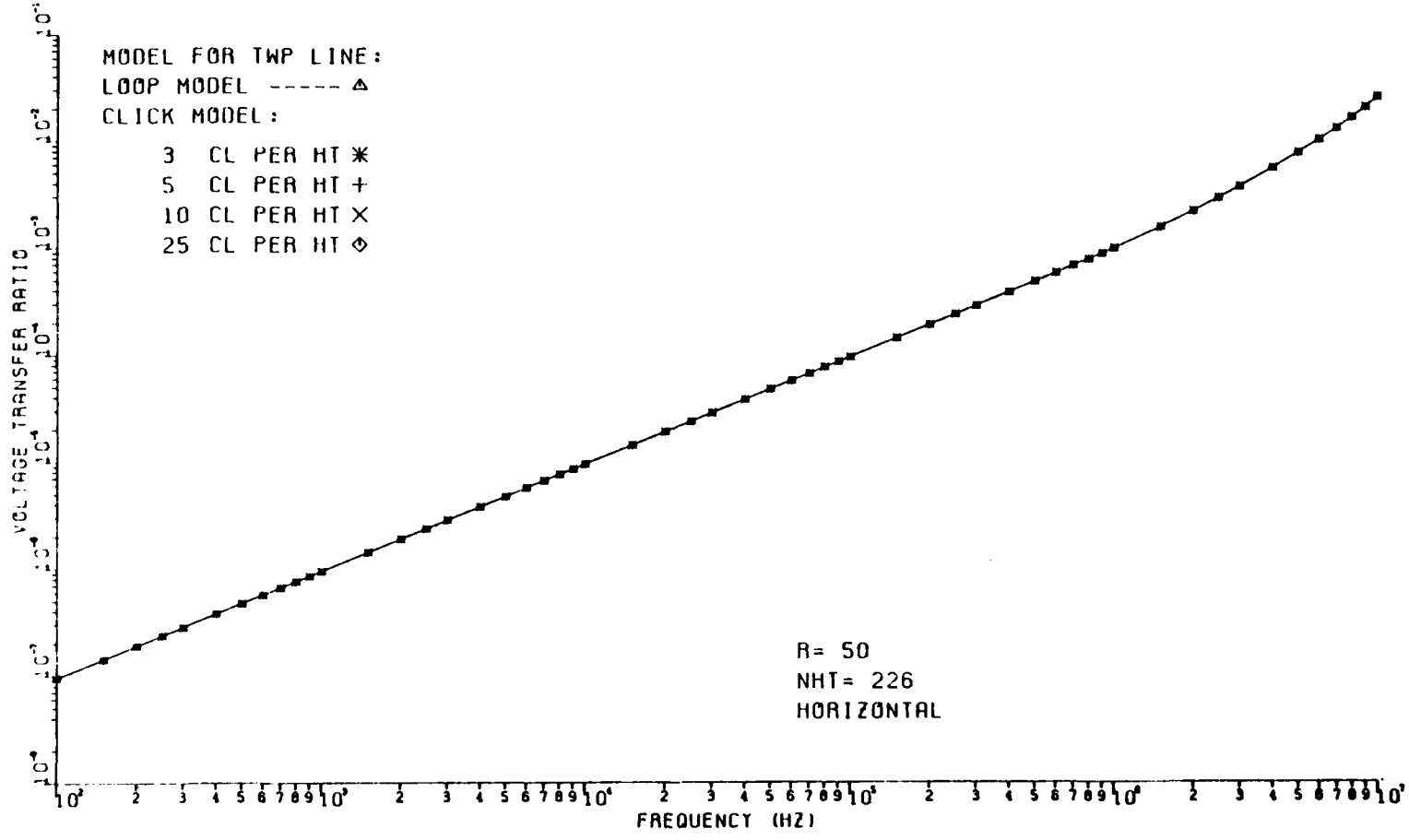
MODEL FOR TWP LINE:
LOOP MODEL ----- △
CLICK MODEL:
3 CL PER HT ✳
5 CL PER HT +
10 CL PER HT ×
25 CL PER HT ◇
VOLTAGE TRANSFER RATIO
FREQUENCY (HZ)
R= 50
NHT= 226
HORIZONTAL

Fig. 3-14

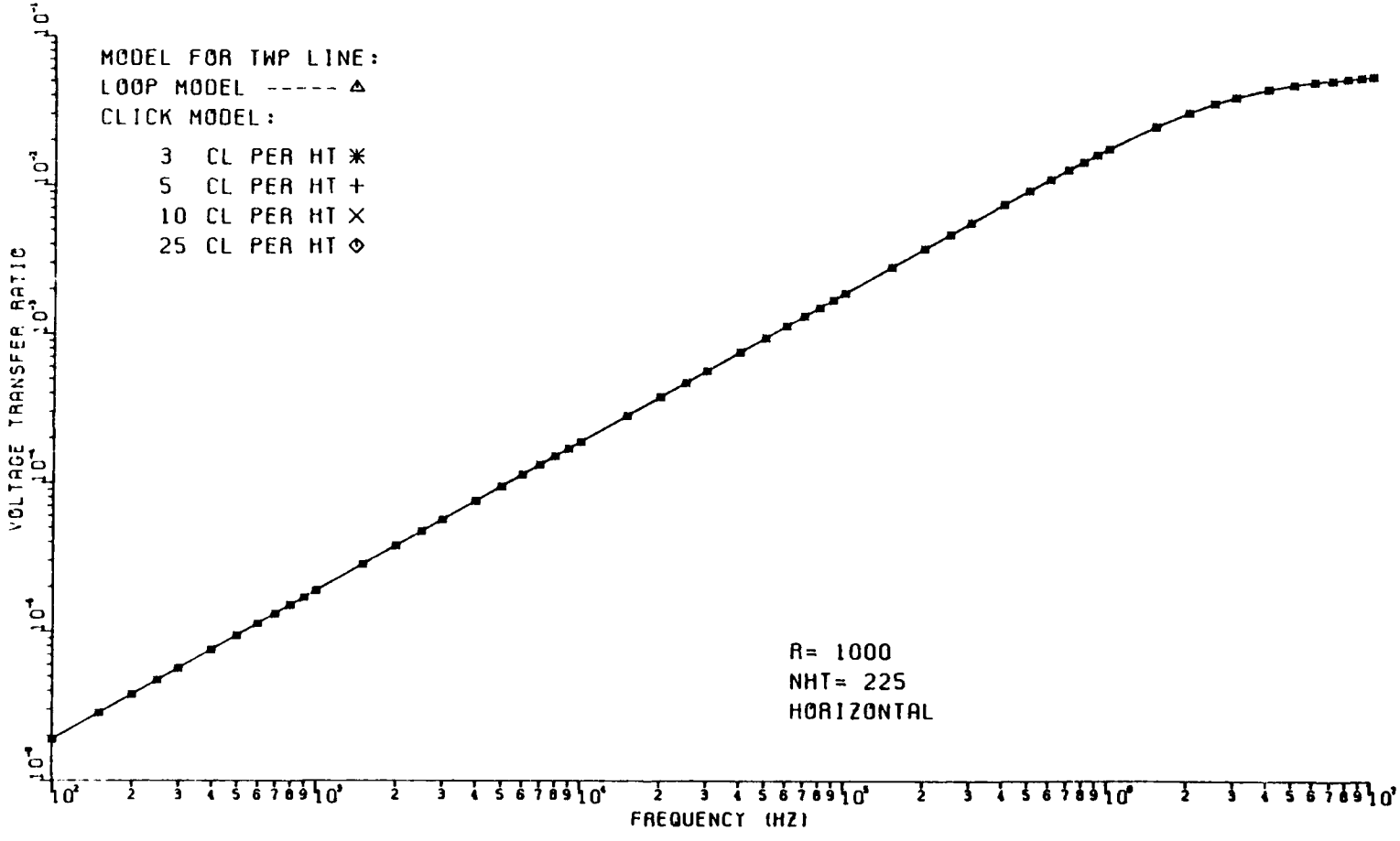
MODEL FOR TWP LINE:
LOOP MODEL ----- △
CLICK MODEL:
3 CL PER HT ✳
5 CL PER HT +
10 CL PER HT ×
25 CL PER HT ◇
VOLTAGE TRANSFER RATIO
FREQUENCY (HZ)
R= 1000
NHT= 225
HORIZONTAL

Fig. 3-15

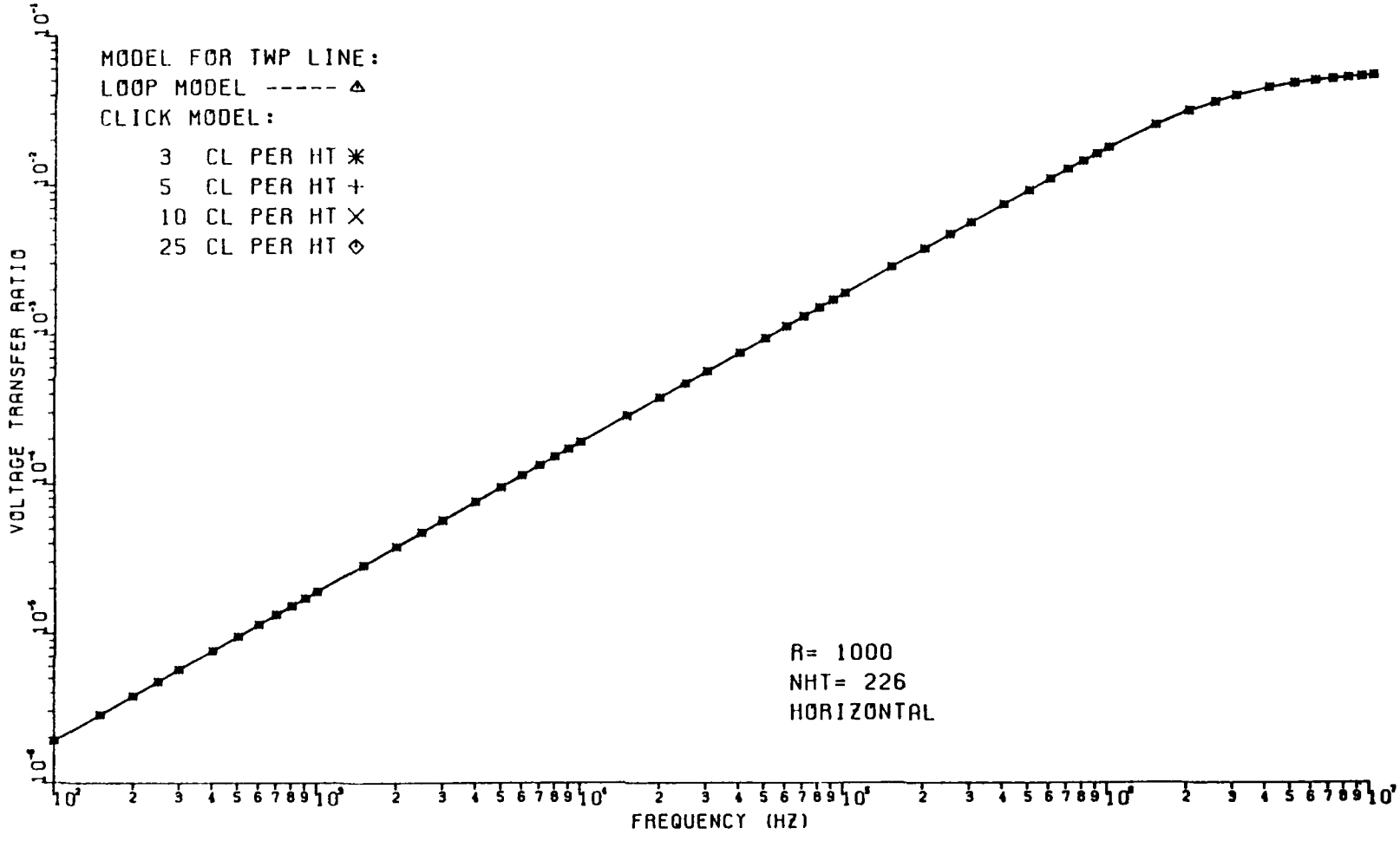
MODEL FOR TWP LINE:
LOOP MODEL ----- △
CLICK MODEL:
3 CL PER HT ✳
5 CL PER HT +
10 CL PER HT ×
25 CL PER HT ◇
R= 1000
NHT= 226
HORIZONTAL
VOLTAGE TRANSFER RATIO
FREQUENCY (HZ)

Fig. 3-16

model prediction and the click model prediction occurs for low impedance line terminations with an odd number of half-twists. The click model prediction of the VTR starts to converge when 25 incremental segments are used to represent one half-twist of the TWP. For an even number of half-twists, both models give the same prediction. Figures 3-17 through 3-24 show the comparison when the initial position of the wire pair was chosen to be vertical with respect to the ground plane. When the TWP starts in the vertical position, the loop model prediction is in close agreement with the click model predicion. The change in VTR prediction, when the initial position of the TWP is changed from horizontal to vertical, is shown in Fig. 3-25 through 3-28, with R=1 ohm and 1k ohm for the loop model and click model (with 25 clicks per half-twist).

The incremental rotation of the segments was also used to change the angular position of the segment of the line attached to the termination blocks. The prediction of the VTR reached a maximum when the angular position of the segment of the twisted pair attached to the load termination block was equal to 60 degrees with respect to the ground plane. The segment attached to the generator termination block was in the horizontal position. The fluctuation of the predicted VTR with respect to the number of half-twists in the line is shown in Fig. 3-29 through Fig. 3-32 for 1 ohm and 3 ohm loads. Changing the direction of rotation of the twist also caused a noticable change in the predicted

VTR. For 50 ohm and 1k ohm loads the VTR remained constant when the number of half-twists in the line were changed. This was in agreement with experimental observations obtained in the sensitivity analysis!

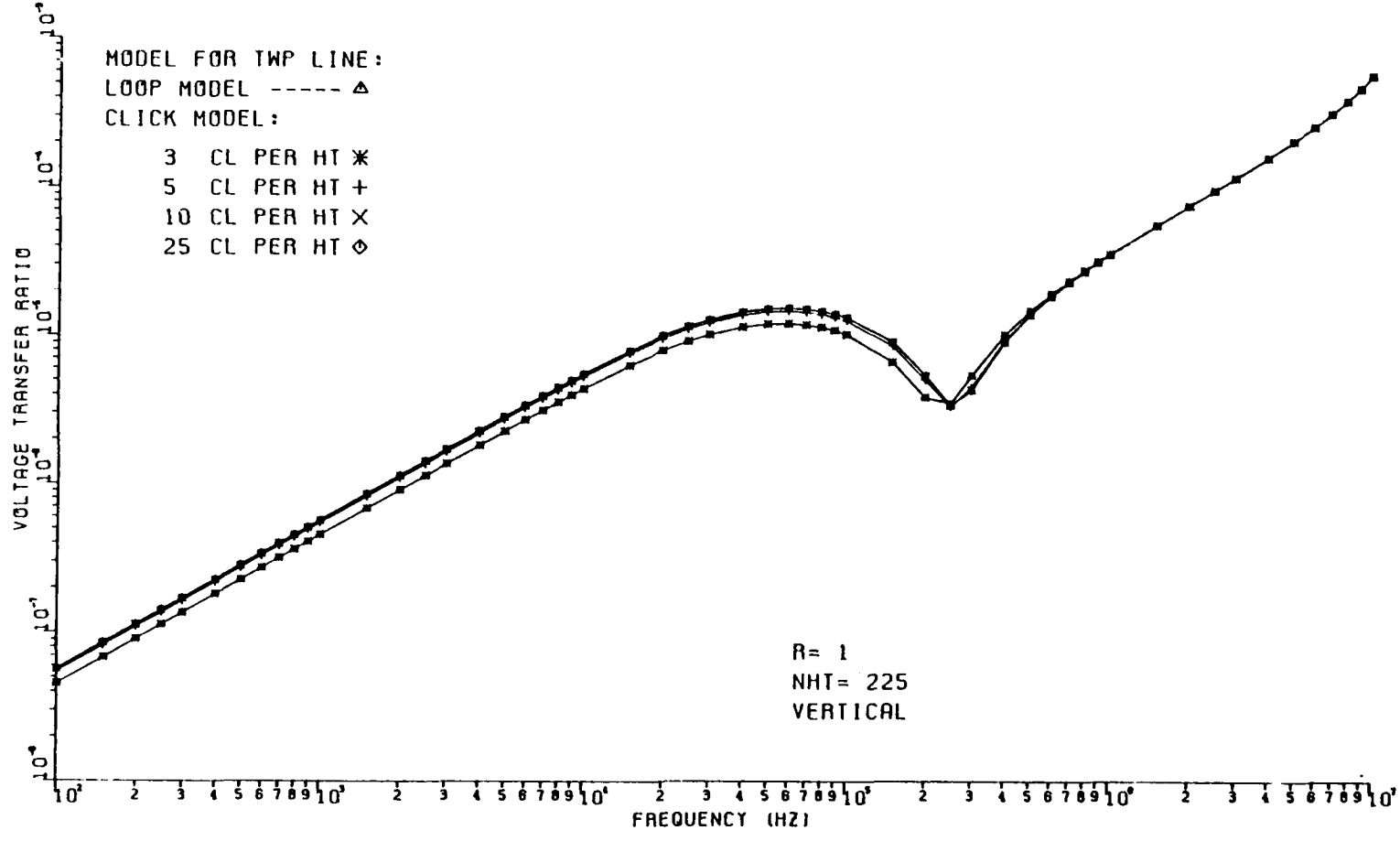
MODEL FOR TWP LINE:
LOOP MODEL ----- Δ
CLICK MODEL:
3 CL PER HT ✳
5 CL PER HT +
10 CL PER HT X
25 CL PER HT ◇
VOLTAGE TRANSFER RATIO
FREQUENCY (HZ)
R= 1
NHT= 225
VERTICAL

Fig. 3-17

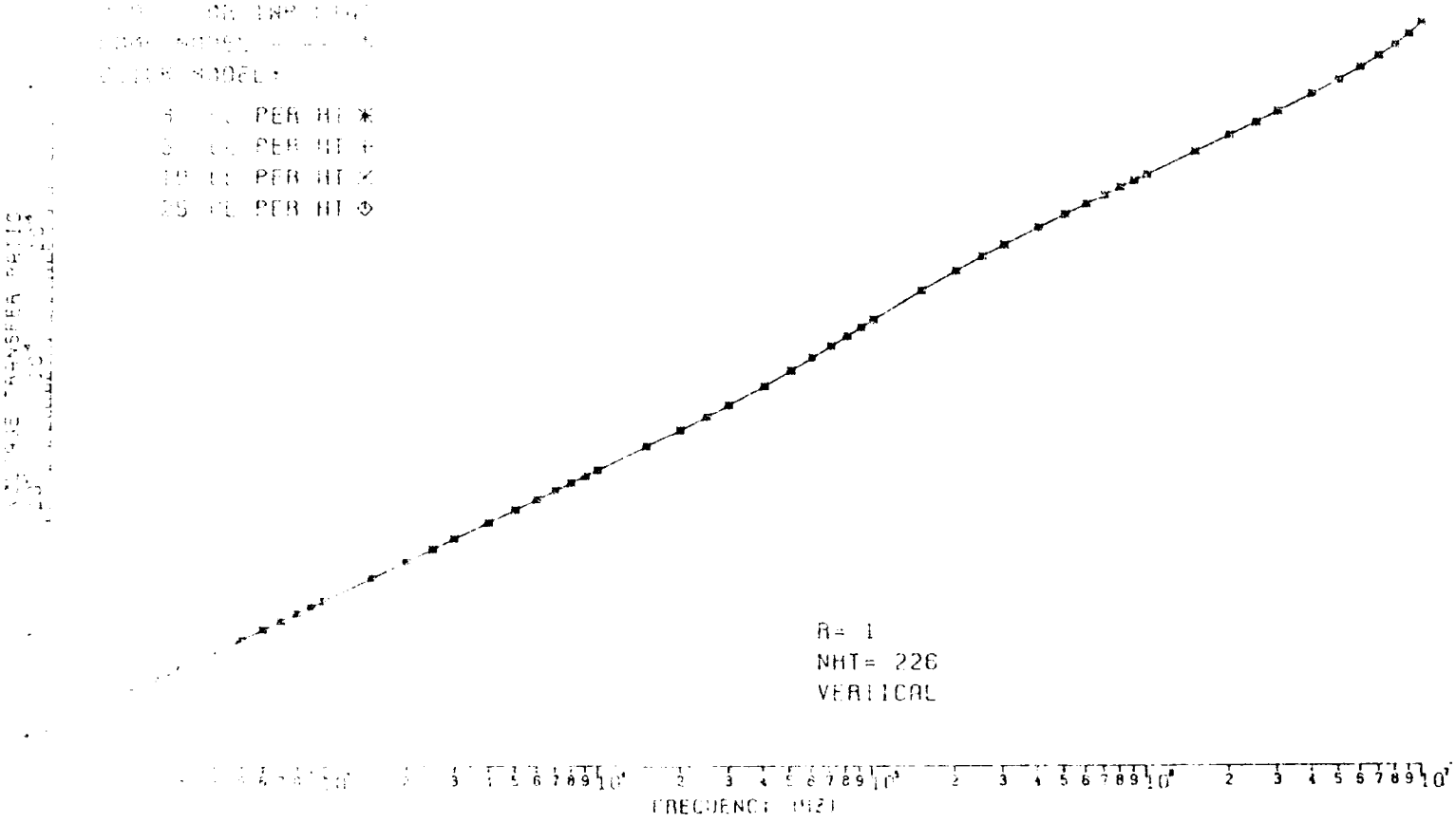

Fig. 3-13

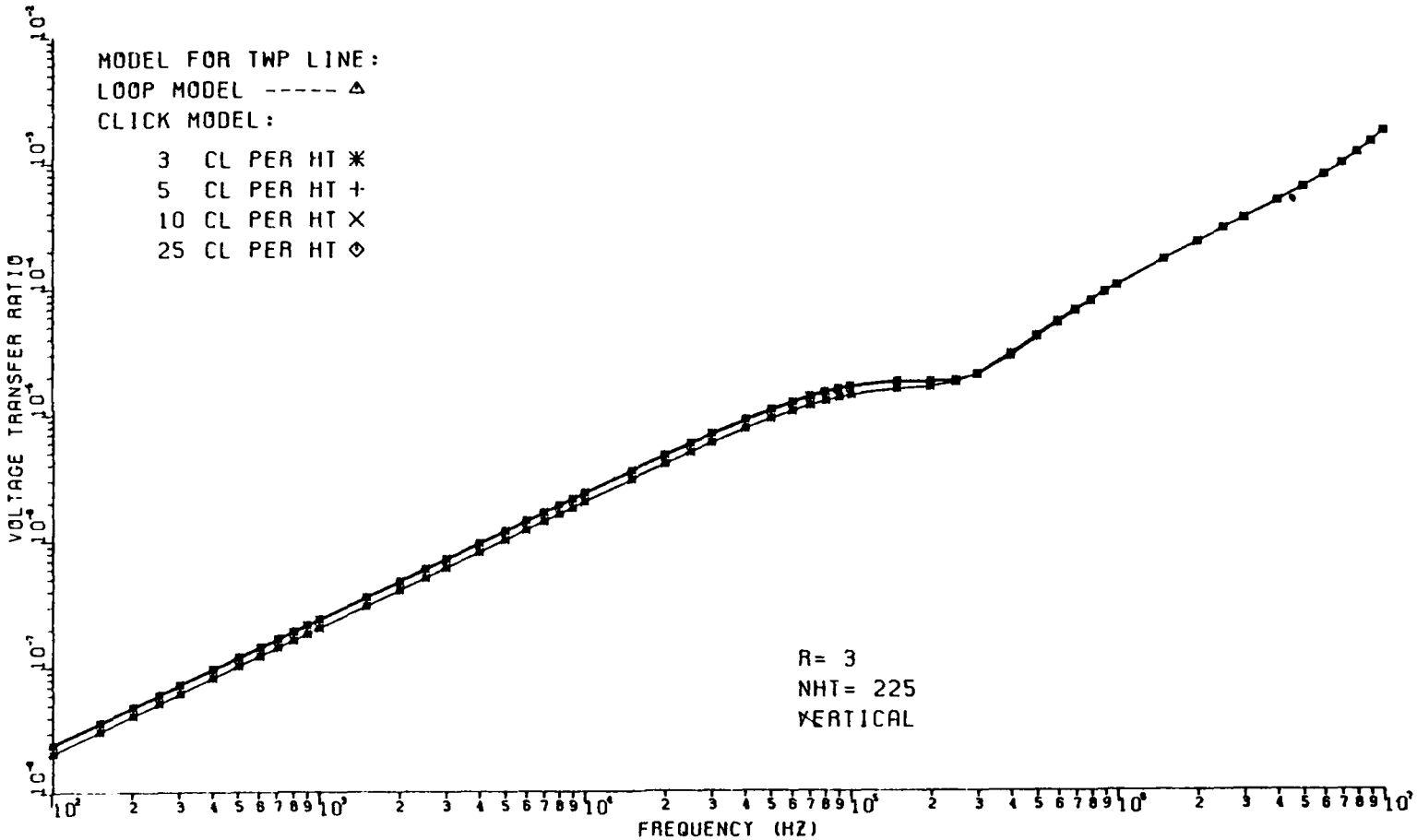
MODEL FOR TWP LINE:
LOOP MODEL ----- Δ
CLICK MODEL:
3 CL PER HT ✳
5 CL PER HT +
10 CL PER HT ×
25 CL PER HT ◇
VOLTAGE TRANSFER RATIO
FREQUENCY (HZ)
R= 3
NHT= 225
VERTICAL

Fig. 3-19

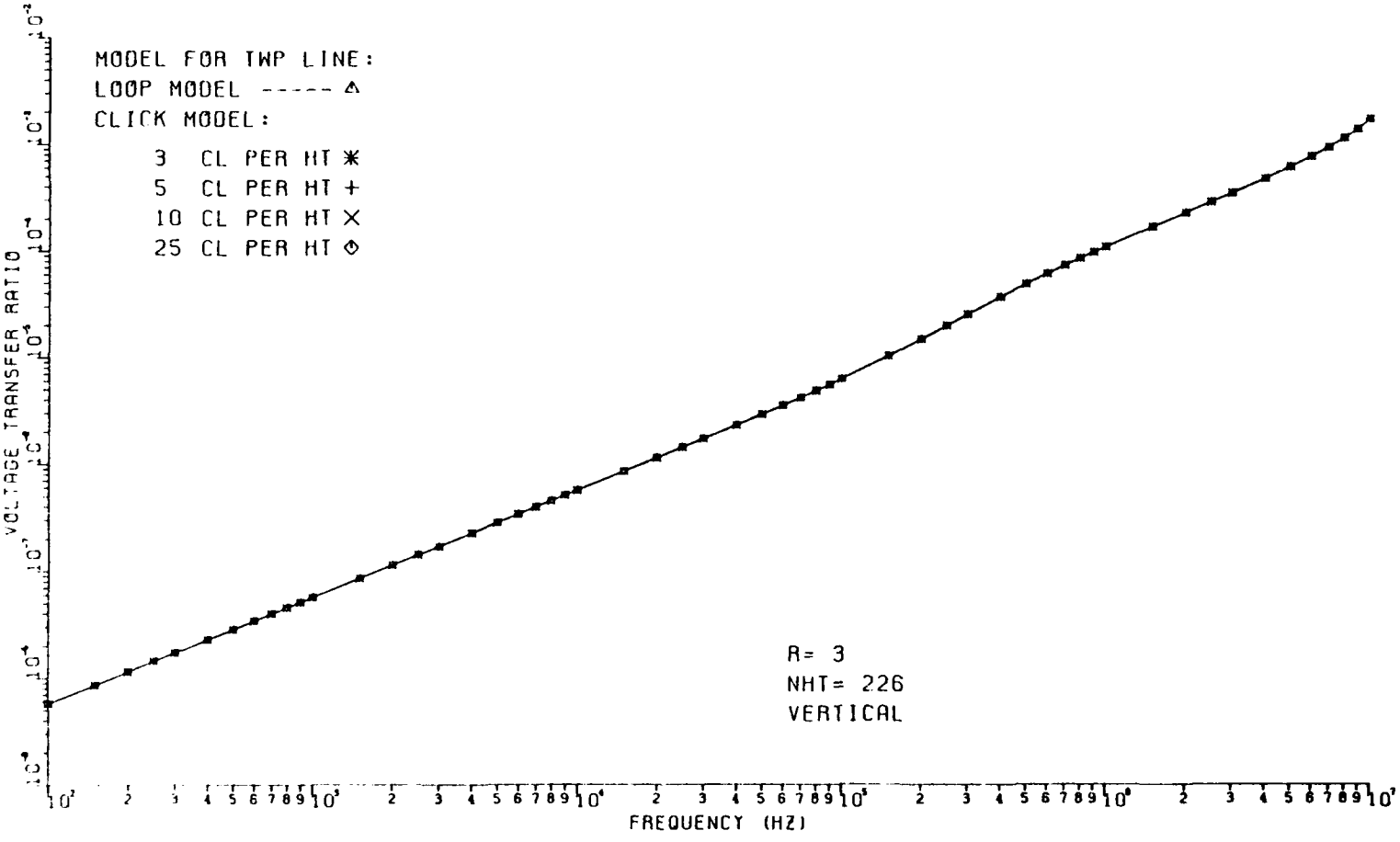
MODEL FOR TWP LINE:
LOOP MODEL ----- △
CLICK MODEL:
3 CL PER HT ✳
5 CL PER HT +
10 CL PER HT ×
25 CL PER HT ◇
R= 3
NHT= 226
VERTICAL
VOLTAGE TRANSFER RATIO
FREQUENCY (HZ)

Fig. 3-20

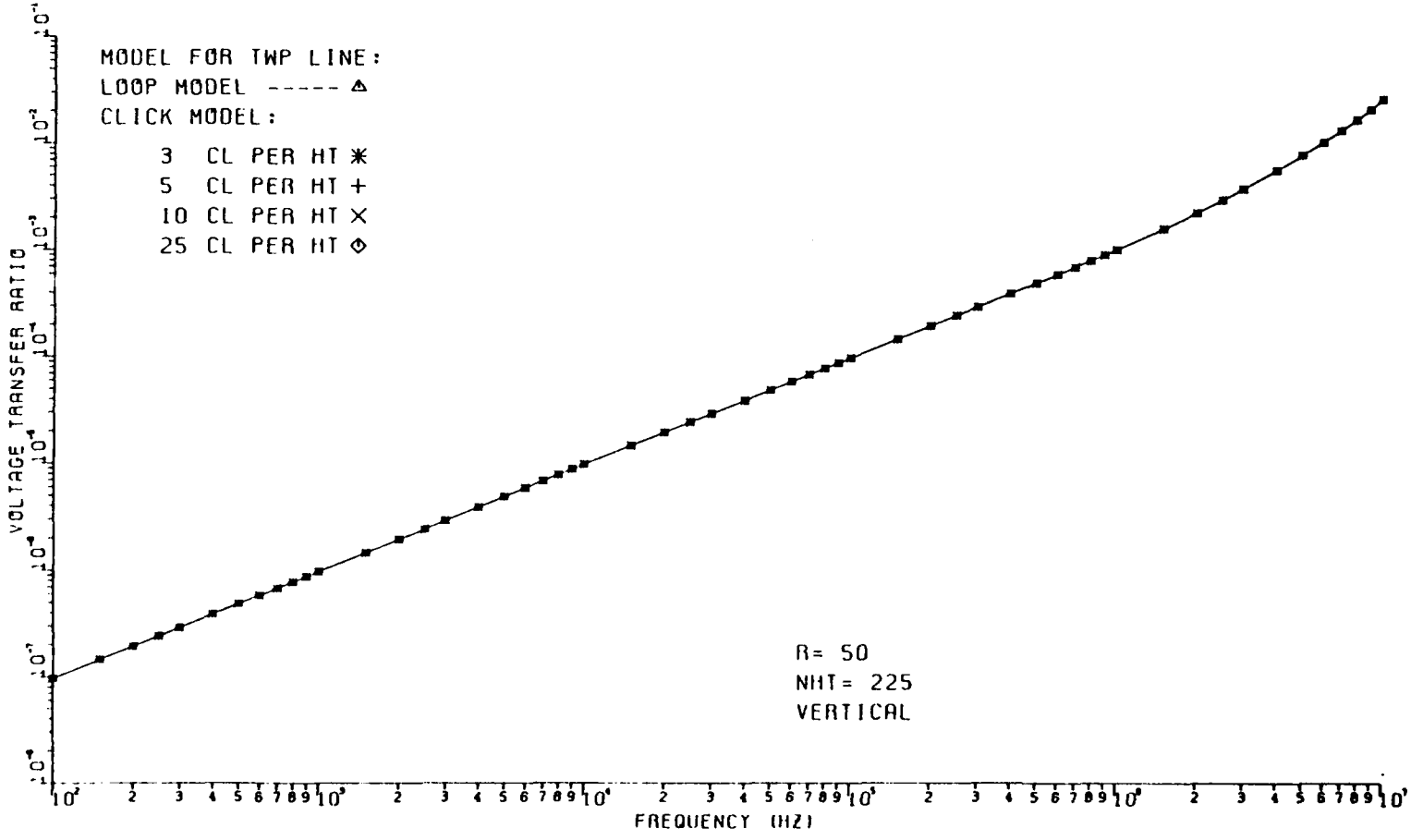
MODEL FOR TWP LINE:
LOOP MODEL ----- Δ
CLICK MODEL:
3 CL PER HT ✳
5 CL PER HT +
10 CL PER HT ×
25 CL PER HT ◇
VOLTAGE TRANSFER RATIO
FREQUENCY (HZ)
R= 50
NHT= 225
VERTICAL

Fig. 3-21

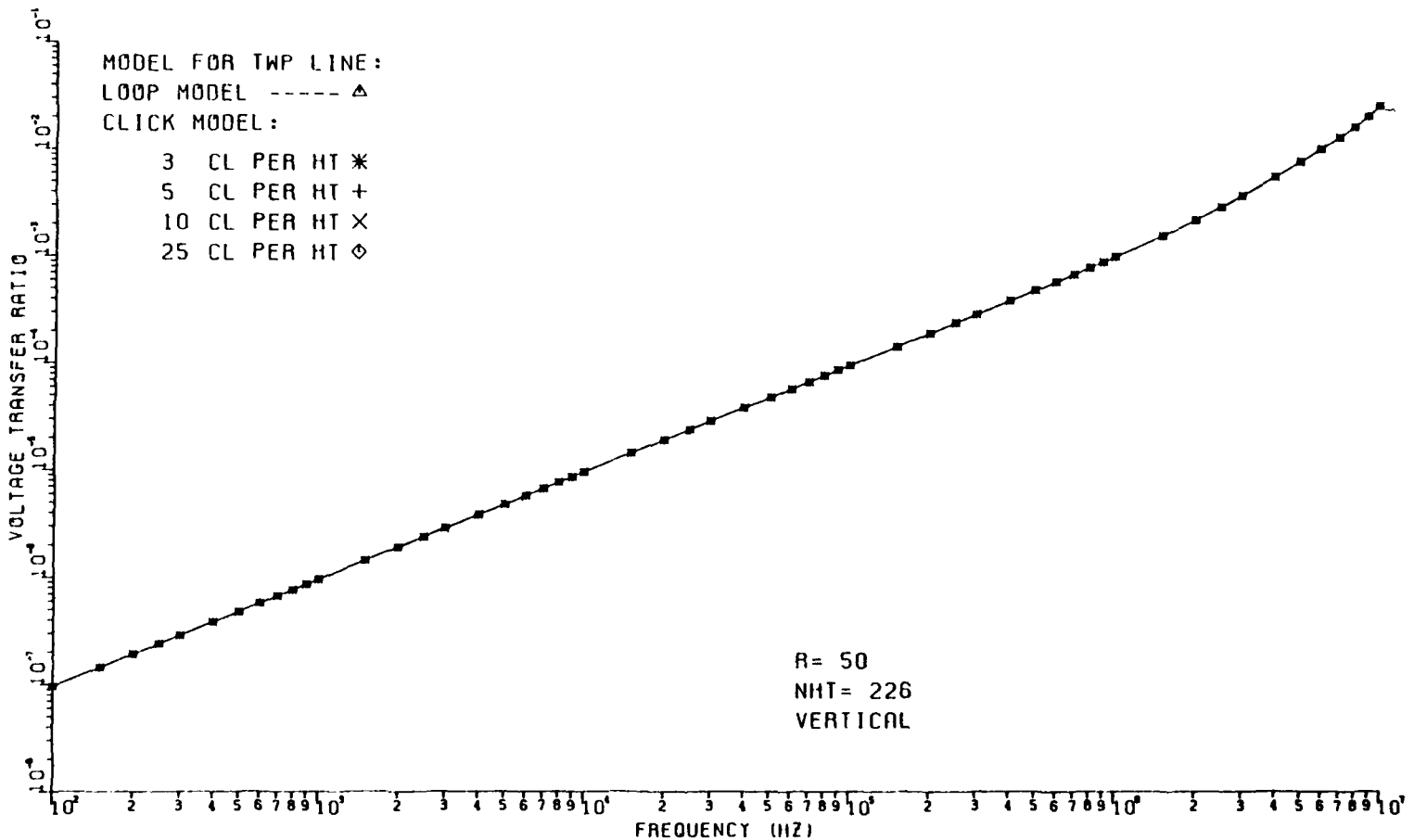
MODEL FOR TWP LINE:
LOOP MODEL ----- Δ
CLICK MODEL:
3 CL PER HT ✳
5 CL PER HT +
10 CL PER HT ×
25 CL PER HT ◇
VOLTAGE TRANSFER RATIO
FREQUENCY (HZ)
R= 50
NHT= 226
VERTICAL

Fig. 3-22

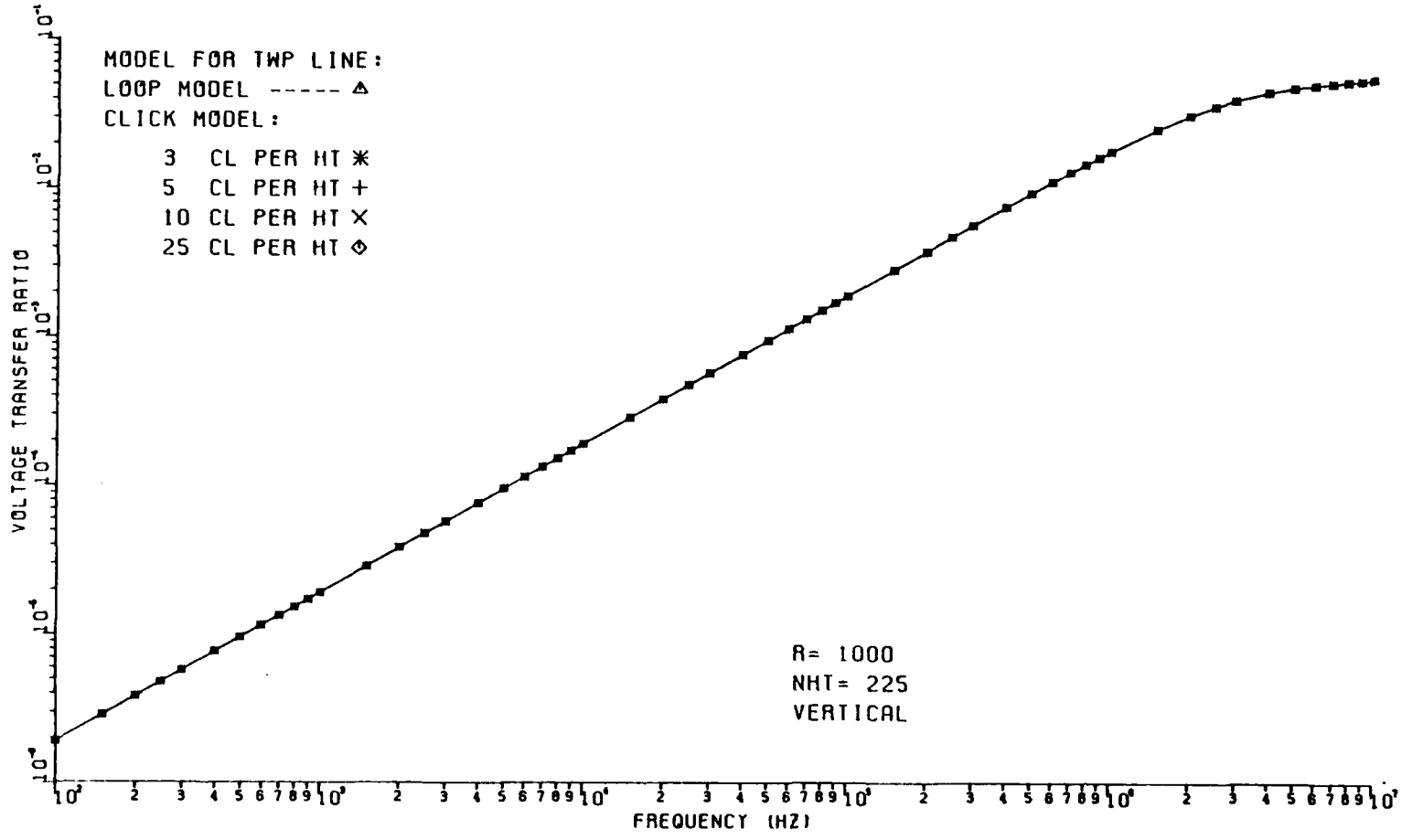
MODEL FOR TWP LINE:
LOOP MODEL ----- Δ
CLICK MODEL:
3 CL PER HT ✳
5 CL PER HT +
10 CL PER HT ×
25 CL PER HT ◇
VOLTAGE TRANSFER RATIO
FREQUENCY (HZ)
R= 1000
NHT= 225
VERTICAL

Fig. 3-23

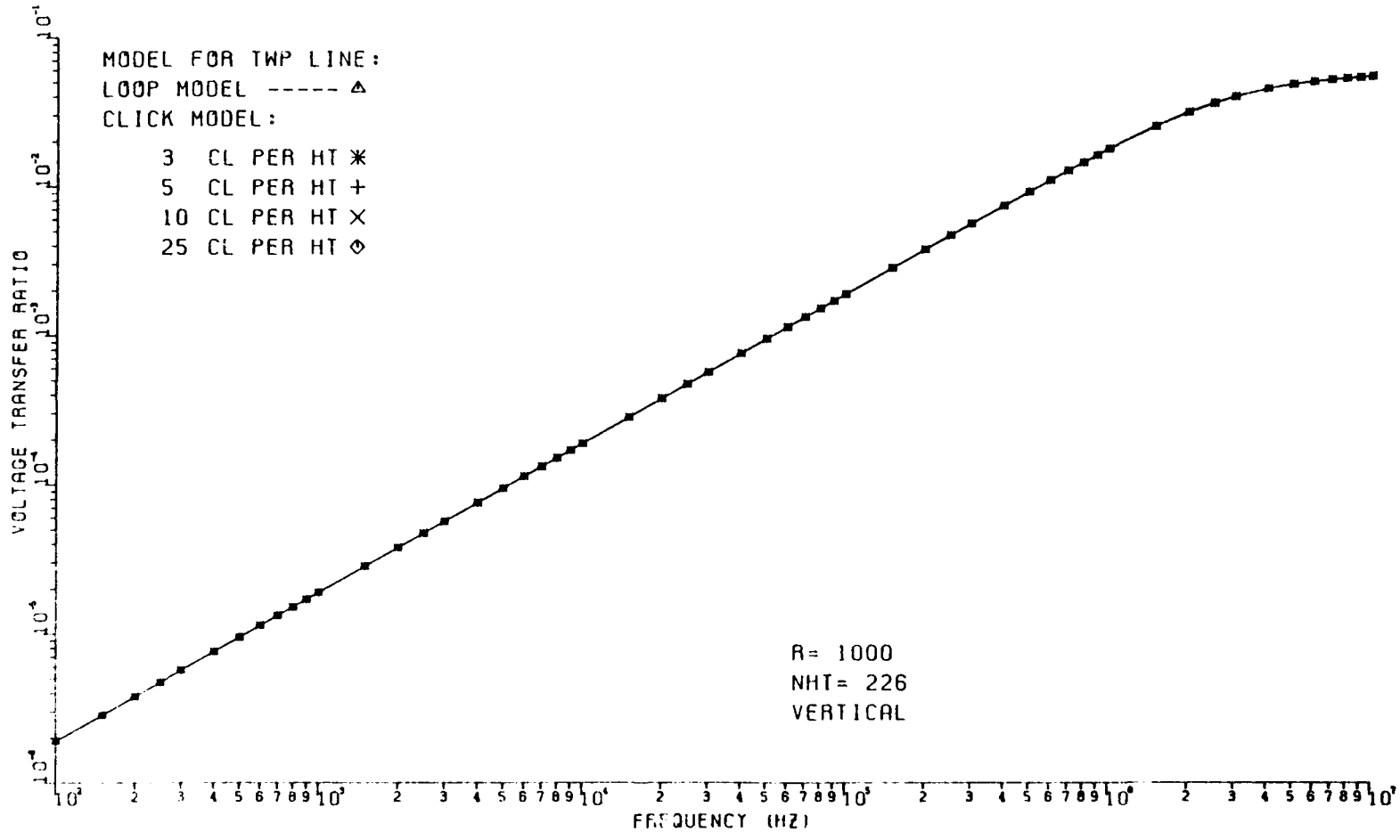
MODEL FOR TWP LINE:
LOOP MODEL ----- △
CLICK MODEL:
3 CL PER HT ✳
5 CL PER HT +
10 CL PER HT ×
25 CL PER HT ◇
VOLTAGE TRANSFER RATIO
FREQUENCY (HZ)
R= 1000
NHT= 226
VERTICAL

Fig. 3-24

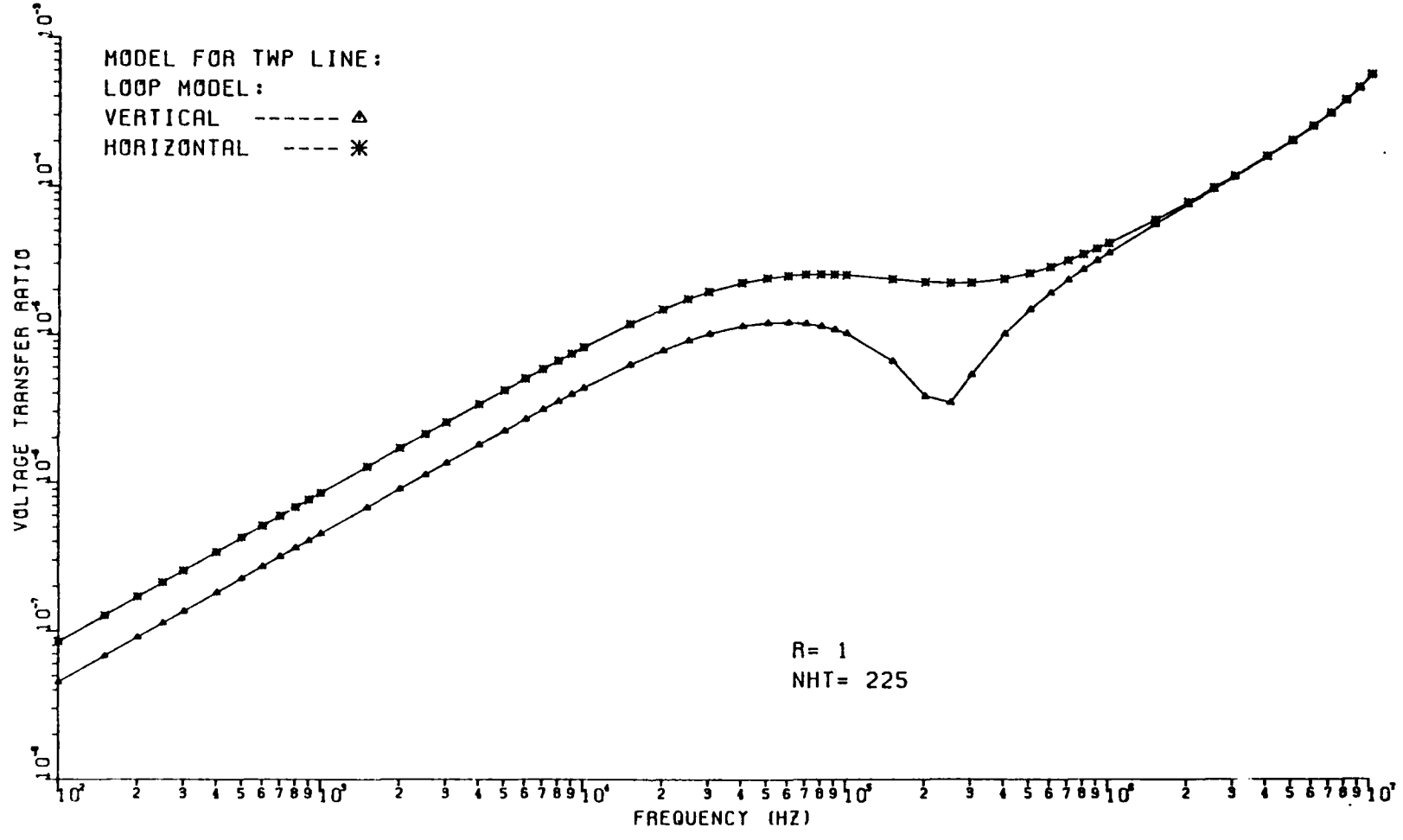
MODEL FOR TWP LINE:
LOOP MODEL:
VERTICAL ------ △
HORIZONTAL ---- ✳
VOLTAGE TRANSFER RATIO
FREQUENCY (HZ)
R= 1
NHT= 225

Fig. 3-25

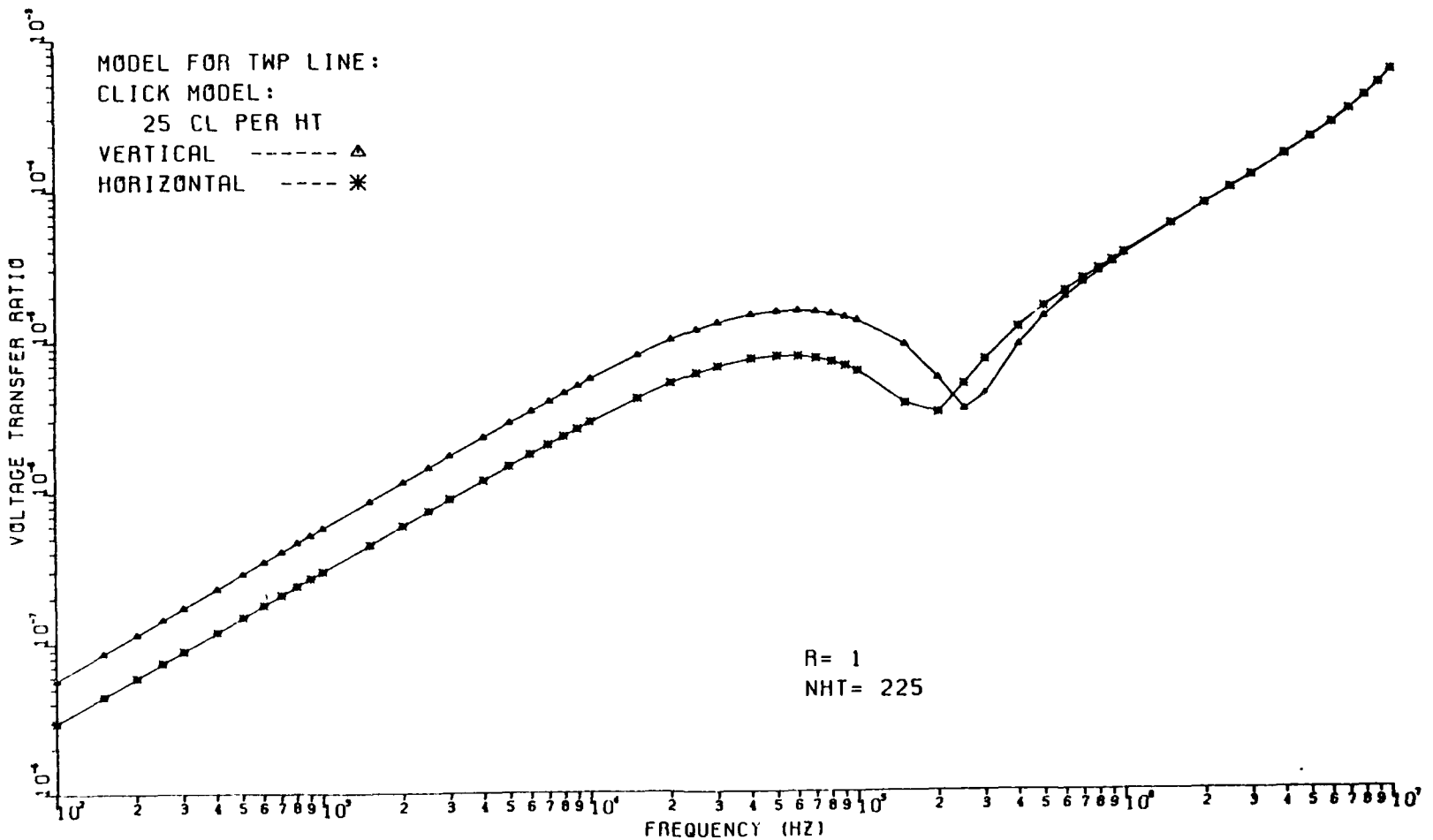
MODEL FOR TWP LINE:
CLICK MODEL:
25 CL PER HT
VERTICAL ------ Δ
HORIZONTAL ---- ✳
VOLTAGE TRANSFER RATIO
FREQUENCY (HZ)
R= 1
NHT= 225

Fig. 3-26

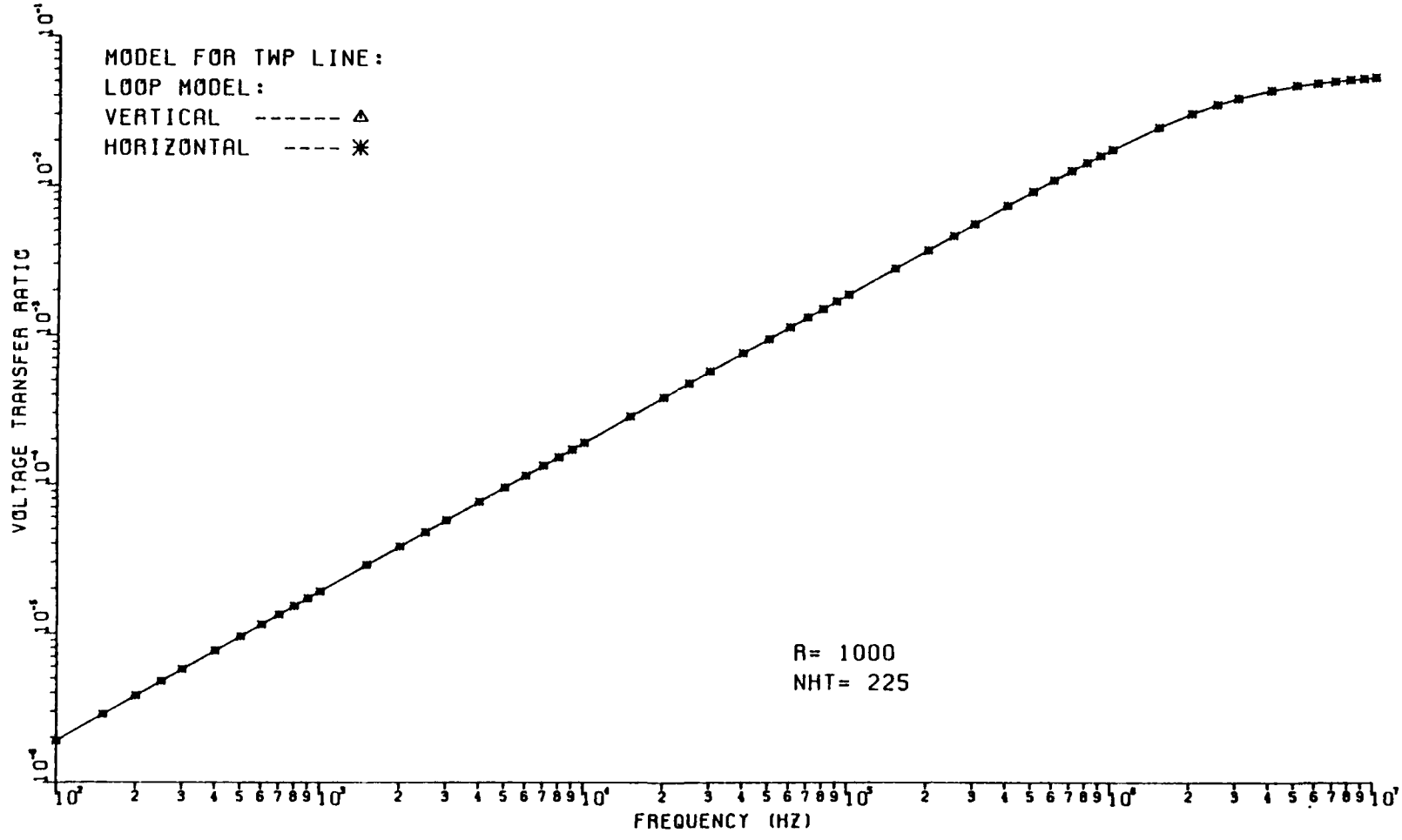
MODEL FOR TWP LINE:
LOOP MODEL:
VERTICAL ------ Δ
HORIZONTAL ---- ✳
VOLTAGE TRANSFER RATIO
FREQUENCY (HZ)
R= 1000
NHT= 225

Fig. 3-27

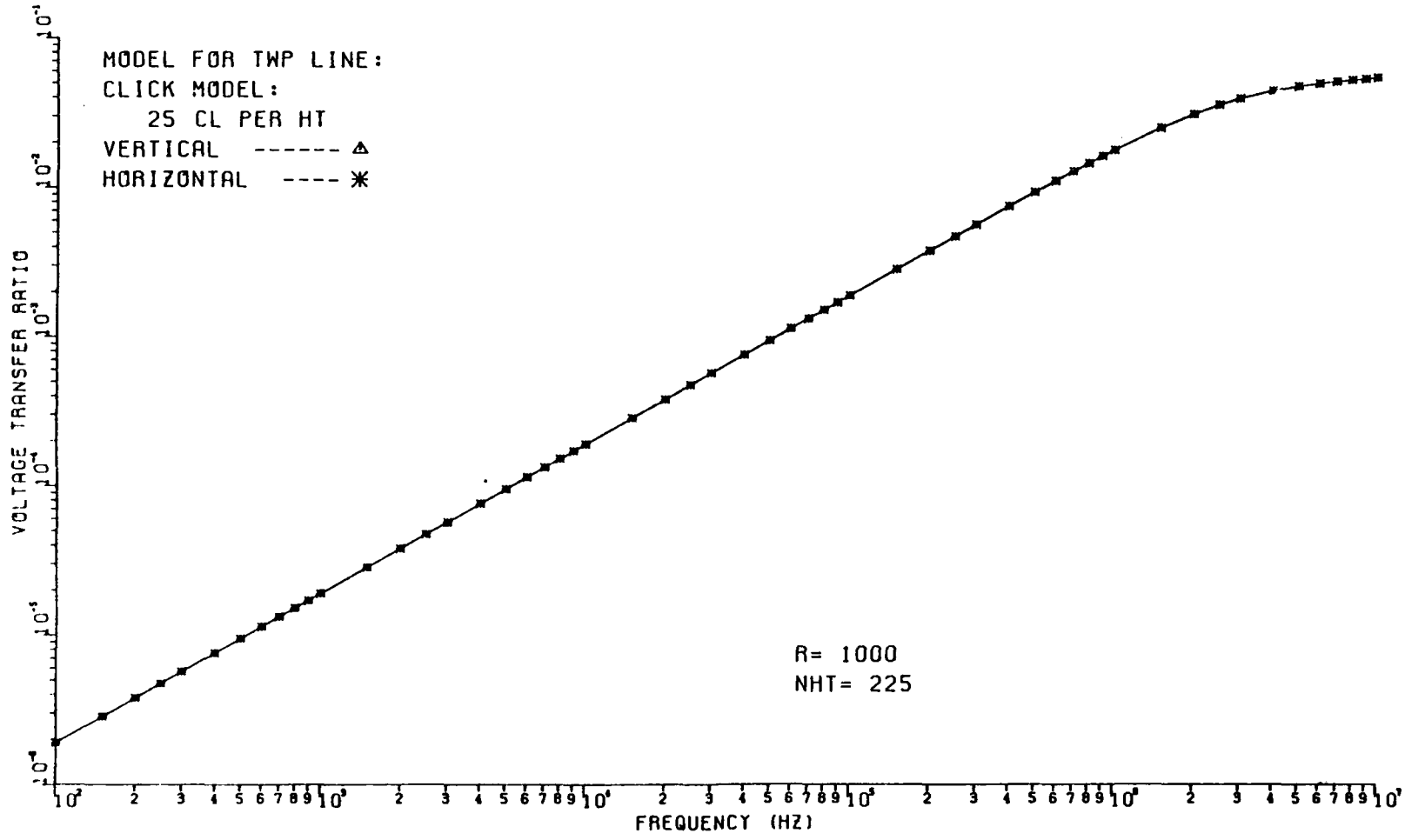
MODEL FOR TWP LINE:
CLICK MODEL:
25 CL PER HT
VERTICAL ------ Δ
HORIZONTAL ---- ✳
VOLTAGE TRANSFER RATIO
FREQUENCY (HZ)
R= 1000
NHT= 225

Fig. 3-28

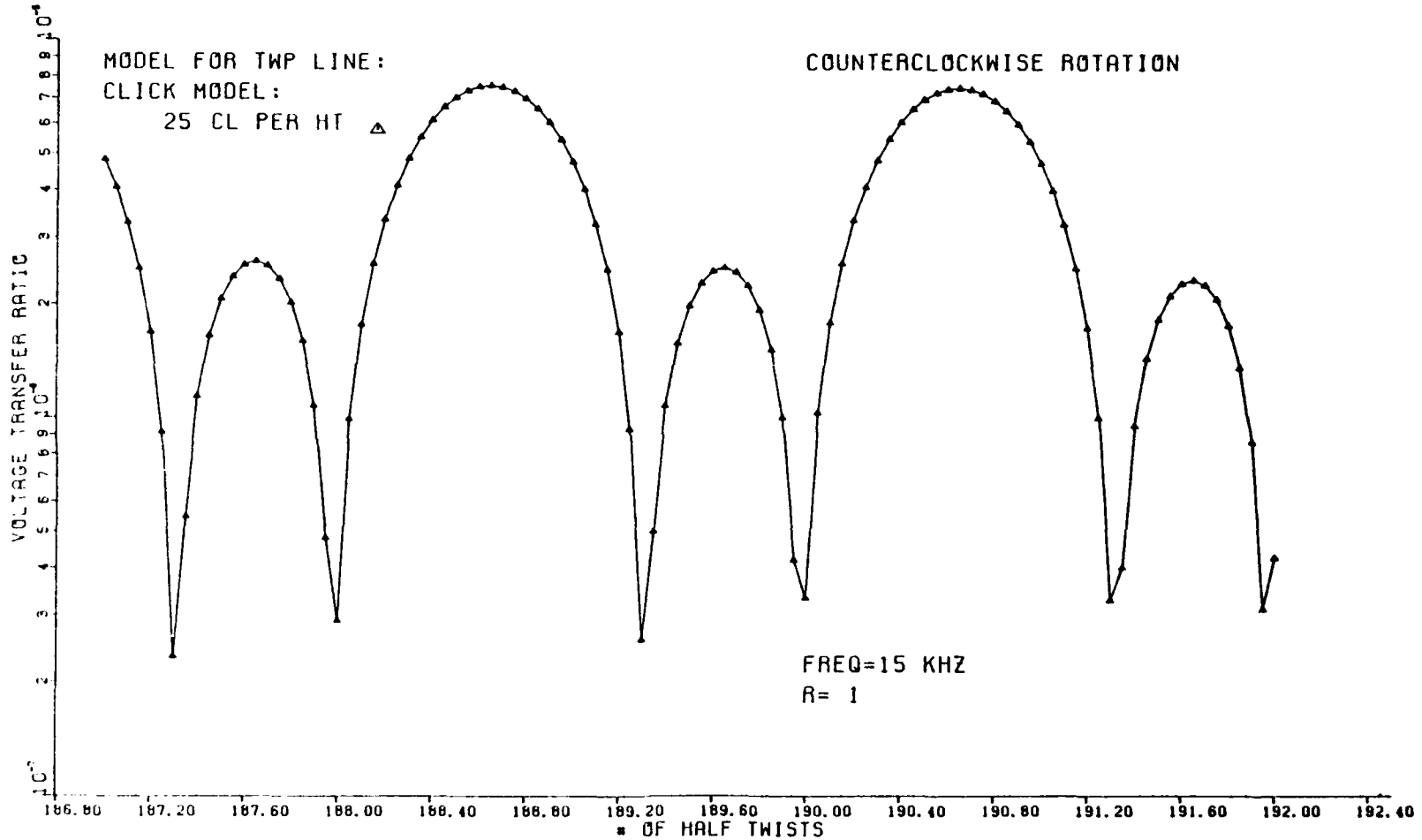
MODEL FOR TWP LINE:
CLICK MODEL:
25 CL PER HT
COUNTERCLOCKWISE ROTATION
FREQ=15 KHZ
R= 1
VOLTAGE TRANSFER RATIO
OF HALF TWISTS
186.80
187.20
187.60
188.00
188.40
188.80
189.20
189.60
190.00
190.40
190.80
191.20
191.60
192.00
192.40

Fig. 3-29

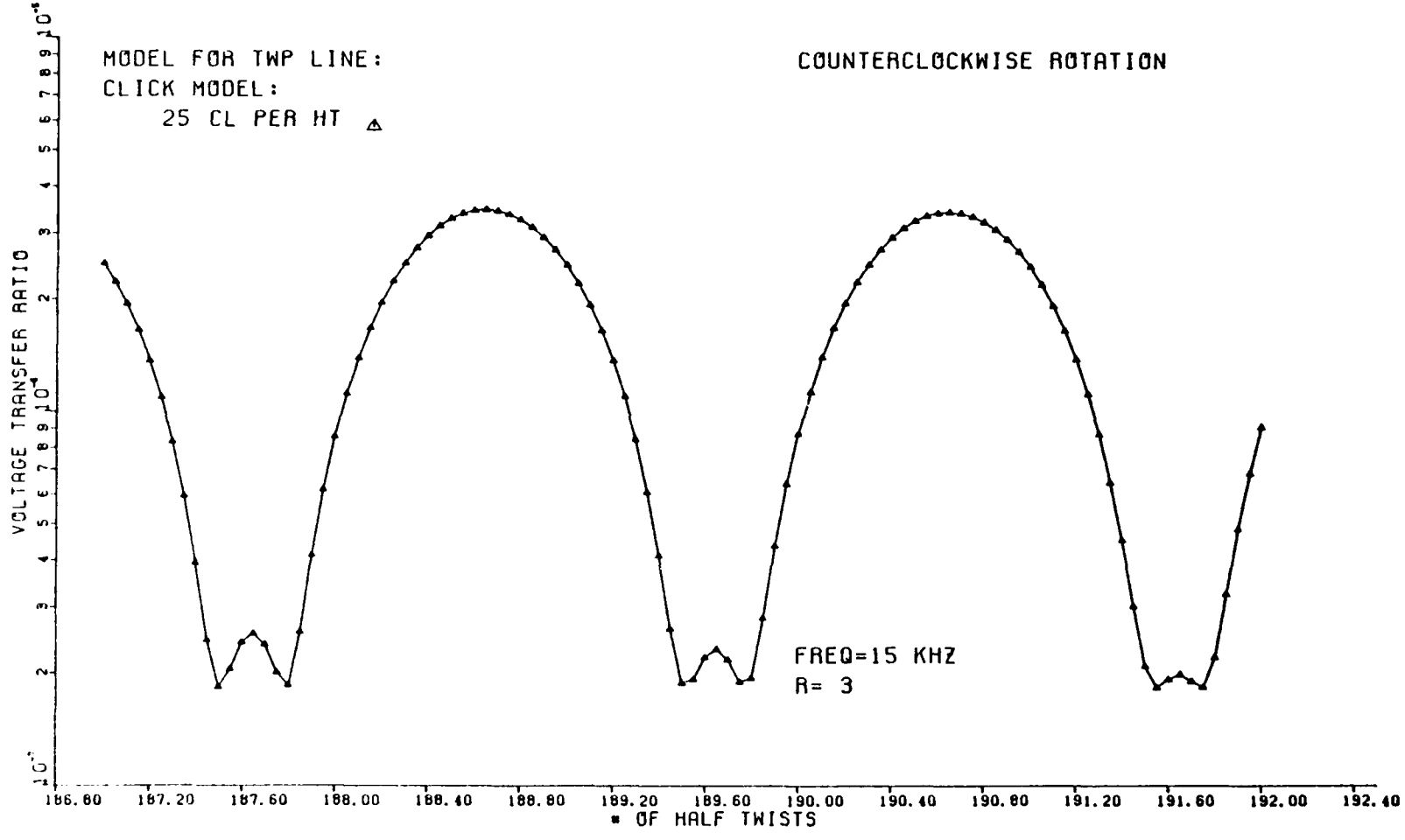
MODEL FOR TWP LINE:
CLICK MODEL:
25 CL PER HT
COUNTERCLOCKWISE ROTATION
VOLTAGE TRANSFER RATIO
FREQ=15 KHZ
R= 3
186.80
187.20
187.60
188.00
188.40
188.80
189.20
189.60
190.00
190.40
190.80
191.20
191.60
192.00
192.40
OF HALF TWISTS

Fig. 3-30

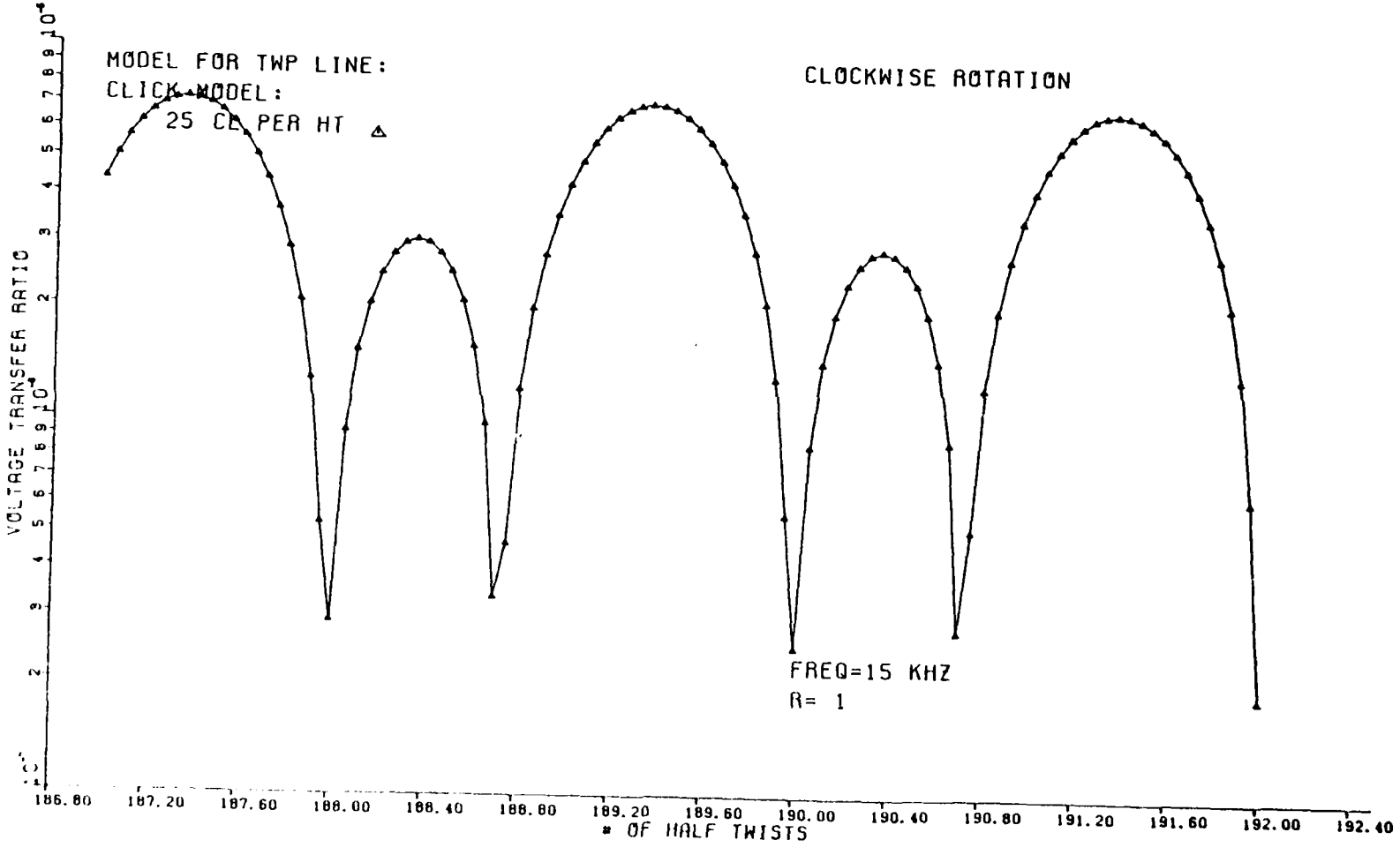
MODEL FOR TWP LINE:
CLICK MODEL:
25 CL PER HT
CLOCKWISE ROTATION
FREQ=15 KHZ
R= 1
VOLTAGE TRANSFER RATIO
OF HALF TWISTS
186.80
187.20
187.60
188.00
188.40
188.80
189.20
189.60
190.00
190.40
190.80
191.20
191.60
192.00
192.40

Fig. 3-31

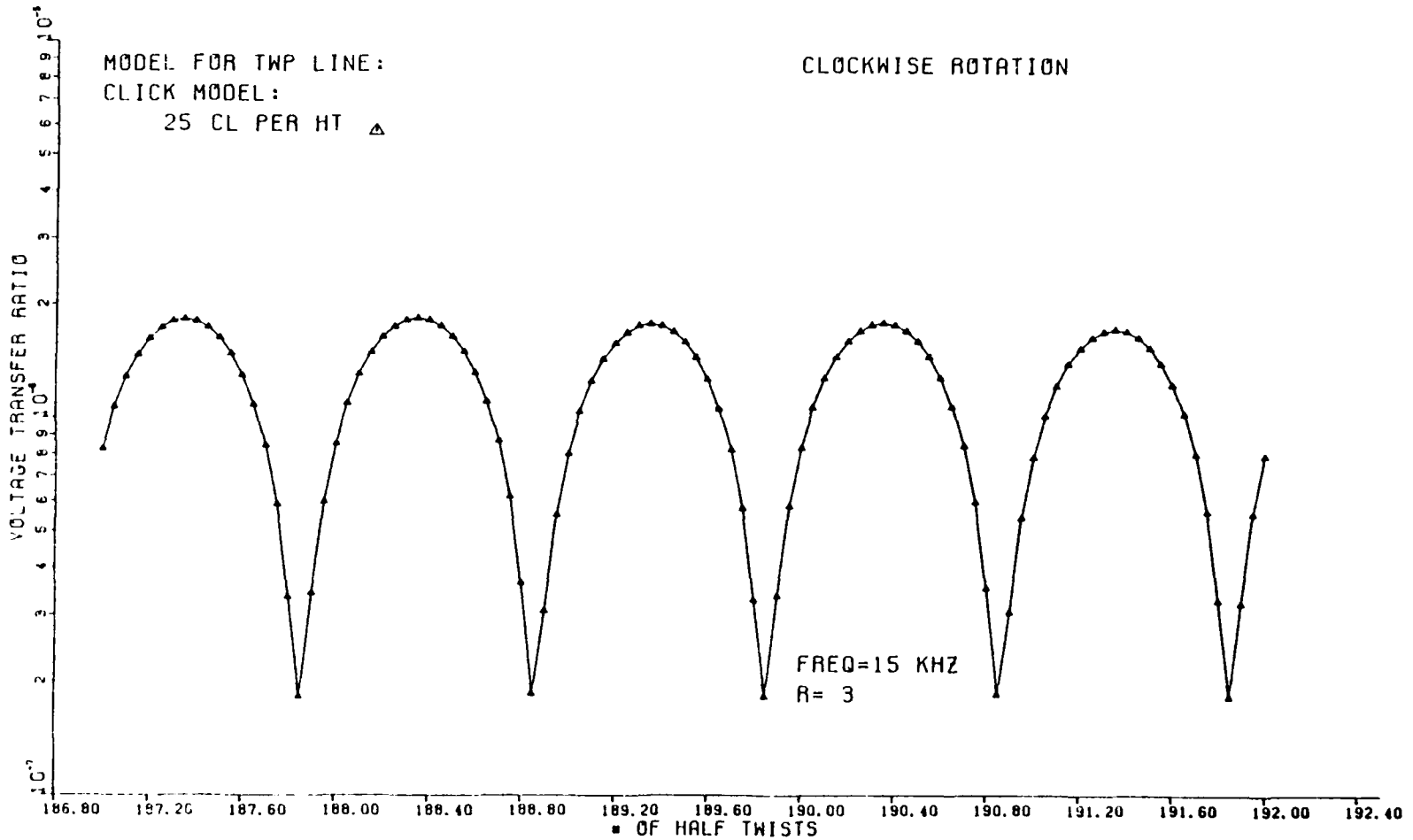
MODEL FOR TWP LINE:
CLICK MODEL:
25 CL PER HT
CLOCKWISE ROTATION
VOLTAGE TRANSFER RATIO
FREQ=15 KHZ
R= 3
186.80
187.20
187.60
188.00
188.40
188.80
189.20
189.60
190.00
190.40
190.80
191.20
191.60
192.00
192.40
OF HALF TWISTS

Fig. 3-32

IV. PREDICTING THE COMMON MODE VOLTAGE OF THE TWP TERMINATED IN A DIFFERENTIAL LINE DRIVER AND DIFFERENTIAL LINE RECEIVER

Most of the digital data used for communication between electronic systems, and subsystems, are transmitted via differential line drivers (DLD) and differential line receivers (DLR) when they are connected to the TWP in the balanced configuration shown in Fig. 4-1. A pair of transmission lines carries the digital signal produced by the DLD to the DLR where the digital logic of the signal is examined. The transmission lines are normally twisted to reduce differential mode coupling to the system. As is shown theoretically in the sensitivity analysis, twisting the lines does not necessarily reduce common mode coupling to the lines. This coupled noise signal, common to both lines, appears at the inputs of the DLR. Although the DLR has a high common mode rejection ratio (CMRR), false data can be interpreted if the common mode noise signal is too large in magnitude. The balanced load configuration for the TWP is investigated to see if the common mode voltage coupled to the TWP can be accurately predicted when the TWP is modeled as a SW and terminated in a DLD and DLR.

Common mode coupling is considered in this analysis because it is less sensitive to the number of twists in the TWP than differential mode coupling and should therefore, be easier to measure with consistent results. As shown in the sensitivity analysis, the differential mode voltage coupled

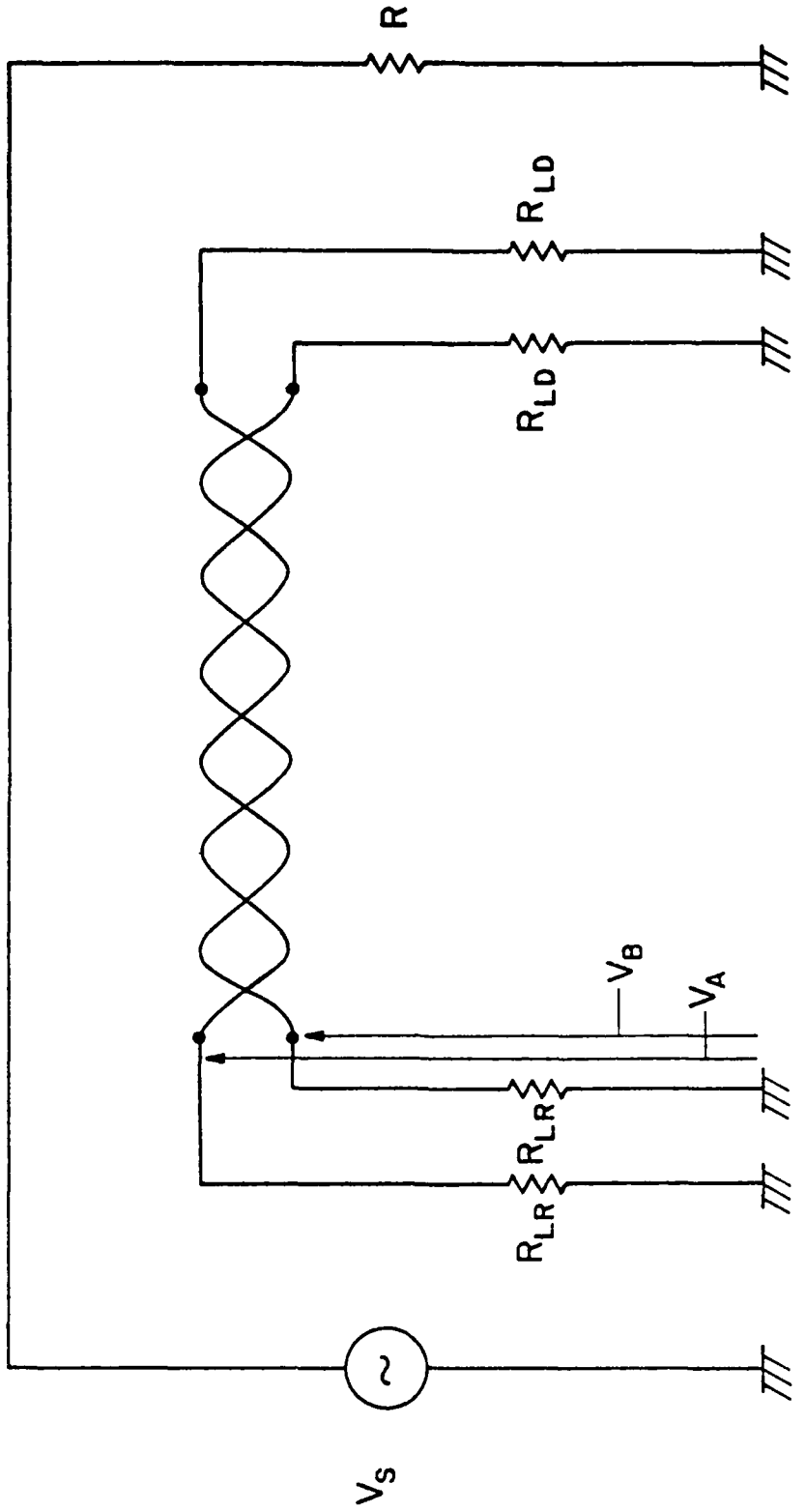

Fig. 4-1

to a twisted pair of lines is very sensitive to the number of twists in the TWP when the line termination impedances are low in magnitude. Any prediction of the differential mode voltage coupled to a TWP would probably be unreliable (from an application point of view) because line twist is difficult to monitor and control when installing the TWP. Common mode voltage coupling to the TWP should be stable with respect to line twist since this coupling is proportional to wire position above the ground plane. As a result of the stability of the common mode voltage coupled to a TWP, experimental results are reproducible with little noise deterioration and the predictions of the common mode VTR prove to be quite accurate.

The balanced TWP configuration shown in Fig. 4-1 was constructed above the aluminum ground plane. The wire height, length, and radius were the same as they were in the sensitivity analysis. The driver and receiver were Texas Instrument SN75114 and SN75115, respectively. The DLD and DLR were mounted on brackets to provide access to their output pins (Fig. 4-2). Both the DLD and DLR are TTL compatible. The DLD converts a common mode digital signal to a differential mode signal which is transmitted between the two wires of the TWP. The output stages of the DLD are similar to TTL totem-pole outputs, and provide both AND and NAND output logic of the input signal. The DLR converts the differential mode digital input voltage to a common mode digital signal. It also provides an internal 130 ohm

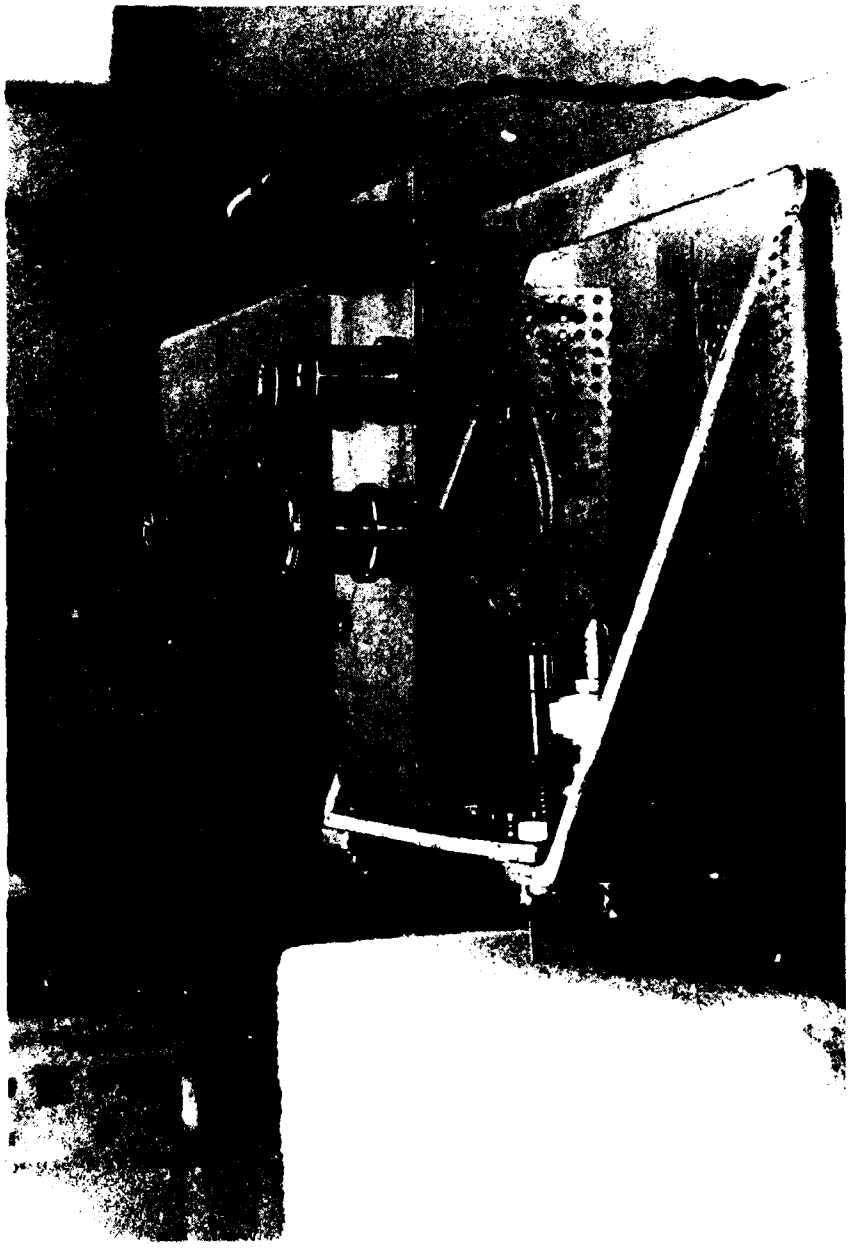

Fig. 4-2a

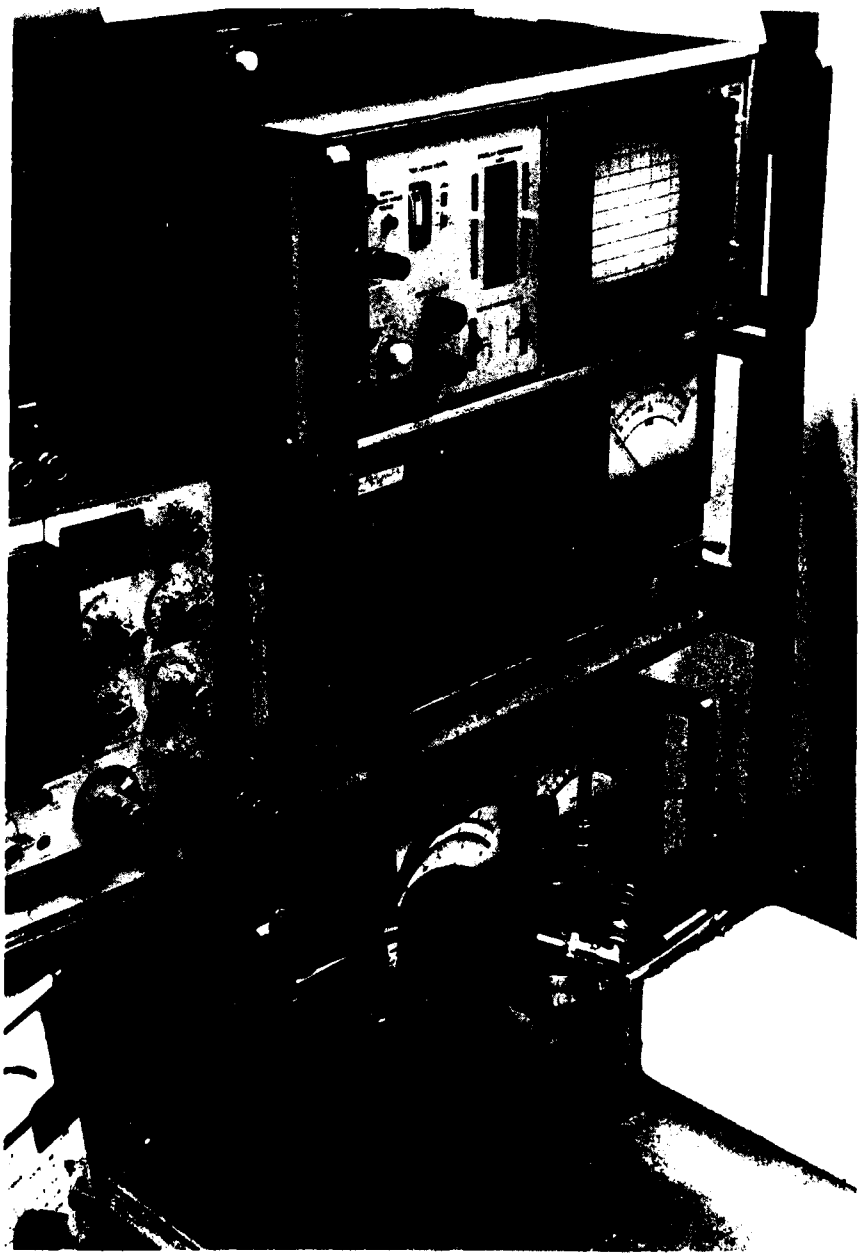

Fig. 4-2b

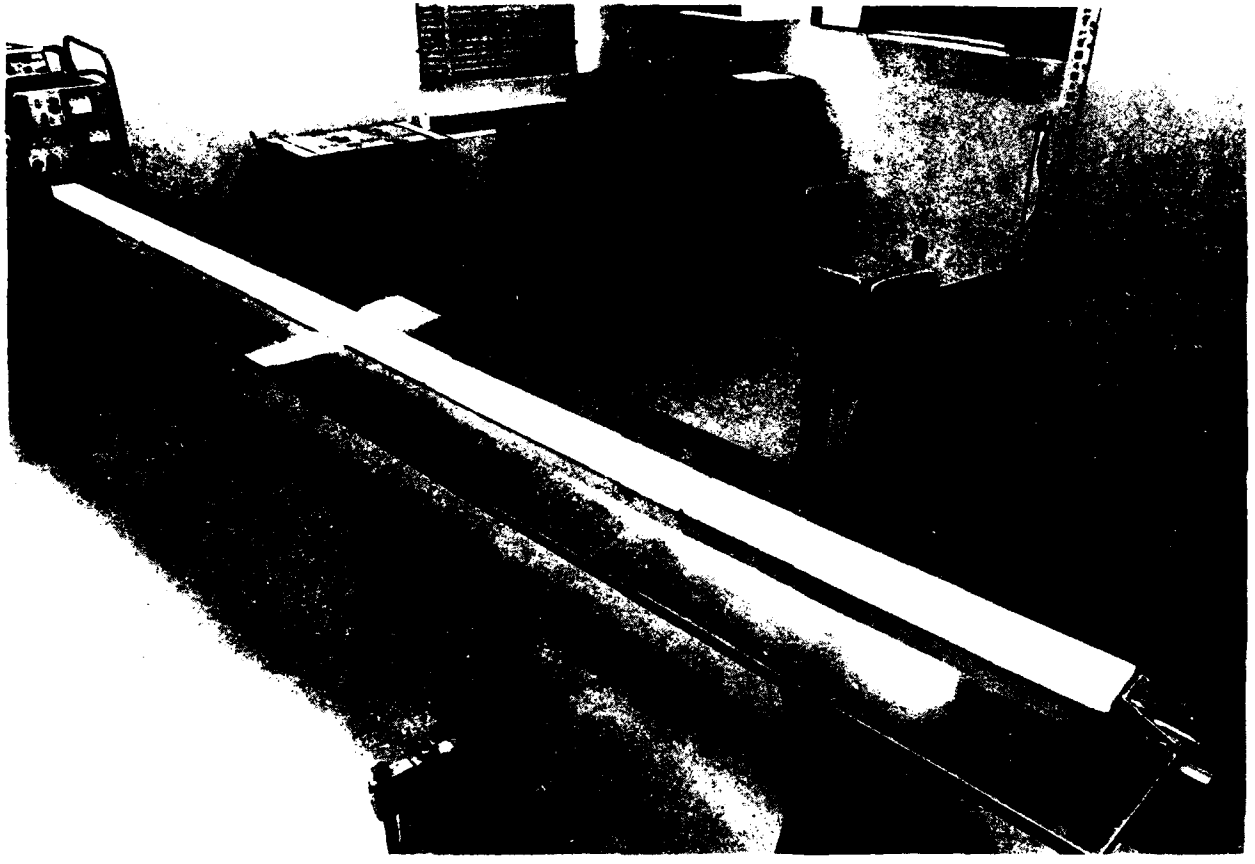

Fig. 4-2c

resistor at its input stage for matching of the TL. A switch was mounted on the line receiver bracket so the 130 ohm resistor, internal to the DLR, could be placed across the end of the TWP when the switch was closed.

Resistive loads (attached to the generator line) of 50 ohms and 1k ohms were used in this experiment. The common mode voltages V_A and V_B at the input to the DLR (see Fig. 1-7 and 4-1) were measured with and without the 130 ohm resistor across the TWP. The input to the DLD was held at a constant voltage while the measurements were taken. Measurements were made over the range of frequencies from 100 Hz to 100 MHz in steps of 1, 1.5, 2, 2.5,3, 4, 5, 6, 7, 8, 9 in each decade. The TWP was then replaced with a SWP and the measurements of the common mode voltage at pins A and B of the DLR were repeated. Upon completion of the SWP voltage measurements, one wire of the SWP was removed and the measurements repeated again to determine the common mode voltage coupling to a single wire (SW). The experimental results are shown in Fig. 4-3 through Fig. 4-10 for the common mode voltages V_A and V_B. The common mode voltages coupled to the TWP, SWP, and SW are shown for comparison. In all three cases the coupled voltages are nearly identical. Even in the higher frequency range, the coupled common mode voltages are independent of the type of transmission line, i.e., TWP, SWP, or a SW.

From the comparison of these results it is apparent (for the length of line and the heights used) that the TWP

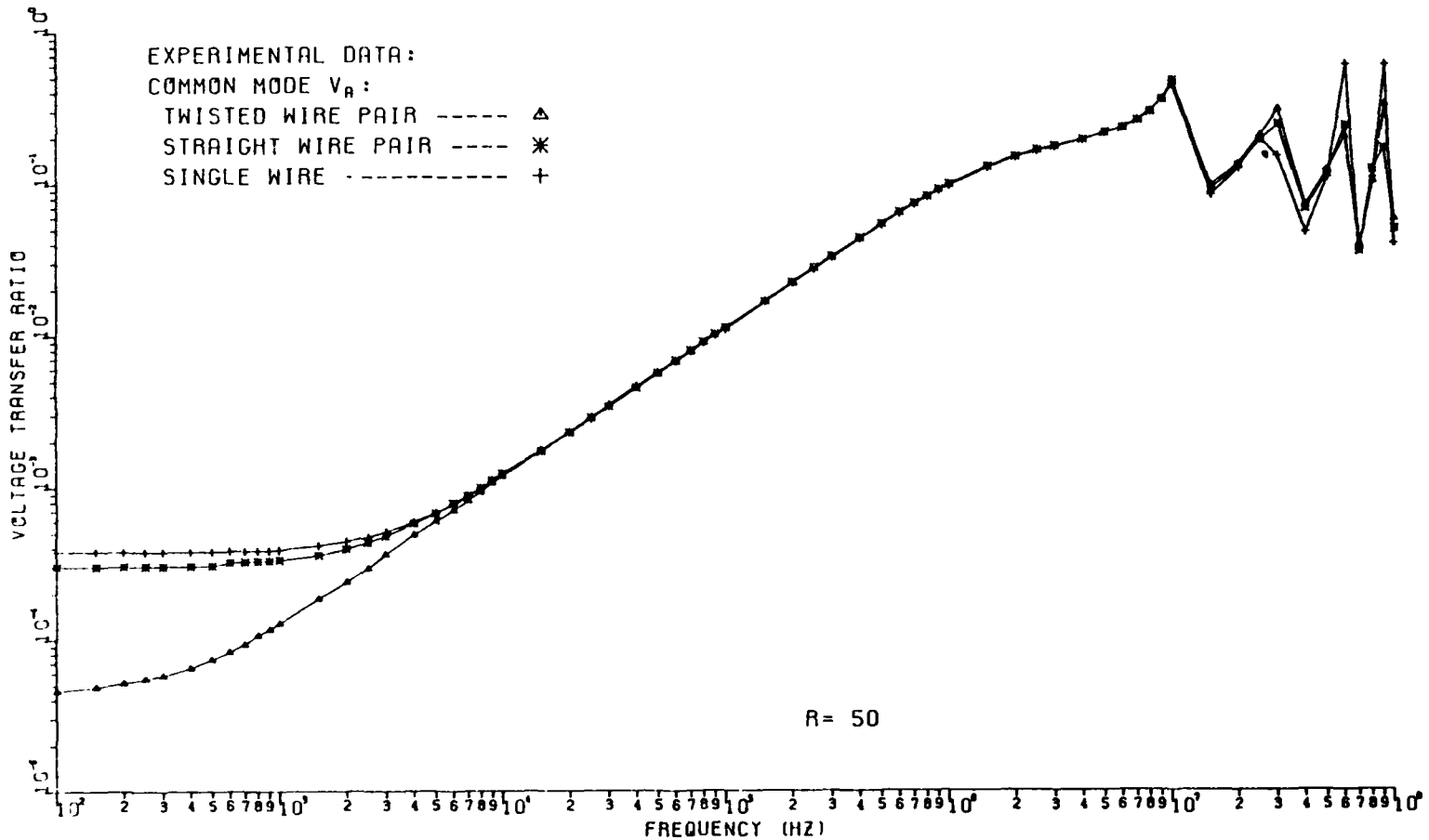
EXPERIMENTAL DATA:
COMMON MODE V_R:
TWISTED WIRE PAIR ----- △
STRAIGHT WIRE PAIR ---- ✳
SINGLE WIRE ---------- +
VOLTAGE TRANSFER RATIO
FREQUENCY (HZ)
R= 50

Fig. 4-3

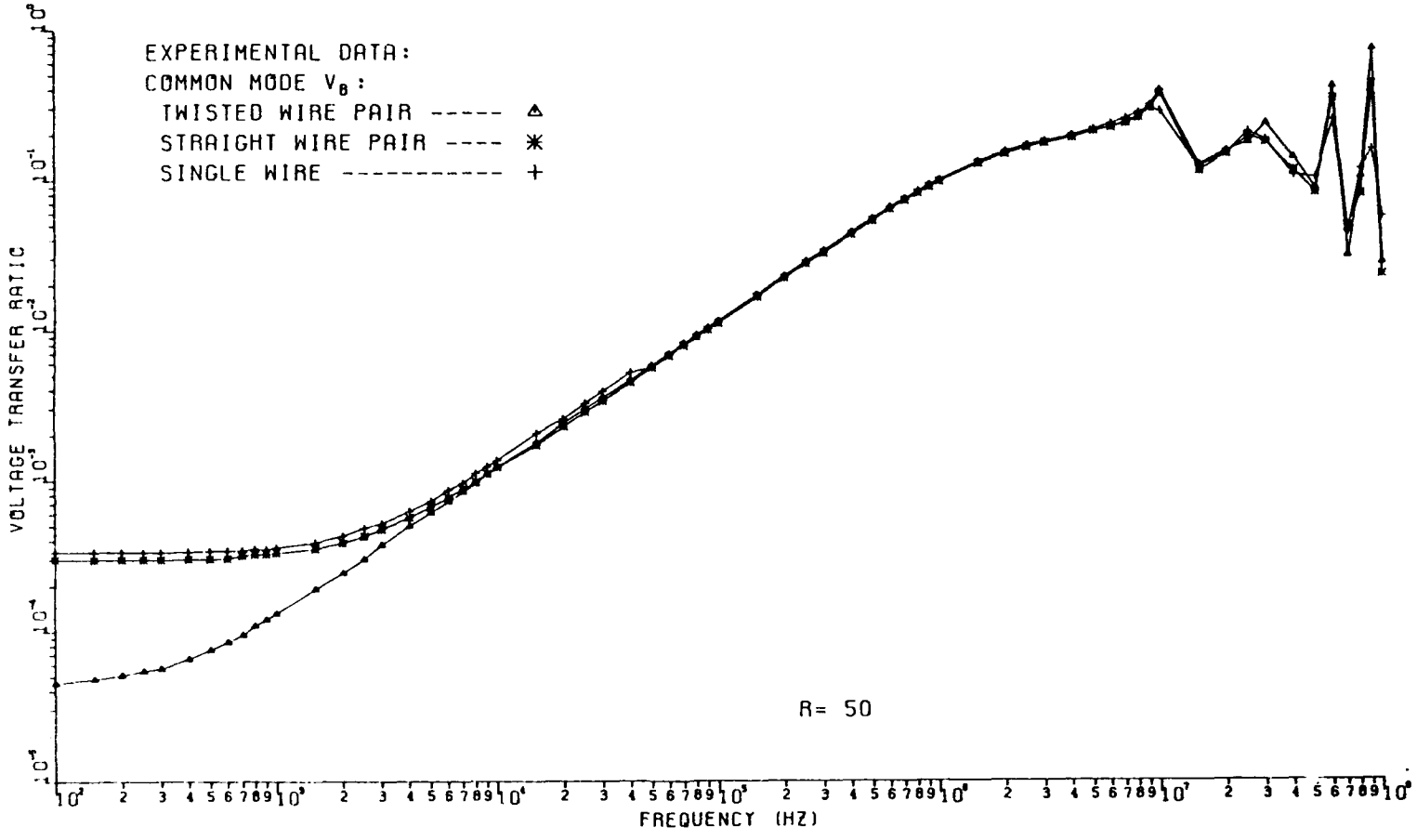
EXPERIMENTAL DATA:
COMMON MODE V_B:
TWISTED WIRE PAIR ----- Δ
STRAIGHT WIRE PAIR ---- ✳
SINGLE WIRE ---------- +
VOLTAGE TRANSFER RATIO
FREQUENCY (HZ)
R= 50

Fig. 4-4

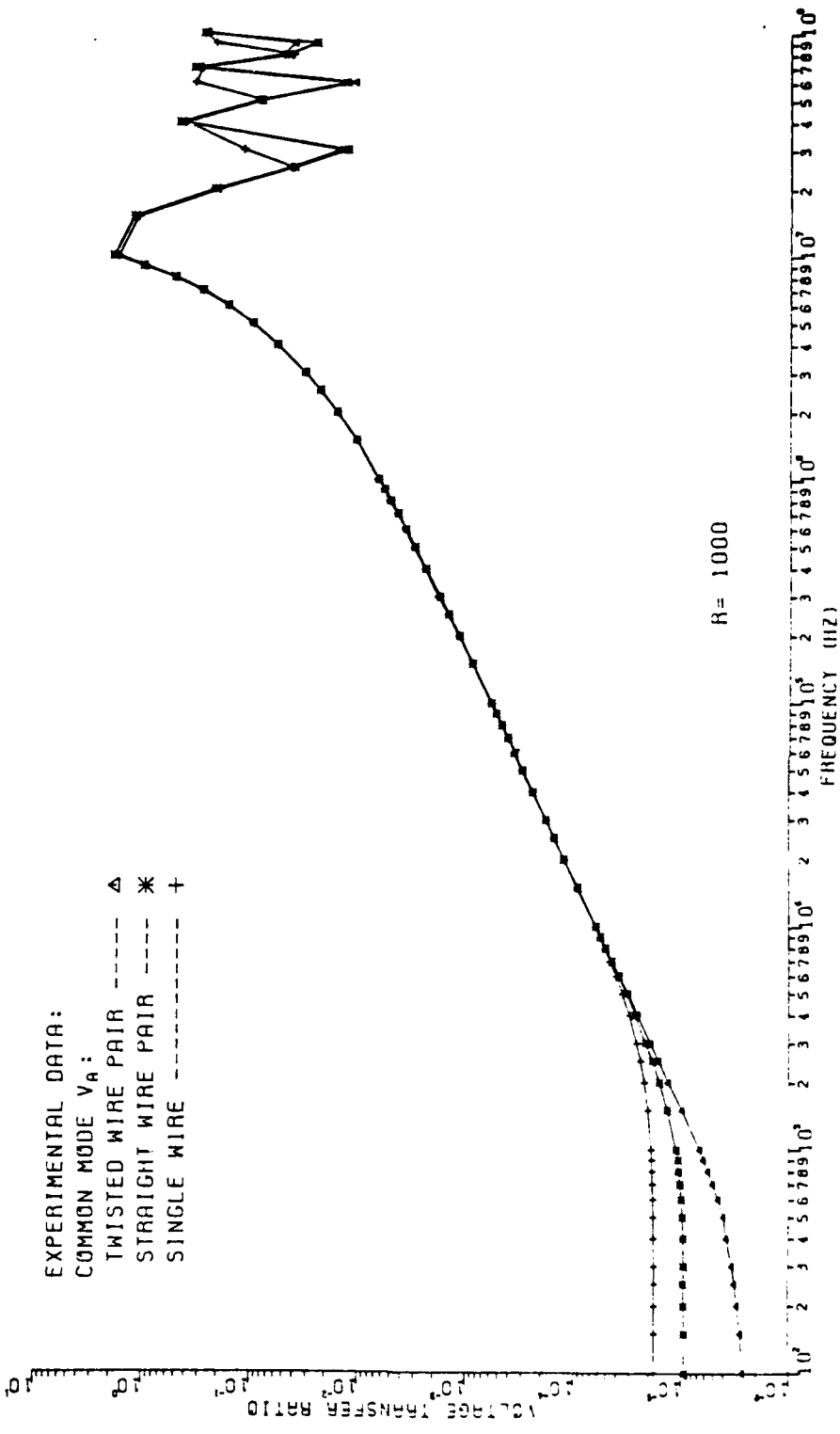
EXPERIMENTAL DATA:
COMMON MODE V_a:
TWISTED WIRE PAIR ----- Δ
STRAIGHT WIRE PAIR ---- ✱
SINGLE WIRE ---------- +
VOLTAGE TRANSFER RATIO
FREQUENCY (HZ)
R= 1000

Fig. 4-5

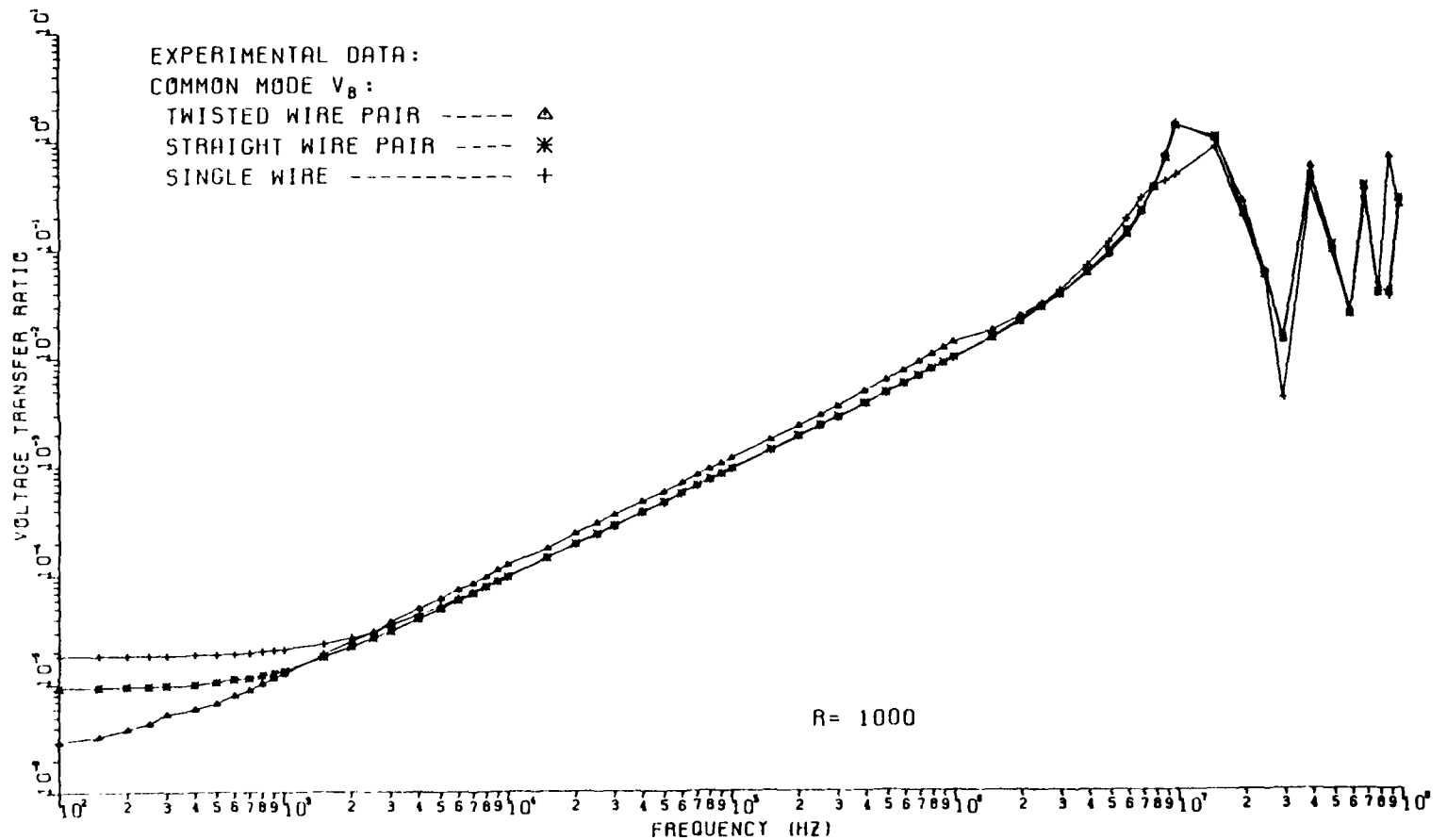
EXPERIMENTAL DATA:
COMMON MODE V_B:
TWISTED WIRE PAIR ----- △
STRAIGHT WIRE PAIR ---- ✳
SINGLE WIRE ---------- +
VOLTAGE TRANSFER RATIO
R= 1000
FREQUENCY (HZ)

Fig. 4-6

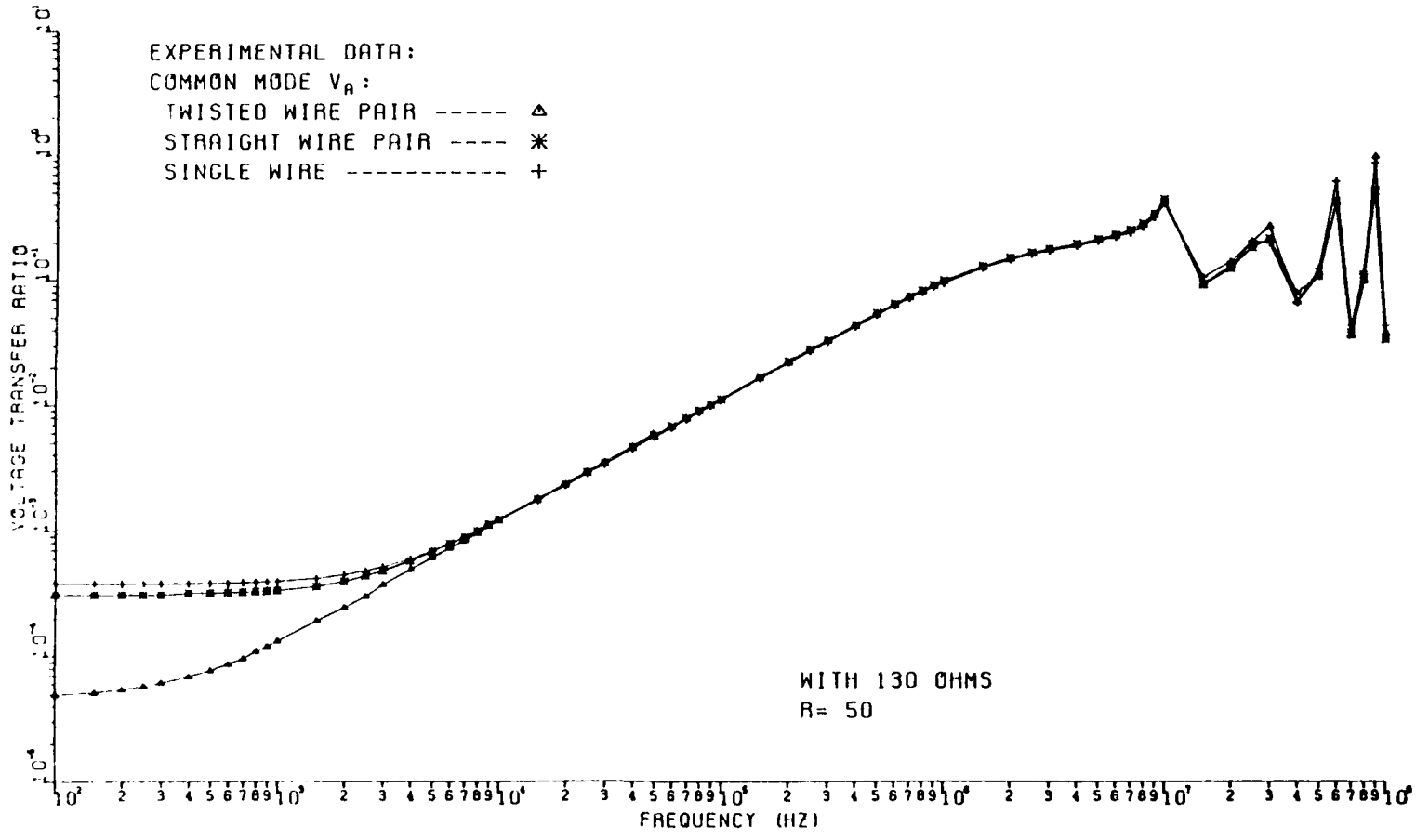
EXPERIMENTAL DATA:
COMMON MODE V_A:
TWISTED WIRE PAIR ----- Δ
STRAIGHT WIRE PAIR ---- ✳
SINGLE WIRE ---------- +
WITH 130 OHMS
R= 50
FREQUENCY (HZ)

Fig. 4-7

AD-A124 863 BASIC EMC TECHNOLOGY ADVANCEMENT FOR C(3) SYSTEMS 2/2
VOLUME IV C CROSSTALK I..(U) SOUTHEASTERN CENTER FOR
ELECTRICAL ENGINEERING EDUCATION INC S..
UNCLASSIFIED M B JOLLY ET AL. NOV 82 F/G 9/3 NL

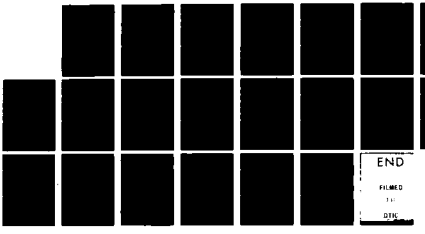

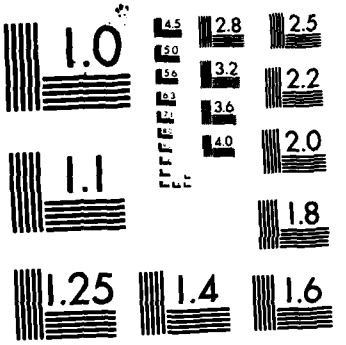

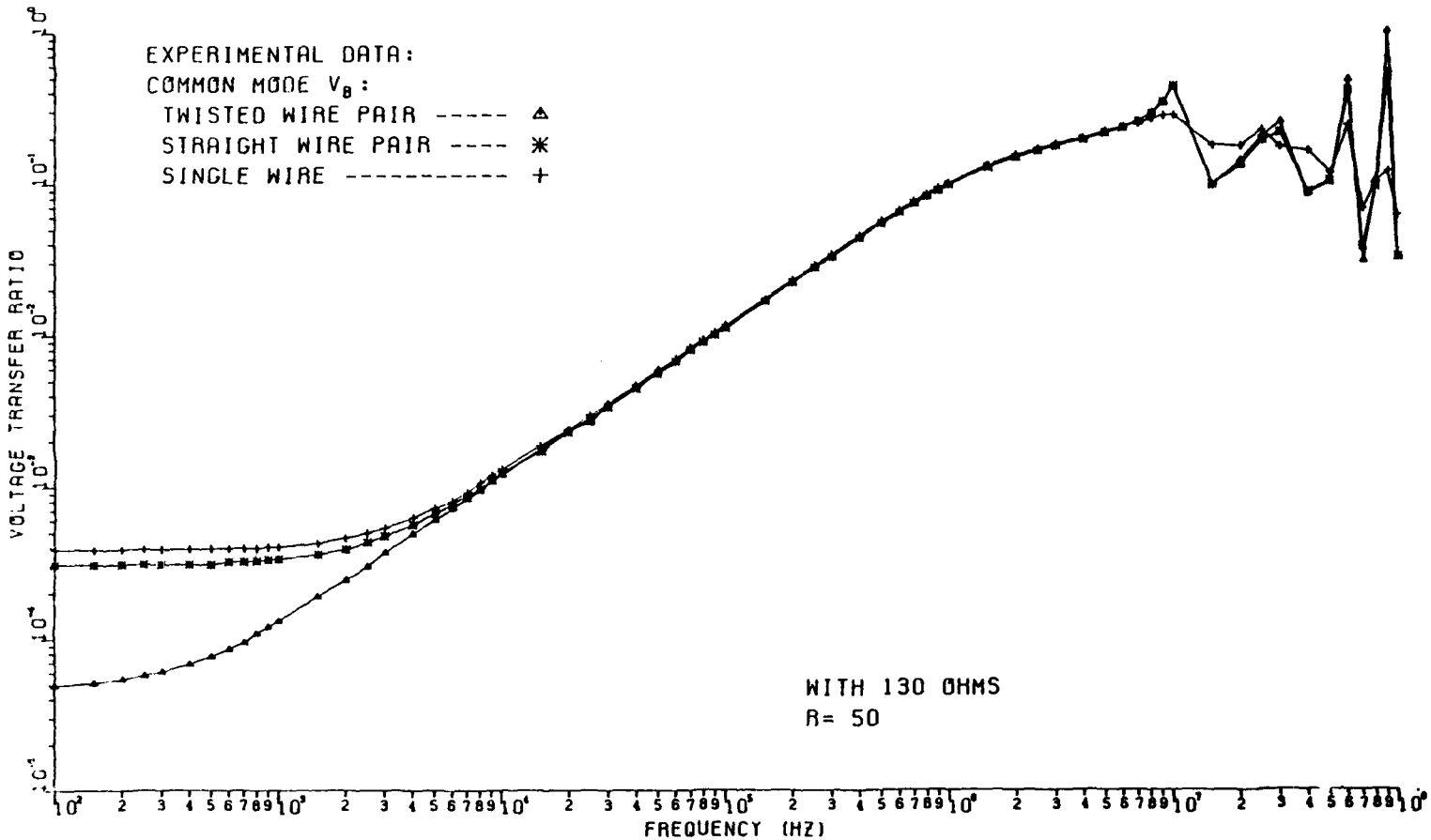
EXPERIMENTAL DATA:
COMMON MODE V_B:
TWISTED WIRE PAIR ----- △
STRAIGHT WIRE PAIR ---- ✳
SINGLE WIRE ---------- +
WITH 130 OHMS
R= 50
VOLTAGE TRANSFER RATIO
FREQUENCY (HZ)

Fig. 4-8

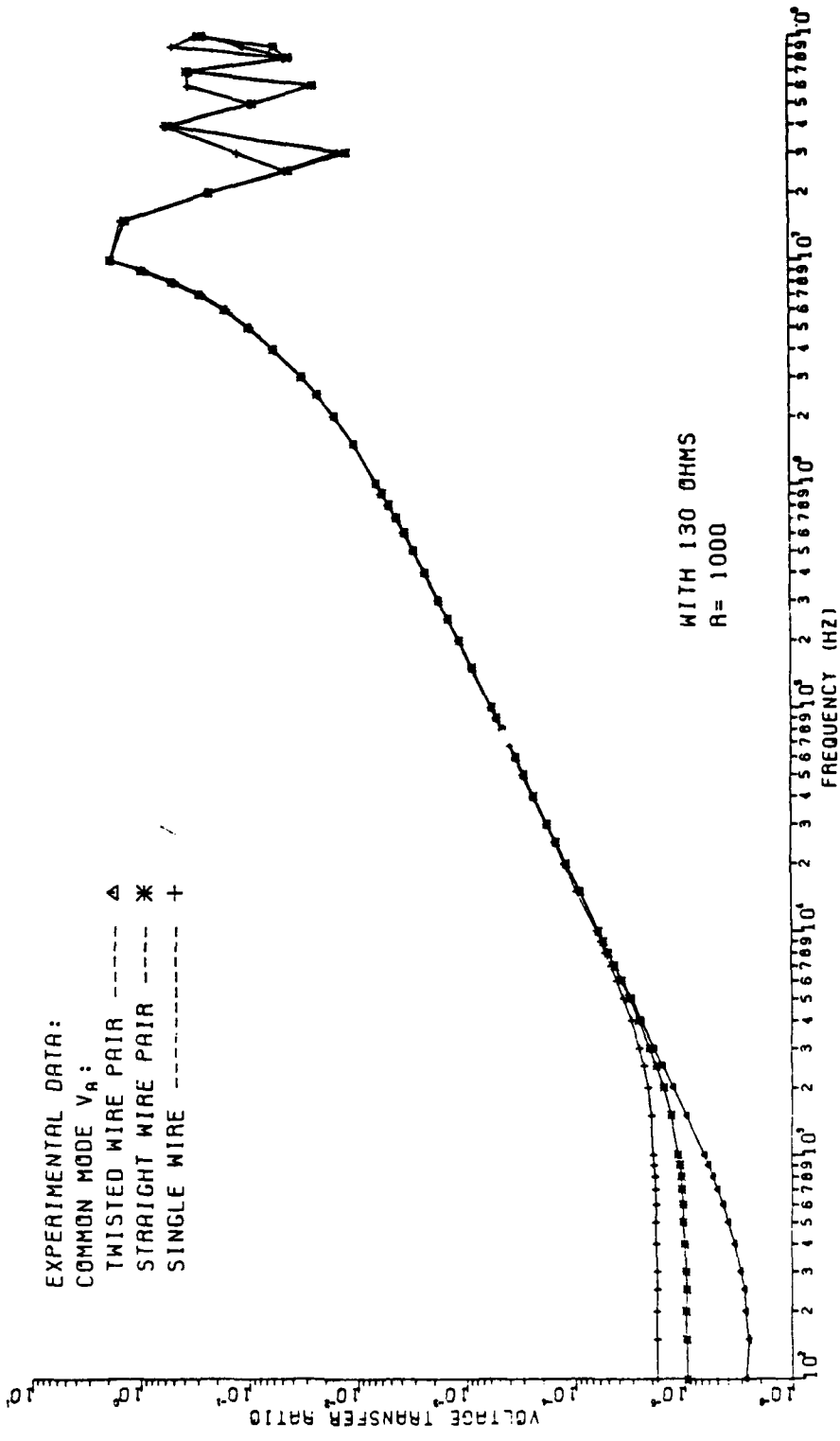
EXPERIMENTAL DATA:
COMMON MODE V_R:
TWISTED WIRE PAIR ----- Δ
STRAIGHT WIRE PAIR ---- *
SINGLE WIRE ---------- +
WITH 130 OHMS
R= 1000
VOLTAGE TRANSFER RATIO
FREQUENCY (HZ)

Fig. 4-9

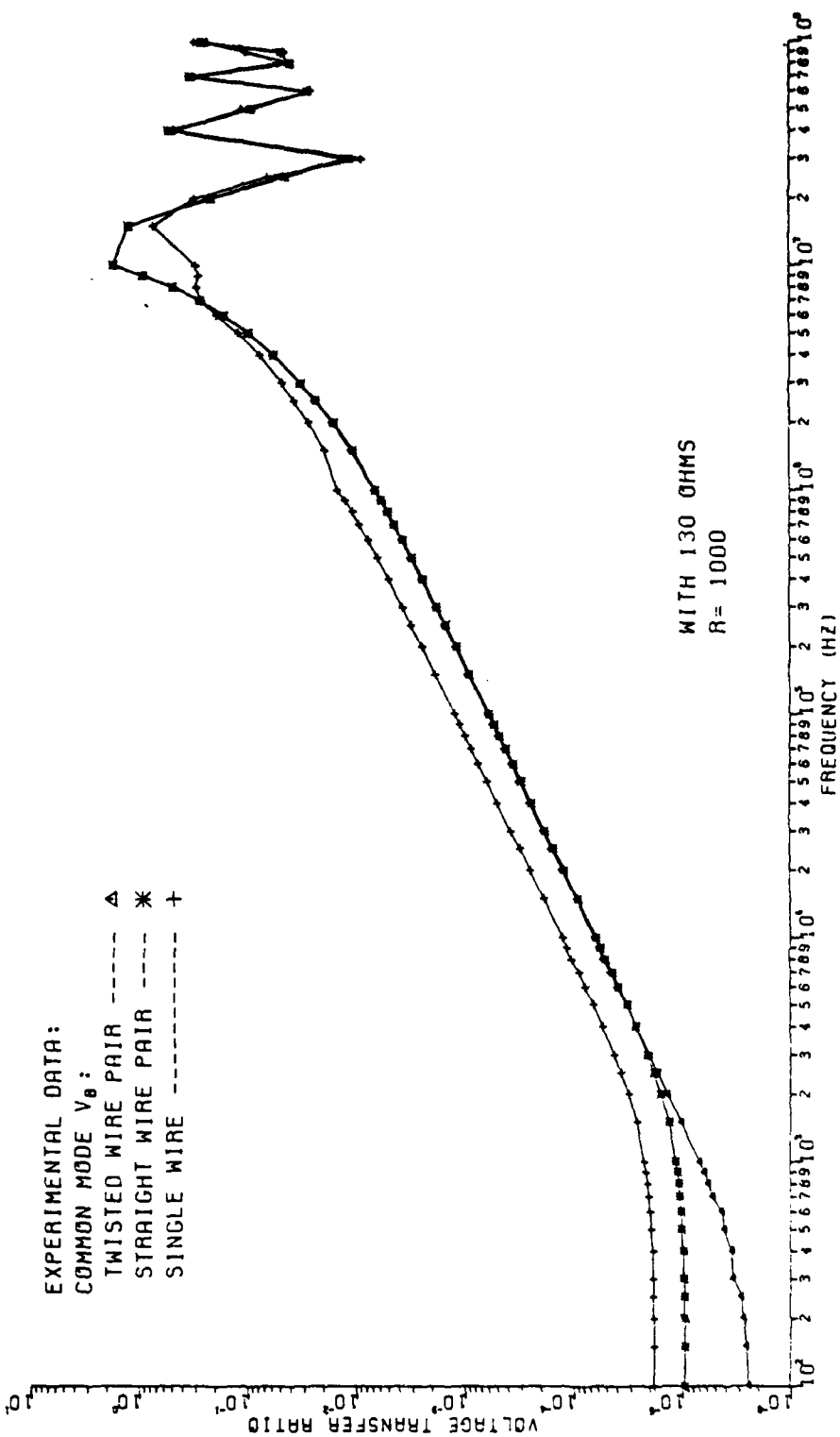
EXPERIMENTAL DATA:
COMMON MODE V_0:
TWISTED WIRE PAIR ----- Δ
STRAIGHT WIRE PAIR ---- ✳
SINGLE WIRE ---------- +
WITH 130 OHMS
R= 1000
VOLTAGE TRANSFER RATIO
FREQUENCY (HZ)

Fig. 4-10

could be replaced with a SW and cause little change in the VTR for the common mode voltage. However, the coupled differential mode voltage would drastically change.

For low frequencies (below 10 kHz) the VTR for the common mode voltage deviated from the 20 dB change per decade and 'leveled out' to a constant transfer ratio. It was noticed that for different line configurations the noise floor of the common mode VTR has a different value of voltage level. Since the line configuration effected a change in the noise floor, something inherent to the three line configurations was suspected of causing the induced circuit noise. As a result, the aluminum ground plane was thought to have a high resistance for these low frequencies, and thereby cause the noise floor.

To further investigate the possible effects of the resistance of the ground plane, a return line, which lay above the ground plane, was provided for the generator signal. With this generator return line present, it was observed that the VTR did not reach a noise floor but continued to roll off at 20 dB per decade.

Using tenative calculations for the resistance of the aluminum ground return, it was found that a value of resistance higher in magnitude than the aluminum could produce was causing the noise floor to occur. The only other possible explanation for the noise floor was that the aluminum support brackets were not in good contact with the ground plane, thus causing a high impedance where they were

joined. To investigate this possible explanation of the noise floor, highly conductive silver grease was used to provide better contact between the aluminum termination brackets and the ground plane. With the silver grease present, it was observed that the common mode VTR rolled off at 20 dB per decade as the frequency was decreased below 10 kHz. Oxidation of the aluminum surfaces appeared to cause a considerable contact resistance to occur between the bracket and the ground plane when the silver grease was not used. This resulted in a constant voltage level occuring at the bracket junctions with the ground plane, as the frequency was reduced below 10 kHz. This constant voltage level was a result of common impedance coupling. The contact resistance at the junction between the termination bracket and the ground plane, R_c, would enter into the balanced wire configuration as shown in Fig. 4-11. The return current from the generating line would induce a voltage across the contact resistance V_{R_c}. This induced voltage acted as a voltage source and induced currents in R_{LR} and R_{LD}. For sufficiently low frequency (below 10 kHz), the induced voltage would dominate the common mode voltage induced via field effects. Hence, a voltage noise floor was created. The silver grease essentially eliminated the noise floor of the common mode VTR which occured below 10 kHz. These experimental results are shown in Figs. 4-12 through 4-19.

The output impedances of the DLD and the input impedances of the DLR were measured by exciting the device

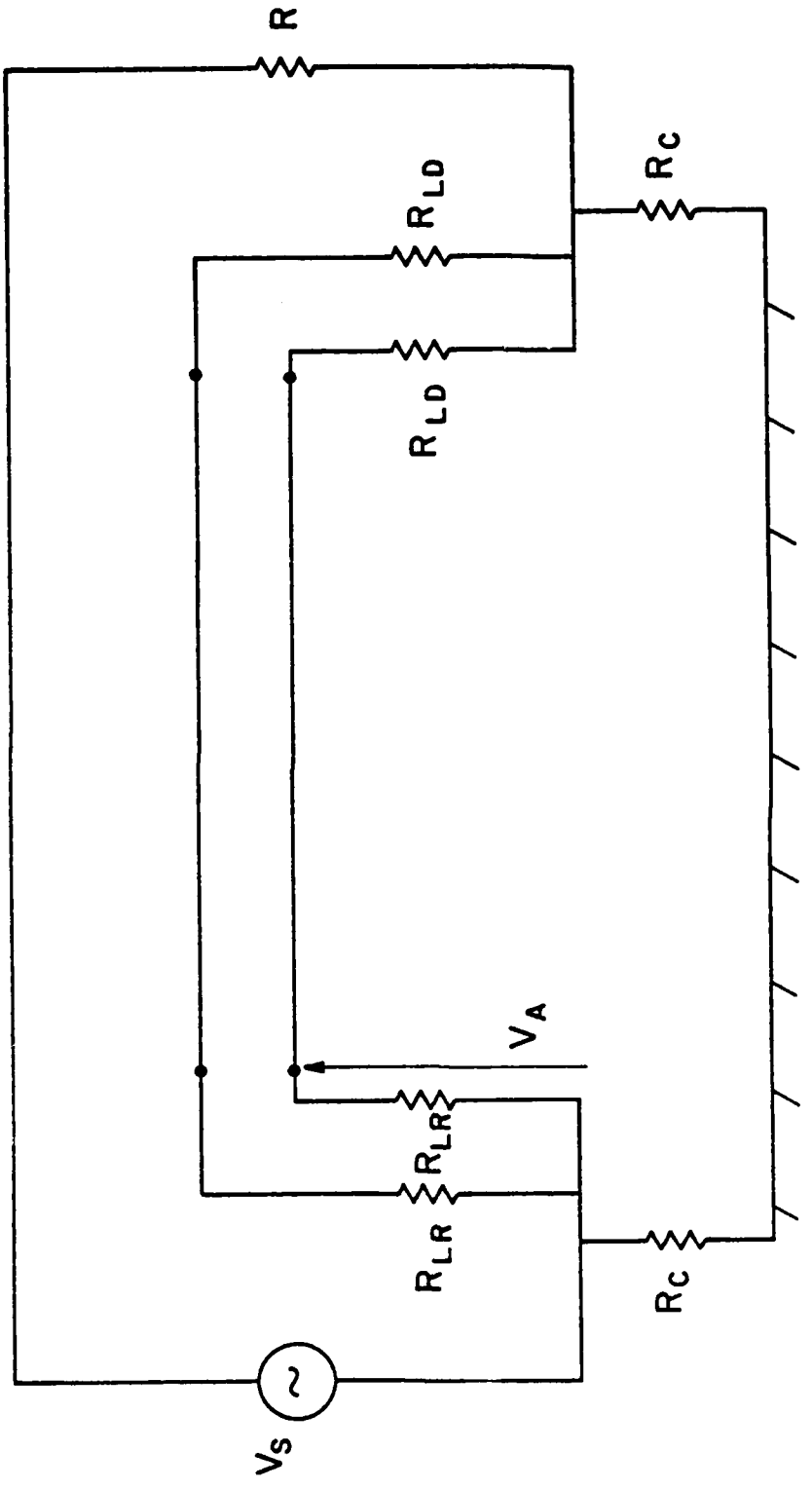

Fig. 4-11a

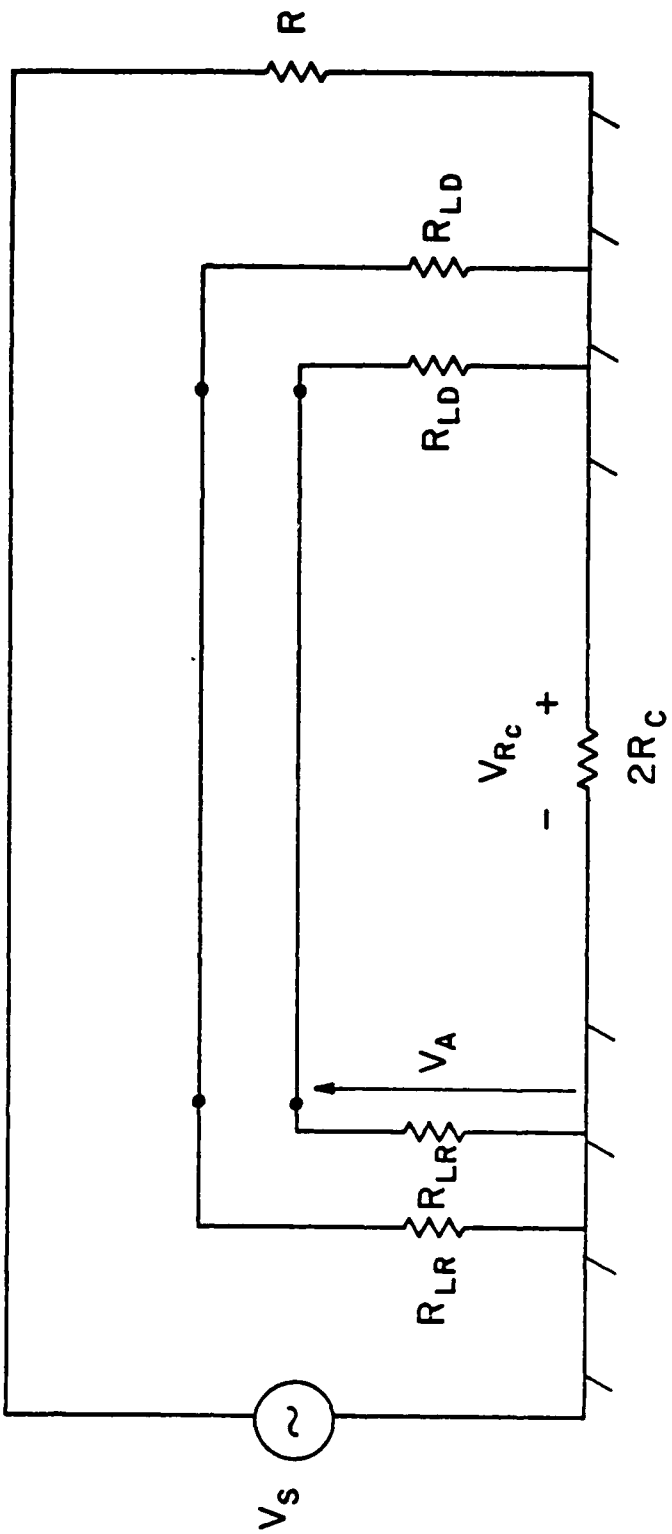

Fig. 4-11b

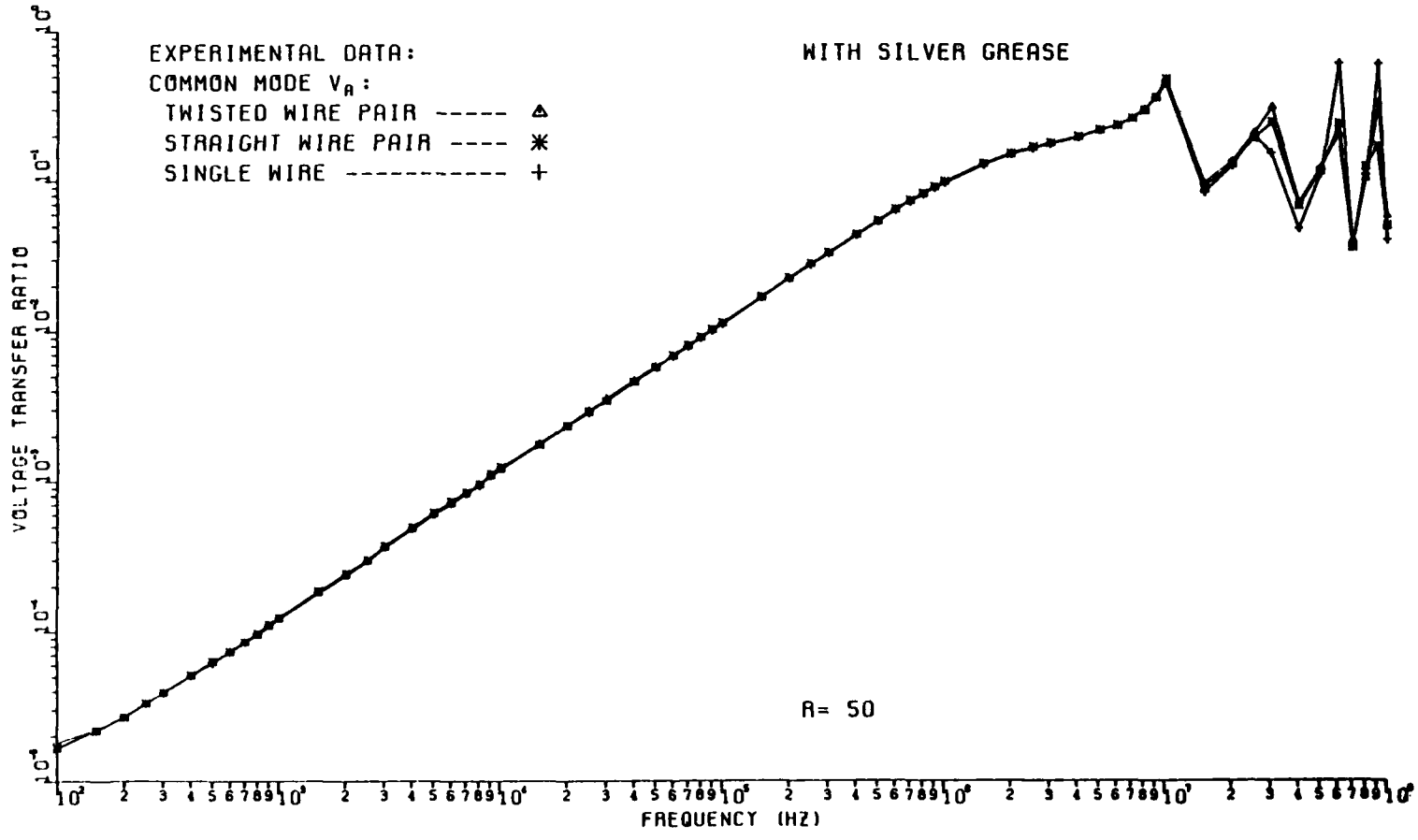
EXPERIMENTAL DATA:
COMMON MODE V_A:
TWISTED WIRE PAIR ----- Δ
STRAIGHT WIRE PAIR ---- ✳
SINGLE WIRE ---------- +
WITH SILVER GREASE
VOLTAGE TRANSFER RATIO
FREQUENCY (HZ)
R= 50

Fig. 4-12

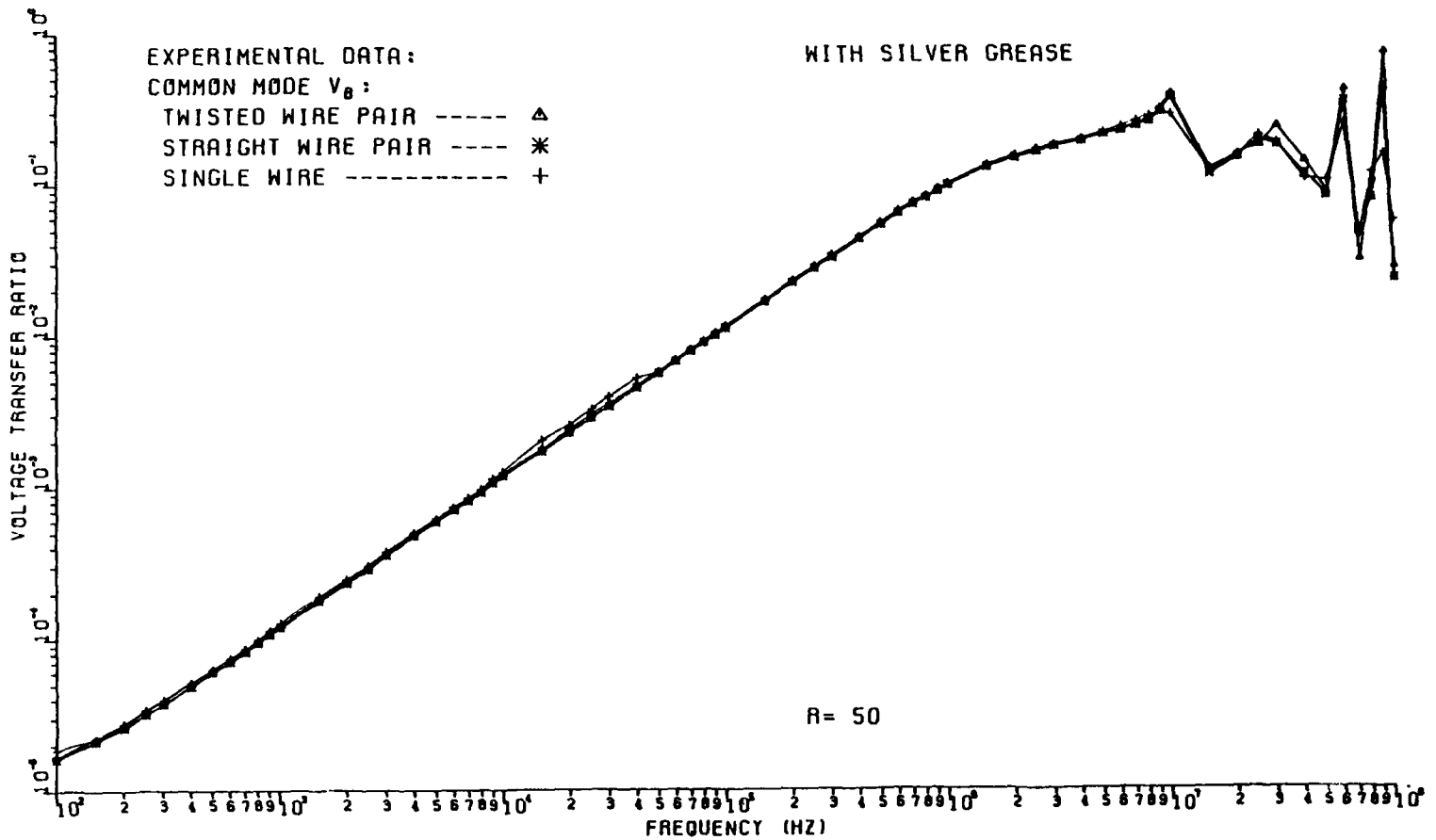
EXPERIMENTAL DATA:
COMMON MODE V_e:
TWISTED WIRE PAIR ----- Δ
STRAIGHT WIRE PAIR ---- ✳
SINGLE WIRE ---------- +
WITH SILVER GREASE
R= 50
VOLTAGE TRANSFER RATIO
FREQUENCY (HZ)

Fig. 4-13

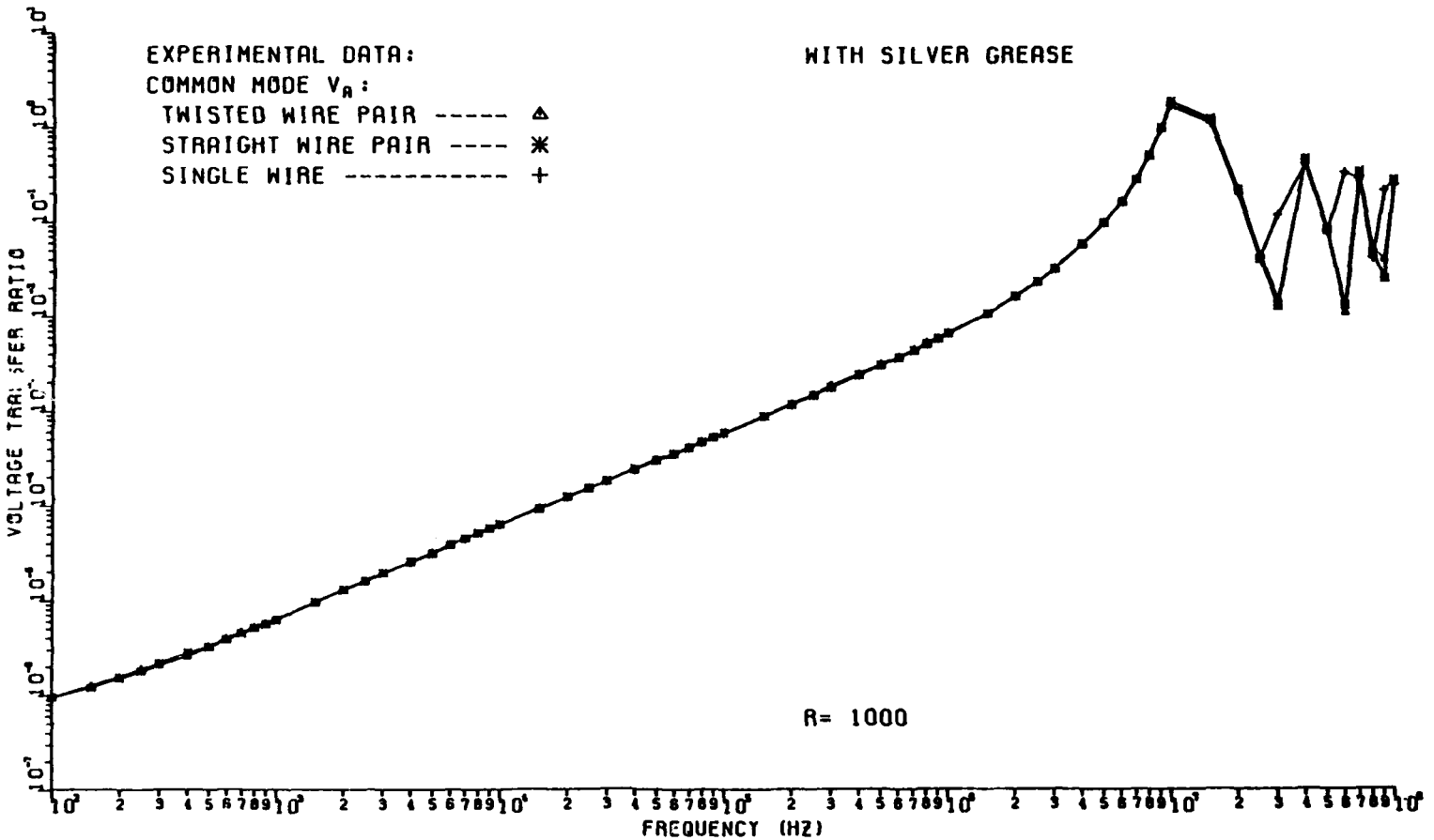
EXPERIMENTAL DATA:
COMMON MODE V_R:
TWISTED WIRE PAIR ----- Δ
STRAIGHT WIRE PAIR ---- ✳
SINGLE WIRE ---------- +
WITH SILVER GREASE
R= 1000
VOLTAGE TRANSFER RATIO
FREQUENCY (HZ)

Fig. 4-14

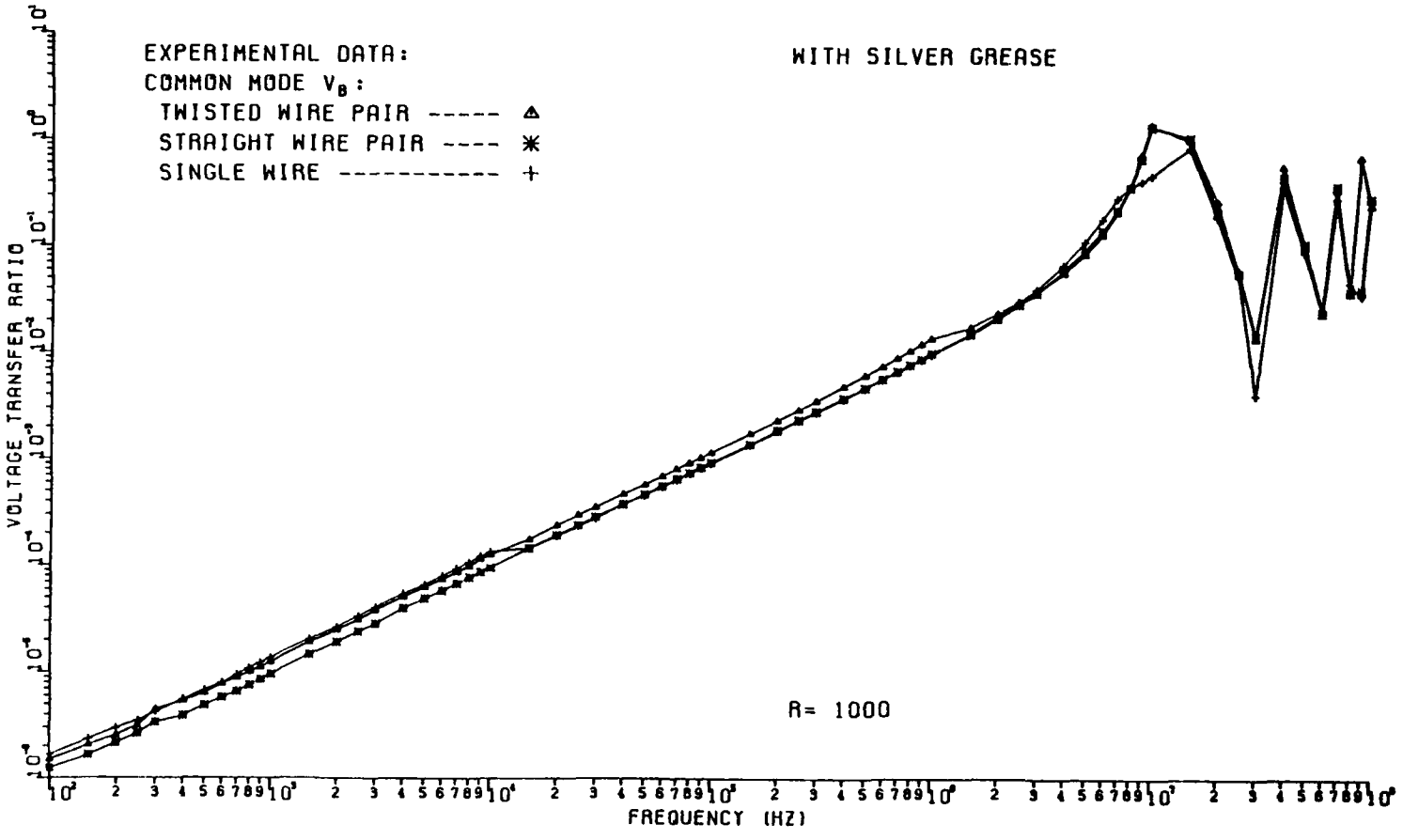
EXPERIMENTAL DATA:
COMMON MODE V_B:
TWISTED WIRE PAIR ----- Δ
STRAIGHT WIRE PAIR ---- ✳
SINGLE WIRE ---------- +
WITH SILVER GREASE
R= 1000
VOLTAGE TRANSFER RATIO
FREQUENCY (HZ)

Fig. 4-15

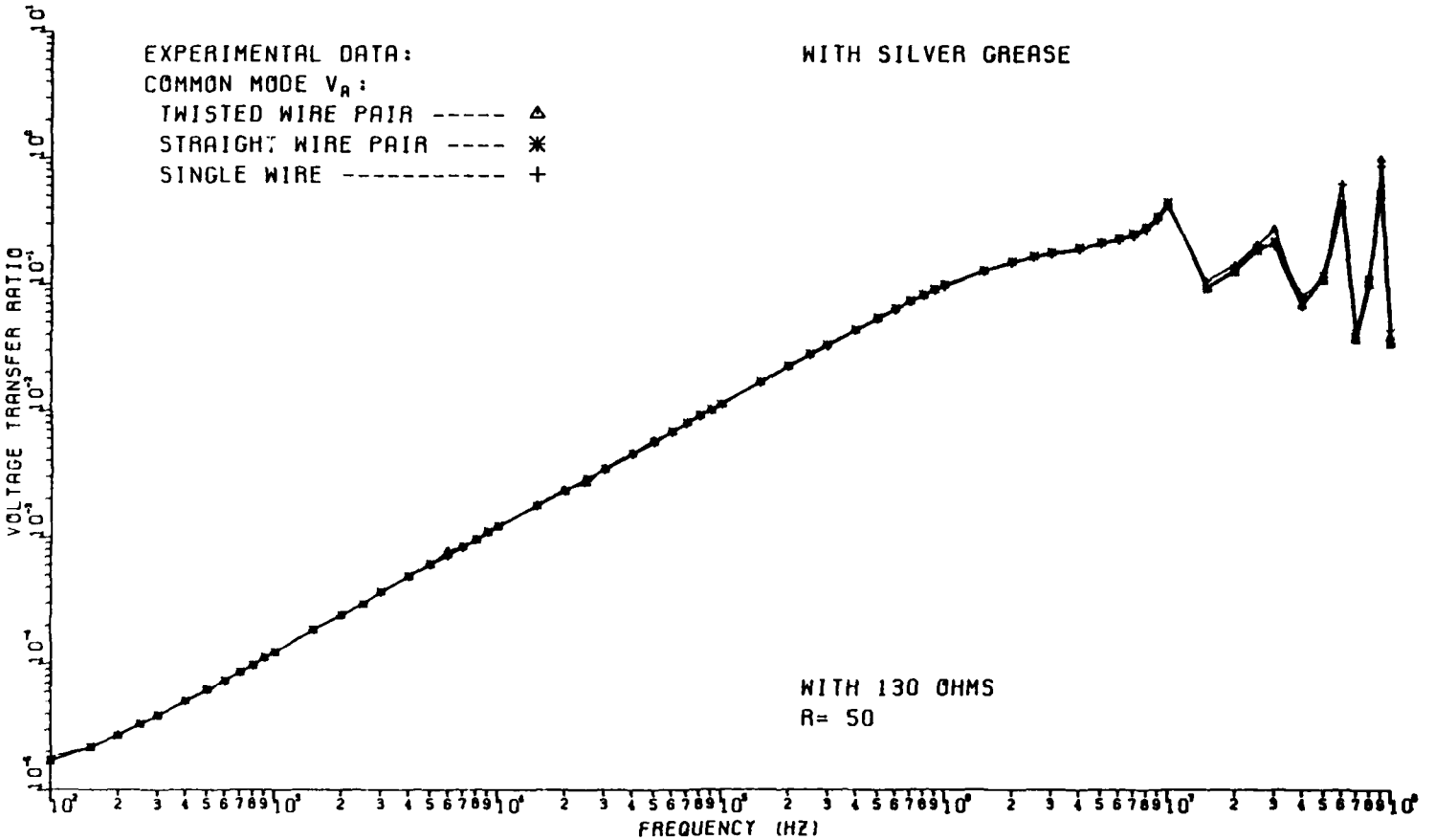
EXPERIMENTAL DATA:
COMMON MODE V_R:
TWISTED WIRE PAIR ----- Δ
STRAIGHT WIRE PAIR ---- ✱
SINGLE WIRE ---------- +
WITH SILVER GREASE
WITH 130 OHMS
R= 50
VOLTAGE TRANSFER RATIO
FREQUENCY (HZ)

Fig. 4-16

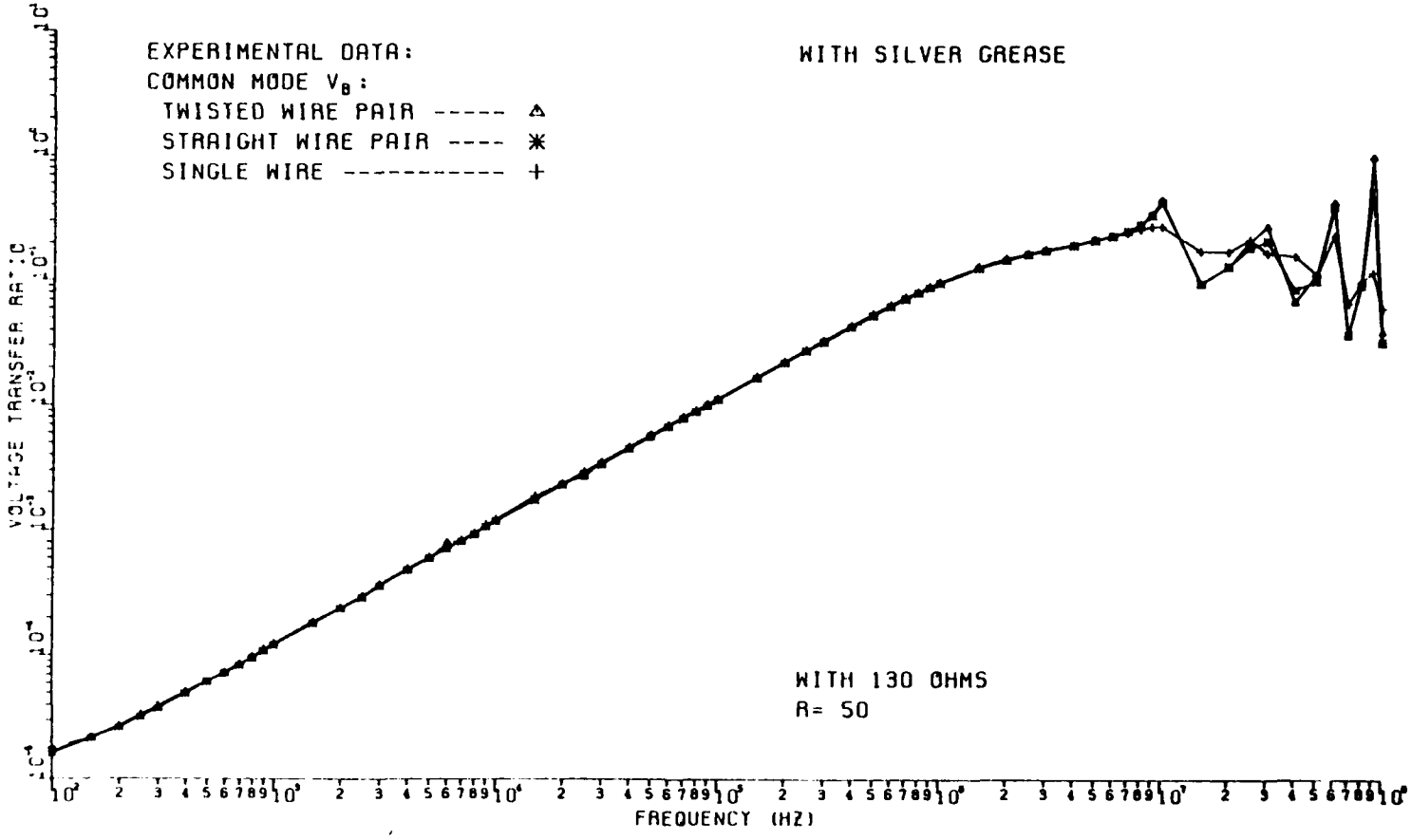
EXPERIMENTAL DATA:
COMMON MODE V_B:
TWISTED WIRE PAIR ----- Δ
STRAIGHT WIRE PAIR ---- ✳
SINGLE WIRE ---------- +
WITH SILVER GREASE
WITH 130 OHMS
R= 50
FREQUENCY (HZ)

Fig. 4-17

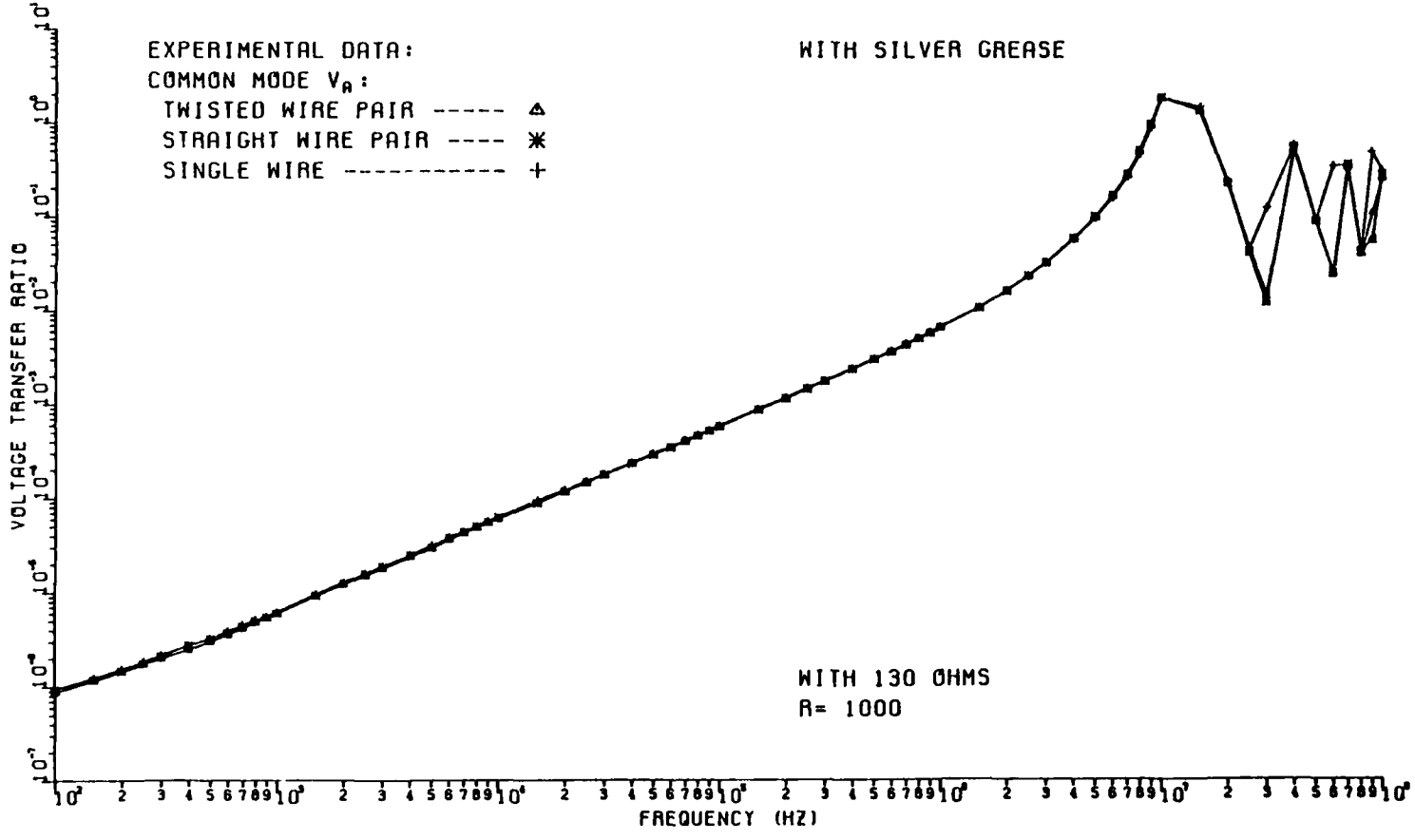
EXPERIMENTAL DATA:
COMMON MODE V_A:
TWISTED WIRE PAIR ----- Δ
STRAIGHT WIRE PAIR ---- ✳
SINGLE WIRE ---------- +
WITH SILVER GREASE
WITH 130 OHMS
R= 1000
VOLTAGE TRANSFER RATIO
FREQUENCY (HZ)

Fig. 4-18

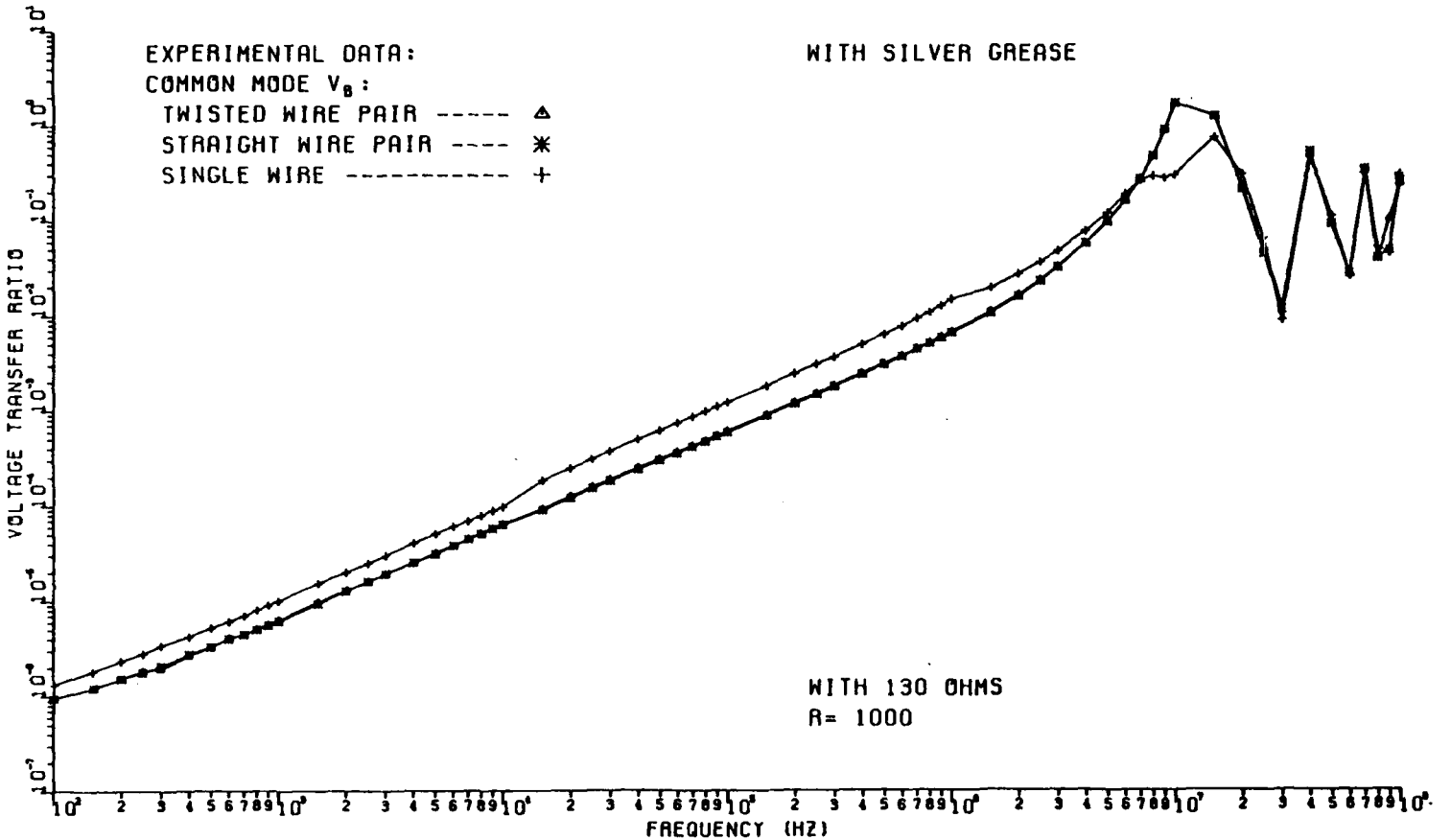
EXPERIMENTAL DATA:
COMMON MODE V_B:
TWISTED WIRE PAIR ----- Δ
STRAIGHT WIRE PAIR ---- ✱
SINGLE WIRE ---------- +
WITH SILVER GREASE
WITH 130 OHMS
R= 1000
VOLTAGE TRANSFER RATIO
FREQUENCY (HZ)

Fig. 4-19

under test with a known voltage and measuring the resulting current. The impedances of the DLD and DLR between each pin and ground were found to be constant for frequencies below 1 MHz. The DLD output impedance, R_{LD}, was equal to 6.55 ohms when the output stage was in the low state, and equal to 12.12 ohms when in the high stage. The input impedance to the DLR, R_{LR}, was found to consist of a single resistor R=4.4 kohms between each pin and ground. The impedance between pins A and B of the DLR was esentially an open circuit.

It was conjectured by Dr. G. T. Capraro of the Rome Air Development Center, Griffiss AFB, NY, that the TWP connecting the DLD and DLR could be replaced by a single wire above ground and have the induced terminal voltages the same as the common mode voltage induced on the TWP, V_A and V_B, when the TWP is connected in the balanced configuration. The prediction model for two wires above a ground plane, presented in [5], will give an accurate prediction of the induced terminal voltages of a single wire above ground. If Dr. Capraro's conjecture is true, this model should also be sufficient for the prediction of the common mode voltage coupled to the TWP and the SWP when they are connected in the balanced wire configuration. Since the experimental results of the SW above the ground plane were in very close agreement with those of the TWP and the SWP above the ground plane, it is expected that the single wire above ground model will give sufficiently accurate predictions.

In [5] it is shown that the overall coupling, between two wires above ground, is the sum of an inductive coupling component, V_{OUT}^{IND}, and a capacitive coupling component, V_{OUT}^{CAP}. The inductive coupling component is due to the mutual inductance, l_m, between the two circuits and the capacitive coupling component is due to the mutual capacitance, c_m, between the two circuits. The results are

$$V_{OUT} = V_{OUT}^{IND} + V_{OUT}^{CAP}$$

where,

$$V_{OUT}^{IND} = \frac{R_{LR}}{R_{LR} + R_{LD}} \, j\omega l_m \mathcal{L} \frac{V_S}{R}$$

$$V_{OUT}^{CAP} = \frac{R_{LR}R_{LD}}{R_{LR} + R_{LD}} \, j\omega c_m \mathcal{L} V_S$$

and $\mathcal{L}$ is the total line length. This low frequency approximation of the coupled voltage to a single wire above ground is illustrated in Fig. 4-20.

It was also shown in [5] that inductive coupling dominates capacitive coupling in $V_R(\mathcal{L})$ if,

$$\frac{R \, R_{LR}}{Z_{CG}Z_{CR}} << 1$$

where $Z_{CG}(Z_{CR})$ is the characteristic impedance of the generator (receptor) circuit in the presence of the receptor

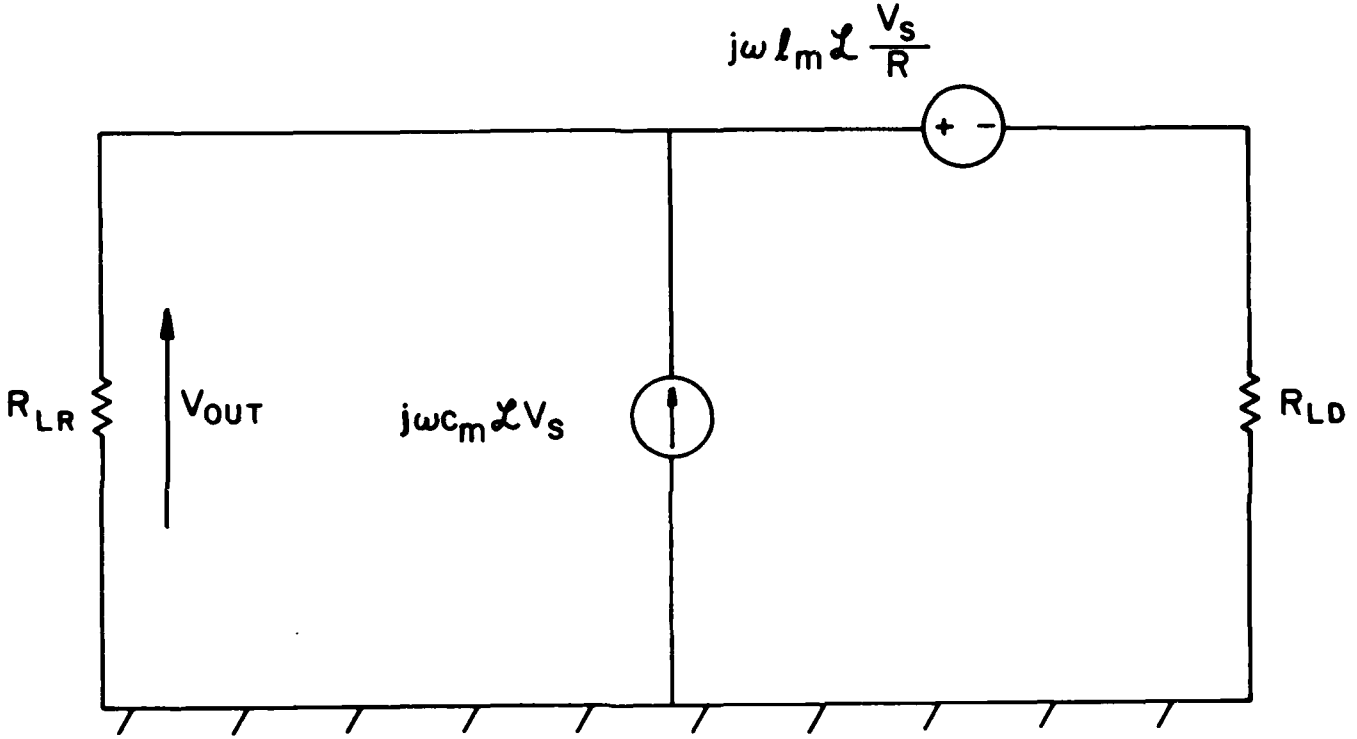
$j\omega l_m \mathcal{L} \frac{V_s}{R}$
+ −
R_{LR}
V_{OUT}
$j\omega c_m \mathcal{L} V_s$
R_{LD}

Fig. 4-20

(generator) circuit.

If inductive coupling component is to dominate the capacitive coupling component in $V_R(0)$ then,

$$\frac{R\,R_{LD}}{Z_{CG}Z_{CR}} << 1$$

Capacitive coupling dominates inductive coupling if these inequalities are reversed.

The solution of the TL equations for a single wire above a ground plane is simplified in [5] to the solution of a single equation with respect to frequency. The prediction results of this single wire model are shown in figures 4-21 through 4-28 in conjunction with the TWP, SWP, and SW experimental results. As can be seen from these figures, the SW model gives a prediction (within 2 dB) of the common mode voltage coupled to the TWP when it is connected in the balanced configuration. If the line length of the wire is electrically short, the simplified TL equation reduces to the low frequency model presented above. Notice that the low frequency model varies linearly with frequency. However, for low frequency (where the line length is electrically short) the VTR of the common mode voltage changes 20 dB per decade and is successfully predicted with the low frequency model. For frequencies above 1 MHz the SW model prediction loses accuracy, but this is expected because the impedances of the DLD and DLR are changing with frequency. They are assumed constant in the SW model

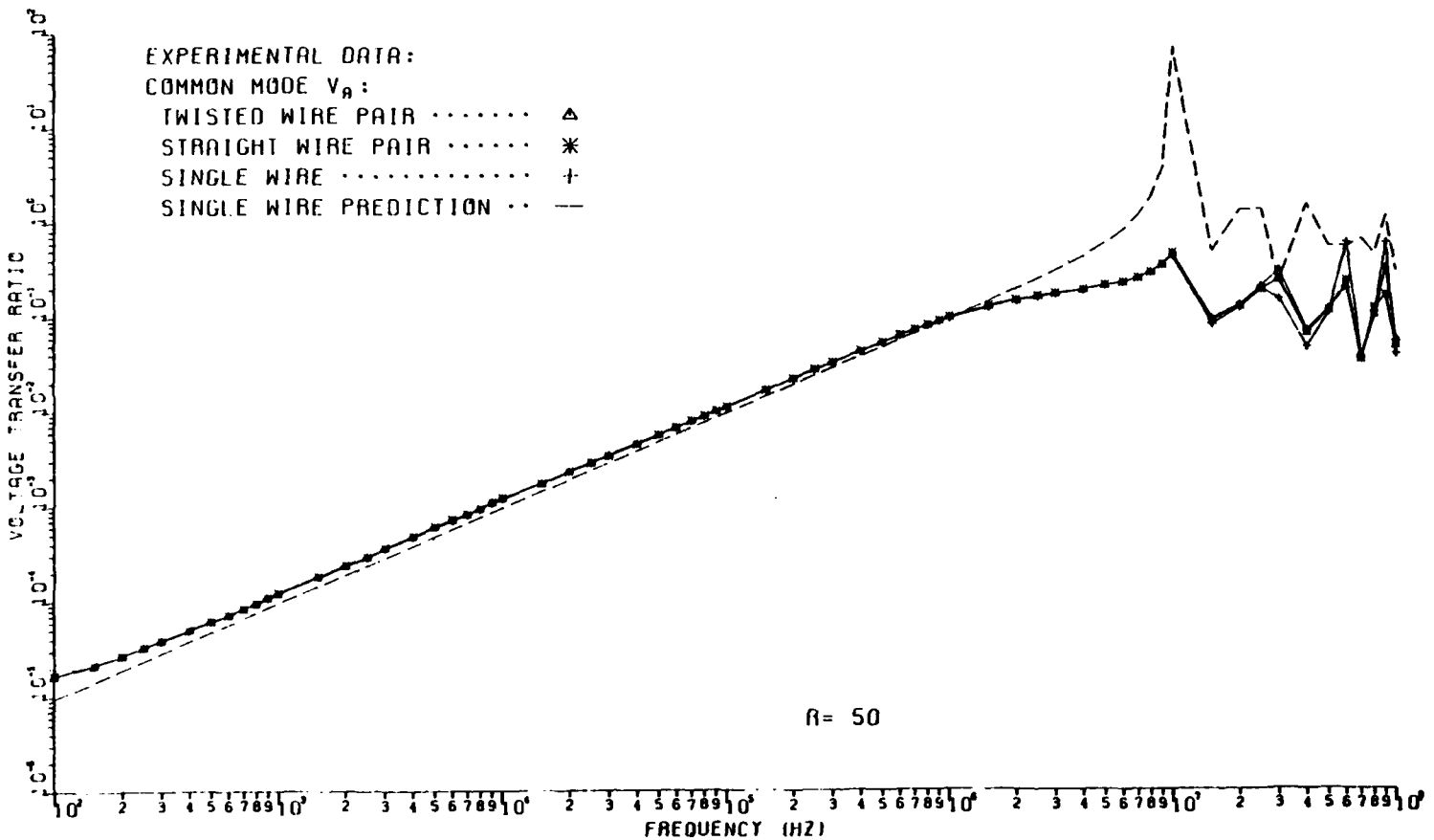
EXPERIMENTAL DATA:
COMMON MODE V_A:
TWISTED WIRE PAIR ····· △
STRAIGHT WIRE PAIR ····· ✳
SINGLE WIRE ····· +
SINGLE WIRE PREDICTION ·· —
VOLTAGE TRANSFER RATIO
R= 50
FREQUENCY (HZ)

Fig. 4-21

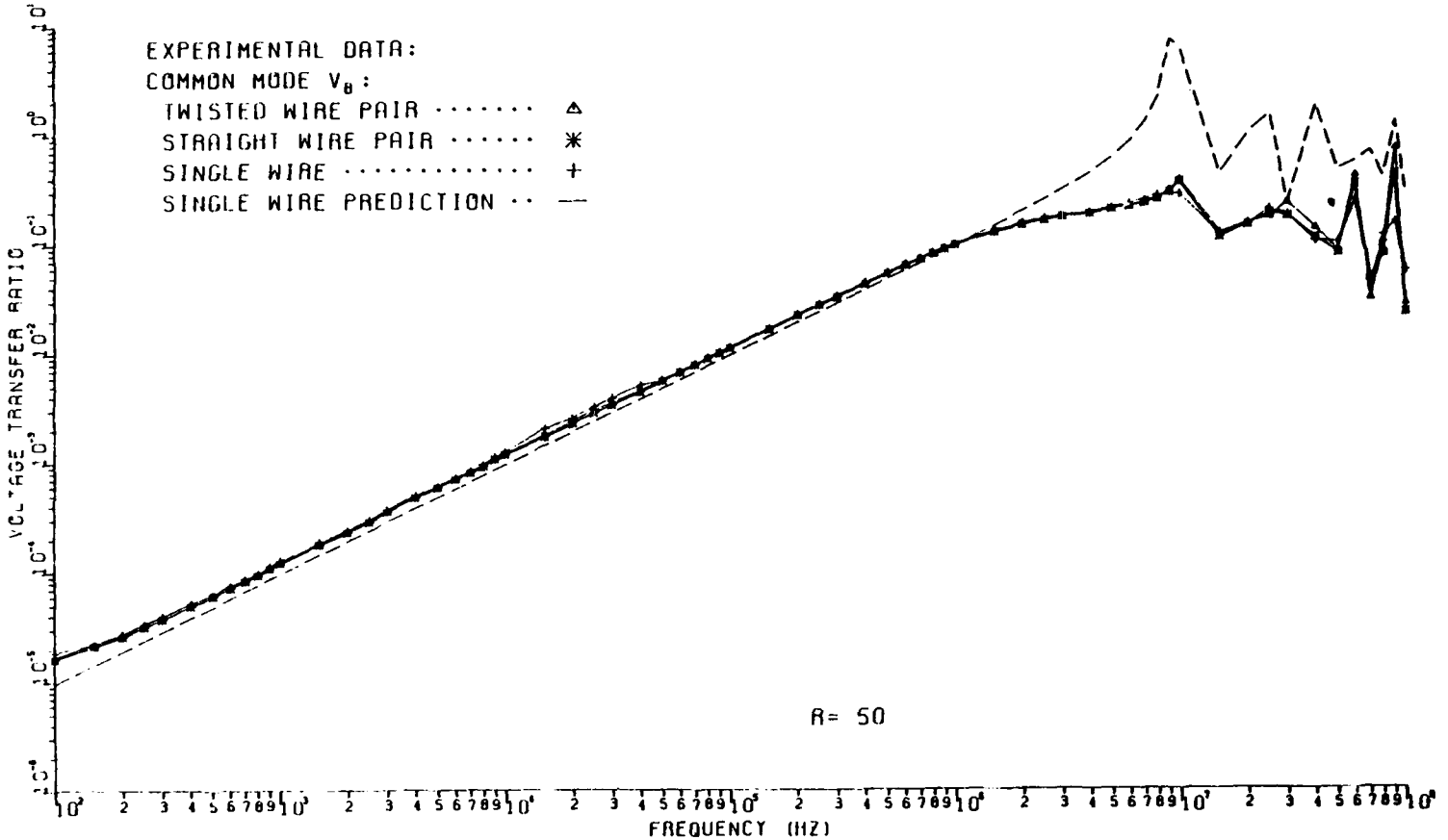
EXPERIMENTAL DATA:
COMMON MODE V_θ:
TWISTED WIRE PAIR ····· △
STRAIGHT WIRE PAIR ····· ✳
SINGLE WIRE ····· +
SINGLE WIRE PREDICTION ·· —
VOLTAGE TRANSFER RATIO
FREQUENCY (HZ)
R= 50

Fig. 4-22

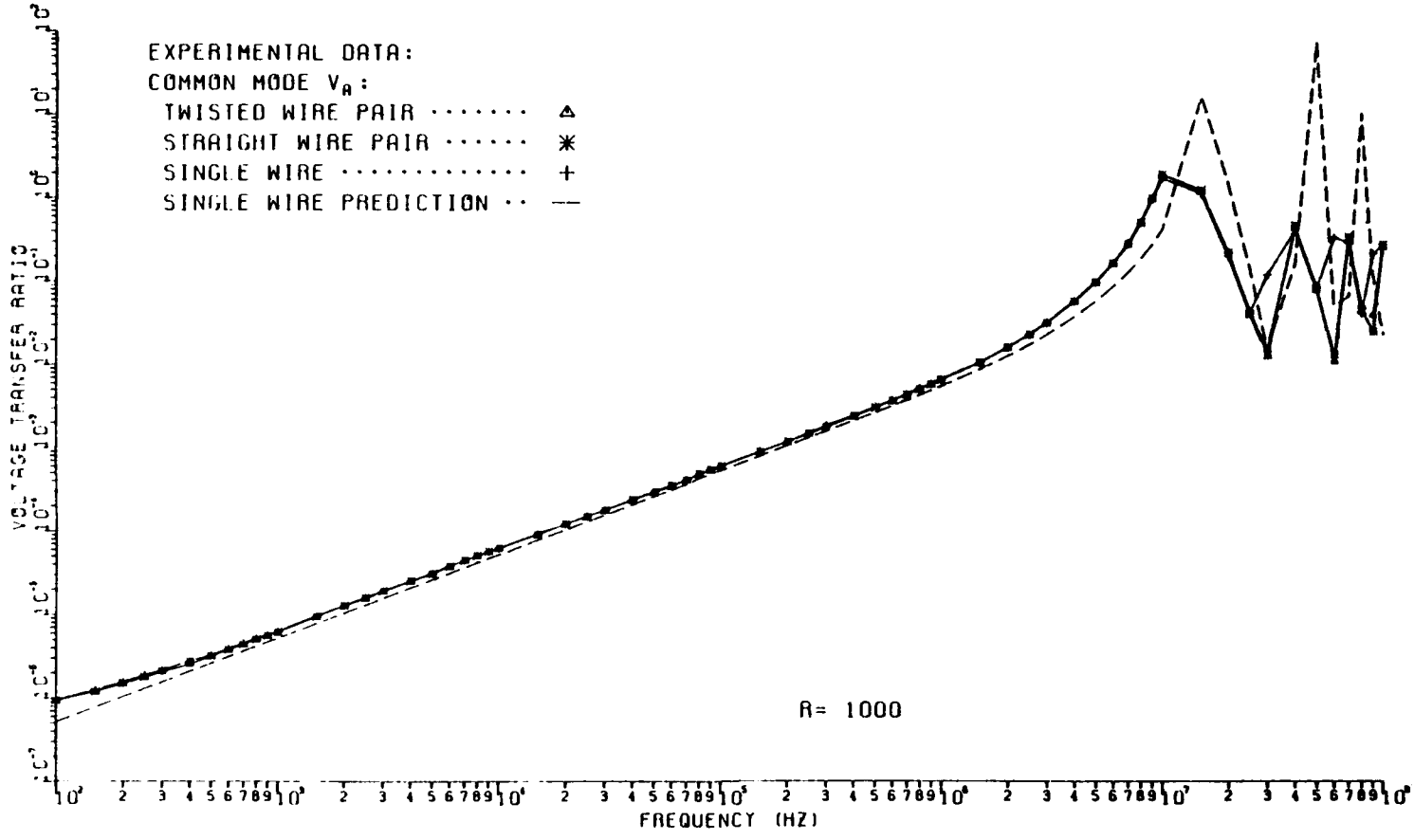
EXPERIMENTAL DATA:
COMMON MODE V_A:
TWISTED WIRE PAIR ····· △
STRAIGHT WIRE PAIR ····· ✳
SINGLE WIRE ····· +
SINGLE WIRE PREDICTION ·· —
R= 1000
FREQUENCY (HZ)

Fig. 4-23

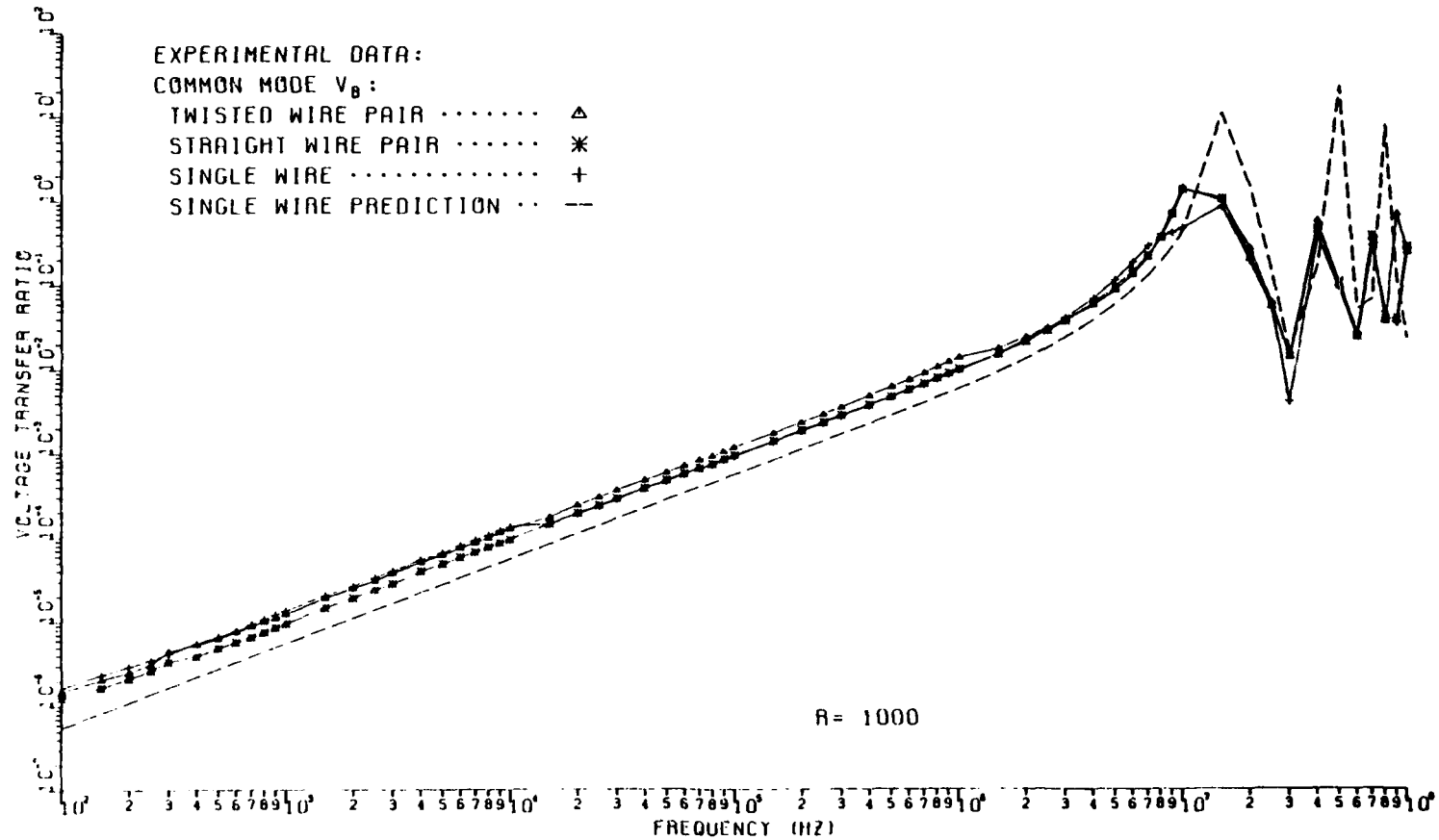
EXPERIMENTAL DATA:
COMMON MODE V_B:
TWISTED WIRE PAIR ····· △
STRAIGHT WIRE PAIR ····· ✳
SINGLE WIRE ····· +
SINGLE WIRE PREDICTION ·· ——
VOLTAGE TRANSFER RATIO
A= 1000
FREQUENCY (HZ)

Fig. 4-24

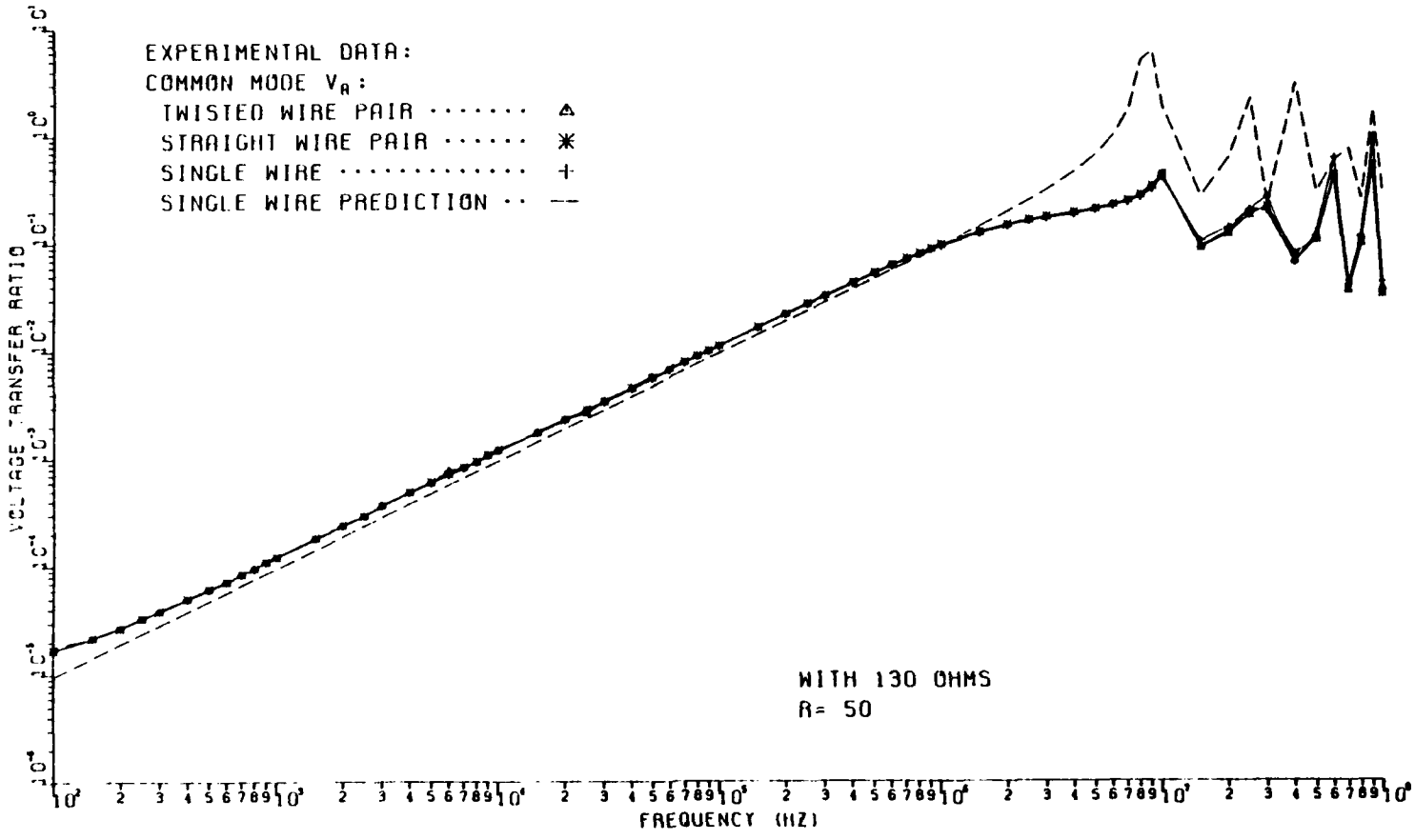
EXPERIMENTAL DATA:
COMMON MODE V_R:
TWISTED WIRE PAIR ····· △
STRAIGHT WIRE PAIR ····· ✳
SINGLE WIRE ····· +
SINGLE WIRE PREDICTION ·· ——
VOLTAGE TRANSFER RATIO
WITH 130 OHMS
R= 50
FREQUENCY (HZ)

Fig. 4-25

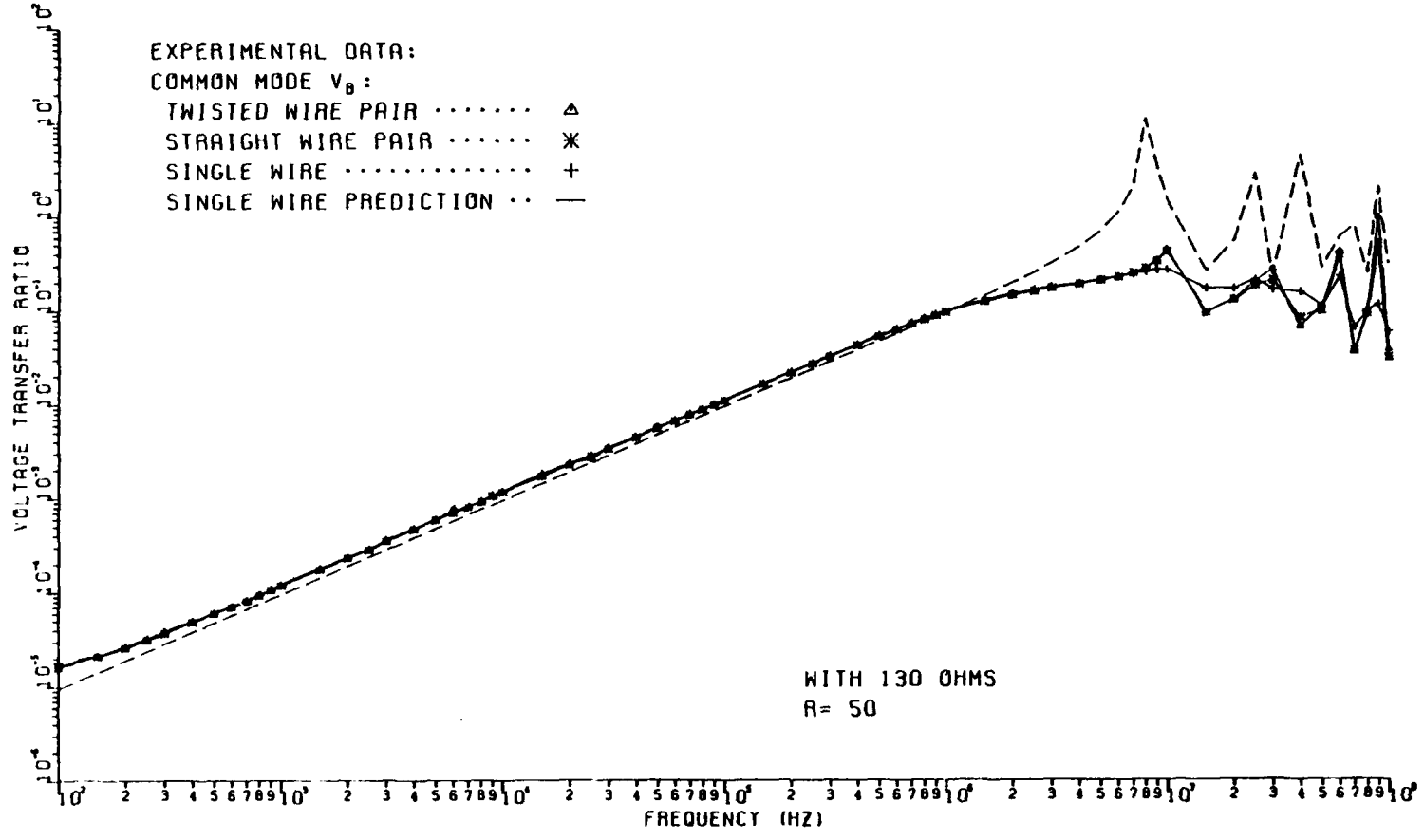
EXPERIMENTAL DATA:
COMMON MODE V_B:
TWISTED WIRE PAIR ····· △
STRAIGHT WIRE PAIR ····· ✳
SINGLE WIRE ····· +
SINGLE WIRE PREDICTION ·· —
WITH 130 OHMS
R= 50
VOLTAGE TRANSFER RATIO
FREQUENCY (HZ)

Fig. 4-26

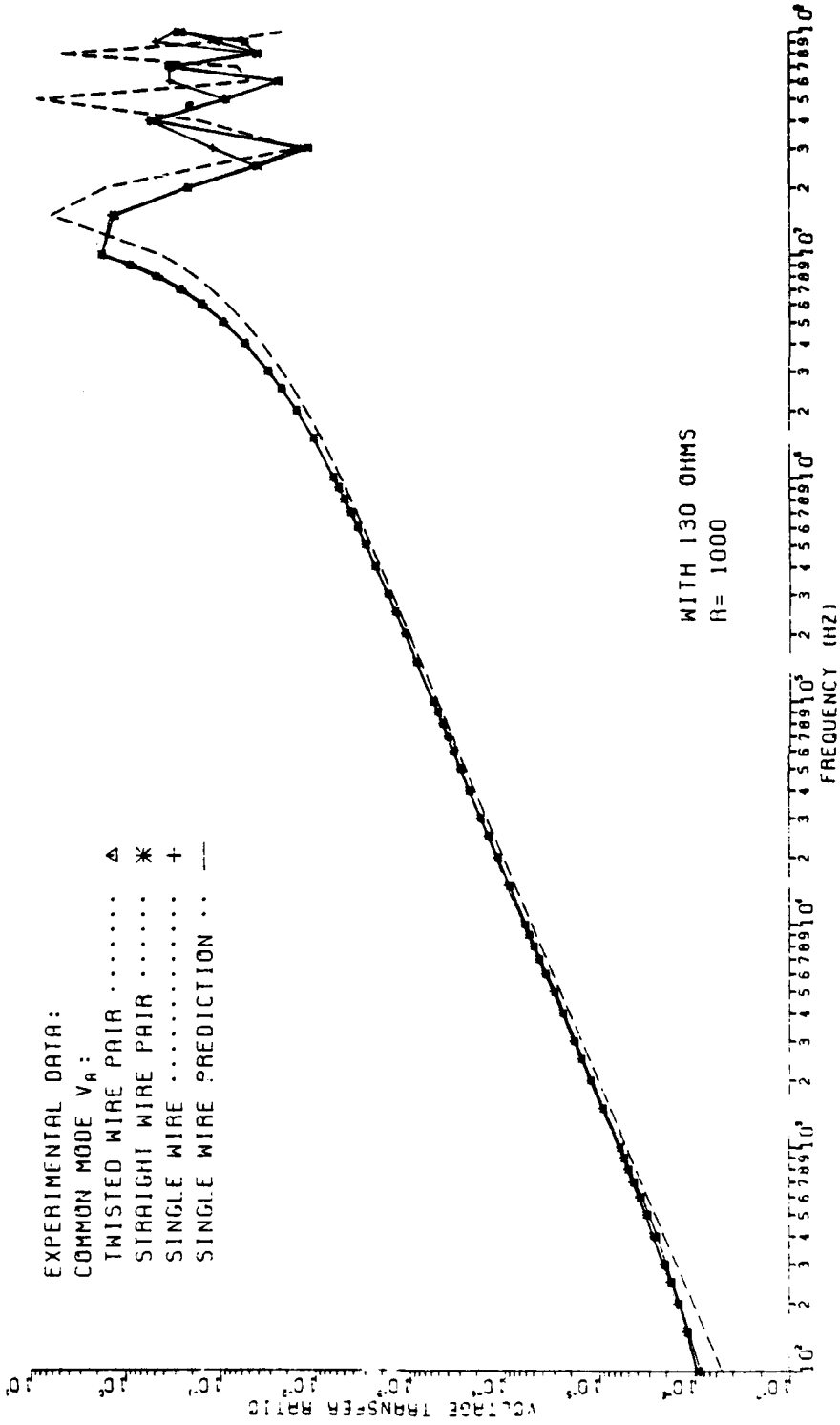
EXPERIMENTAL DATA:
COMMON MODE V_R:
TWISTED WIRE PAIR ..... Δ
STRAIGHT WIRE PAIR ..... ✳
SINGLE WIRE ..... +
SINGLE WIRE PREDICTION .. —
WITH 130 OHMS
R= 1000
VOLTAGE TRANSFER RATIO
FREQUENCY (HZ)

Fig. 4-27

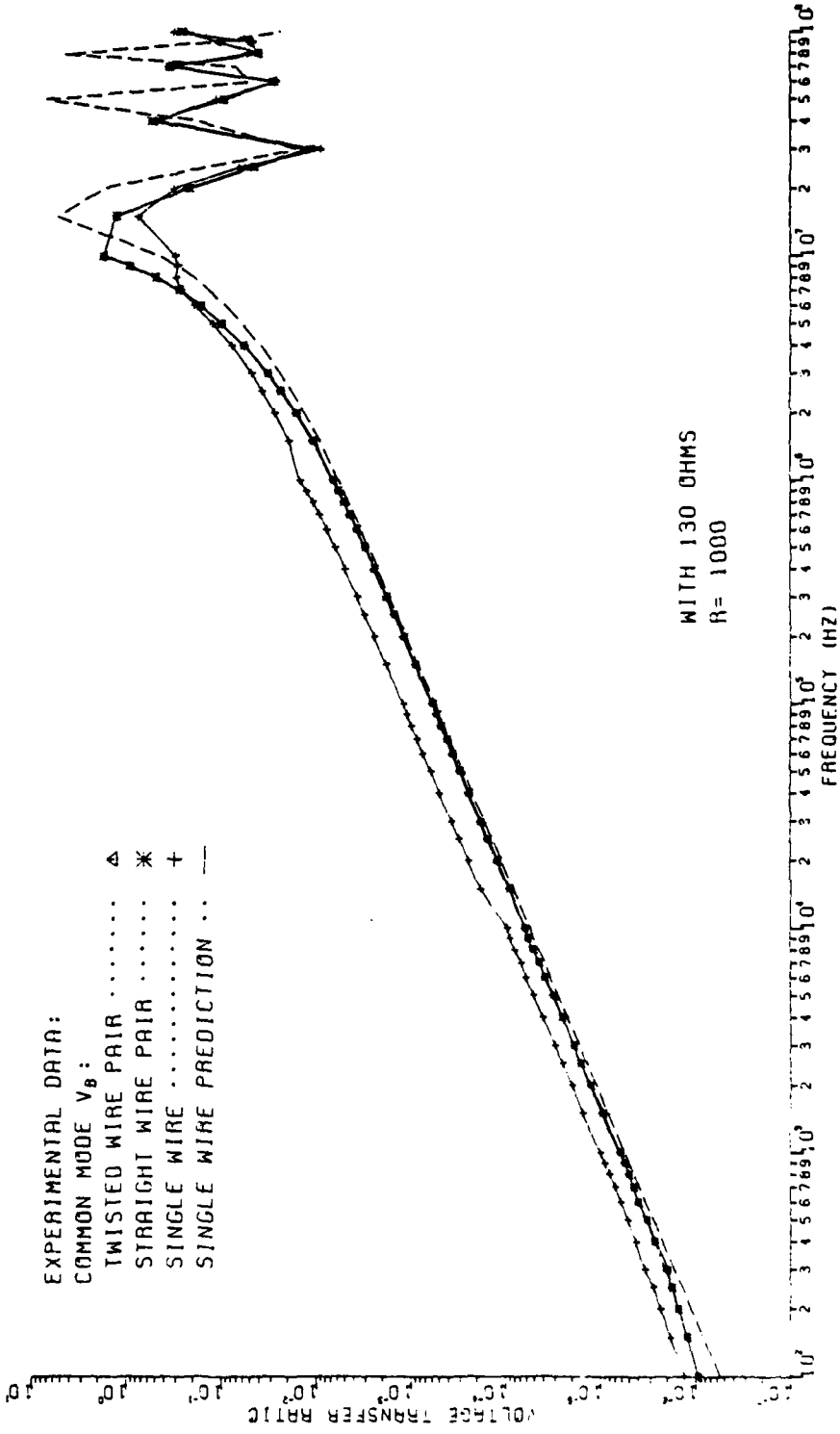
EXPERIMENTAL DATA:
COMMON MODE V_B:
TWISTED WIRE PAIR ..... Δ
STRAIGHT WIRE PAIR ..... ✳
SINGLE WIRE ..... +
SINGLE WIRE PREDICTION .. —
WITH 130 OHMS
R= 1000
VOLTAGE TRANSFER RATIO
FREQUENCY (HZ)

Fig. 4-28

prediction. The effects of the common impedance coupling due to the contact resistance still causes a slight rolloff of the VTR to occur for very low frequencies. The common impedance coupling was not considered in the SW model predictions, because it is very difficult to calculate. The use of different generator impedances would probably not change these results since inductive coupling is dominant for both 50 ohms and 1k ohm. The DLD and DLR impedances are virtually identical with those of similar devices made by Fairchild (9614 and 9615) and National Semiconductor (DS 55114 and DS 55115) so the given results would seem to apply to other devices.

V. SUMMARY AND CONCLUSIONS

The experimental results of the sensitivity analysis have shown that the differential mode voltage coupled to a TWP is very sensitive to line twist for low impedance loads but relatively insensitive to line twist for high impedance loads. This lead to the conclusion that reducing inductive coupling by twisting the lines has little effect in the overall coupled voltage when capacitive coupling is dominant. It also has shown that accurate prediction of the coupled voltage to the TWP for low impedance loads would not be practical from an application point of view, because the overall coupling is very sensitive to line twist.

A new computer model for the TWP, which incorporated the rotation of the twisted pair, gave moderate improvement in the prediction of the coupled voltage to the TWP when it was terminated in low impedance loads. The model also predicted the maximum coupling to the twisted pair when the angular position of the segment attached to the load termination was approximately equal to 60 degrees. This angle was observed in the sensitiviy analysis to produce maximum coupling to the twisted pair.

It was found that the prediction of the common mode voltage to a balanced TWP terminated in a differential line driver and line receiver could be accurately achieved when the TWP was modeled as a single wire. This greatly simplifies the prediction model and avoids the sensitivity

associated with the coupled differential mode voltage.

Work is currently under way at Syracuse University, under the direction of Professor D. D. Weiner, that is investigating the degradation of the receivers to various types of common mode signals. It is anticipated that the combination of the results of this report and the work at Syracuse University will result in an overall prediction model for the vulnerability of this common data transmission system.

BIBLIOGRAPHY

[1] J. W. McKnight and C. R. Paul, Applications of Multiconductor Transmission Line Theory to the Prediction of Cable Coupling, Volume V, Prediction of Crosstalk Involving Twisted Wire Pairs. Technical Report, Rome Air Development Center, Griffiss AFB, N.Y., RADC-TR-76-101, Volume V, February 1978.

[2] Clayborne D. Taylor and J. Philip Castillo, "On the Response of a Terminated Twisted-Wire Cable Excited by a Plane-Wave Electromagnetic Field", IEEE Trans. on Electromagnetic Compatibility, Volume EMC-22, No. 1, pp. 16-19, February 1980.

[3] S. Shenfeld, "Magnetic Fields of Twisted-Wire Pairs", IEEE Trans. on Electromagnetic Compatibility, Volume IMC-11, No. 4, pp. 164-169, November 1969.

[4] C. R. Paul and A. E. Feather, "Computation of the Transmission Line Inductance and Capacitance Matrices from the Generalized Capacitance Matrix", IEEE Trans. on Electromagnetic Compatibility, Volume EMC-18, No. 4, pp. 175-183, November 1976.

[5] C. R. Paul, "Solution of the Transmission Line Equations for Three-Conductor Lines in Homogeneous Media", IEEE Trans. on Electromagnetic Compatibility, Volume EMC-20, No. 1, pp. 216-222, February 1978.

MISSION
of
Rome Air Development Center

RADC plans and executes research, development, test and selected acquisition programs in support of Command, Control Communications and Intelligence (C^3I) activities. Technical and engineering support within areas of technical competence is provided to ESD Program Offices (POs) and other ESD elements. The principal technical mission areas are communications, electromagnetic guidance and control, surveillance of ground and aerospace objects, intelligence data collection and handling, information system technology, ionospheric propagation, solid state sciences, microwave physics and electronic reliability, maintainability and compatibility.